# STABILIZING PARAMETERIZATION
# FOR UNCERTAIN DELAY SYSTEMS

**LE BINH NGUYEN**

(B. Eng (Hons), UPG)

A THESIS SUBMITTED

FOR THE DEGREE OF DOCTOR OF PHILOSOPHY

DEPARTMENT OF ELECTRICAL AND COMPUTER

ENGINEERING
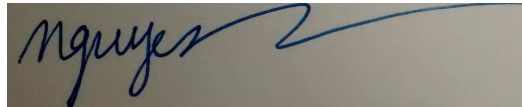
NATIONAL UNIVERSITY OF SINGAPORE

2013

# DECLARATION

I hereby declare that this thesis is my original work
and it has been written by me in its entirety.
I have duly acknowledged all the sources of
information which have been used in the thesis.

This thesis has also not been submitted for any
degree in any university previously.



Le Binh Nguyen

13th December 2013

# Acknowledgement

First and foremost, I would like to express my heartfelt gratitude to Professor Wang Qing-Guo for his fundamental role in my doctoral work. Without Professor Wang, I could hardly find better role model with tremendous inspirational, supportive, and patience. I appreciate his time, ideas and advices to train me in the last four and a half years. Without him, this thesis would not be possible.

I wish to take this opportunity to thank my co-supervisor Professor Lee Tong Heng for his constant support, guidance and encouragement. His enthusiasm and inspiration play an important role in my time here at NUS. I also would like to extend my special thanks to all lecturers and tutors from ECE department that have built my academic background.

My sincere thanks go to Mr Yu Chao, Mr Li Xian, Dr. Qin Qin, Dr. Lee See Chek and many others in the Advanced Control Technology Lab (Center for Intelligent Control) who have in one way or another given me their kind help. I am also grateful to the National University of Singapore for the research scholarship.

Lastly, I am deeply thankful to my family for their love, support and encouragement. Their faith in my PhD journey has been invaluable. I would like to dedicate this thesis to them and hope that they would find delight in this humble achievement.

# Contents

# Summary

The focus of this thesis is on stabilizing parameterization for uncertain delay processes. The first part of the thesis presents a method to find PID stabilizing region in controller's parameter plane. The concept of stability boundaries in D-decomposition technique is extend to the parameterized stability boundary , which transform boundary curves into boundary bands when one of the controller gains varies in a range. This eliminates the difficulty of using 3D graph to solve the problem with 3 parameters while maintaining the advantage of 2D method.

In the second part, the thesis deals with the problem of determining the stabilizing controller gain and process delay ranges for a general delay process in feedback configuration. In general, such a problem admits no analytical solutions. Instead, the condition of the loop Nyquist plot's intersection with the critical point is graphically employed to determine stability boundaries in the gain-delay space. The stability of regions that are divided by these boundaries is decided with helps of a new perturbation analysis of delay on change of closed-loop unstable poles. As a result, all the stable regions can be obtained and each stable region can capture the full information on the stabilizing gain intervals versus any delay of the process.

In the third part of the thesis, the aforementioned problem for a bi-proper process is investigated. A bi-proper process is rare but causes great

complication for the method, due to the new phenomena that do not exist for a strictly proper process, such as a non-zero gain at infinity frequency, which may cause infinite intersections of boundary functions within a finite delay range. A detail study into the properties of boundary functions from such processes shows that finite boundary functions are sufficient to determine all stable regions for finite parameter intervals. The formula is given for calculating this number. Moreover, the algorithms are established to find exact stabilizing gain and delay ranges, and they are illustrated by many kinds of processes including stable/unstable poles and minimum/non-minimum zeros. These new results, together with those in the previous part, provide a complete solution for numerical parameterization of stabilizer for a general delay SISO process in terms of proportional control gain and delay.

Finally, the graphical method is also extended to two-input two-output processes with time delay. For those processes with fixed coefficients, an effective method is suggested to exactly compute the loop gain margins. For a class of systems with time-varying delay, the common gain ranges can be obtained. The proposed graphical method for parameterized processes can be used for any process with a square transfer function.

# List of Tables

# List of Figures

# Chapter 1

# Introduction

## 1.1. Motivation

The Proportional-Integral-Derivative (PID) controllers are widely implemented in industrial application because of their simple structure and reasonable robustness to system uncertainties [1]. Despite its popularity in applications as well as in theory studies, the problem of determining the stabilizing regions in the PID's parameter space is still a hard topic that gets a lot of attention. D-decomposition technique [2], [3] is one of the most popular tool that is employed to obtain stability boundary in the controller's parameter plane. In [4]–[6], this technique was applied to determine the stability boundary in the 3D space $(K_p, K_i, K_d)$ and find the stable regions of such space. However, the stabilizing graph produced by this approach is difficult to visualize. Another approach in employing D-decomposition technique is to fix one parameter of the controller and consider the stabilizing problem with the other two variable gains [7], [8]. This approach produces a 2D stabilizing graph with stability boundary curves which are easy to display. Obviously, the limitation of this method is the fixed parameter which reduces the size of stabilizing controller gain set. Thus, our motivation in this thesis is to develop a method to eliminate this restriction while maintaining the advantage of the 2D visualization.

Time delay is present in many practical processes, mainly due to transport and propagation phenomena of their inner dynamics [9]–[11]. In most cases,

they are small and ignorable. But when they are significant, they could be sources of instability and oscillation that would lead to poor system's performance. Thus, a time-delay is usually regarded as negative and undesirable effect in control applications. Stability analysis and stabilization for processes with time delays have attracted a lot of attention in control community. Delay-range dependent stability has been addressed extensively in the last decade. In [12]–[16], the free-weighting matrices technique was employed to study time-delay dependent stability conditions and to provide less conservative stability analysis of time delay processes. However, these methods do not tell the exact stabilizing parameter regions. To design stabilizer and controller for delay processes, time delay compensation is a popular choice. A well known control scheme is Smith Predictor (SP) [17]. Note that the SP uses the full model of the process. Thus, the SP control system is not internally stable if the process is unstable, and the use of SP is limited to only stable processes [18]. Many modified SP structures have been proposed to overcome this limitation [19]–[23]. Finite spectrum assignment has also been employed to stabilize unstable processes with time delay [24], [25].
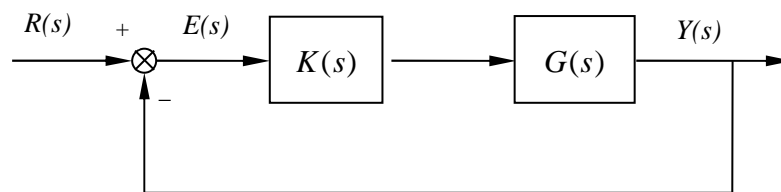


Figure 1.1: Unity output feedback control system.

Because of the dominance of PID controller in the industrial world, this class of controller has been employed widely to stabilize and control time delay processes as well. Consider the unity output feedback system in Figure

1.1, in the context of stabilization, the early studies focused on the simple normalized first-order plus delay model:

$$G(s) = \frac{1}{s-1} e^{-Ls},$$

where $L > 0$ is the equivalent dead time. Great efforts were made to find controller gain ranges in terms of time delay. For P control, $K(s) = k$, the necessary and sufficient condition is $L < 1$. For other types of PID controllers, two or three parameters are involved. The D-decomposition method was introduced to identify the stability domain in space of controller parameters [8], [26], [27]. The stability boundary is obtained by solving the transcendental characteristic equation with regard to two chosen parameters while the third is gridded. The Hermite-Biehler theorem was employed to study quasi-polynomials and determine the range of stabilizing gains [28]–[30].

It is noted that many industrial processes cannot be well approximated as first-order processes. Thus, stabilizing high-order and more complex processes is necessary. Recently, Xiang et al. [31] obtained stabilizability conditions on delay ranges for second-order unstable delay processes without any zero by P, PI, PD and PID controllers using the Nyquist criterion. This work was extended to all-pole unstable delay process in Lee et al. [32], unstable first-order plus delay process with a zero in [33] and an unstable delay process of higher-order and zero dynamics in [34]. The types of normalized processes and respective stabilizability conditions are summarized in Table 1.1. One can see that these analytical sufficient and necessary stabilizability conditions are available for limited classes of processes. To the best of our knowledge, stabilization of a general SISO process with any delay range and right half plane poles and/or zeros remains as an open problem.

Table 1.1: Stabilizability results for unstable SISO delay processes

| Process | P/PI | PD/PID |
|---|---|---|
| $\dfrac{1}{s(s-1)\prod_{k=1}^{n}(T_k s+1)}e^{-L}$ | None | $L<1-\sum_{k=1}^{n}T_k$ |
| $\dfrac{1}{(s-1)\prod_{k=1}^{n}(T_k s+1)}e^{-Ls}$ | $L<1-\sum_{k=1}^{n}T_k$ | $L<\sqrt{1+\sum_{k=1}^{n}T_k^2}+1-\sum_{k=1}^{n}T_k$ |
| $\dfrac{\alpha s+1}{(s-1)\prod_{k=1}^{n}(T_k+1)}e^{-Ls}$ | Necessary condition<br><br>$L<\sqrt{1+\sum_{k=1}^{n}T_k^2}-\sum_{k=1}^{n}T_k+1$<br><br>$\alpha>-1$<br><br><br>Sufficient condition<br><br>$-1<\alpha<\sqrt{1+\sum_{k=1}^{n}T_k^2},$<br><br>$L<\alpha+1-\sum_{k=1}^{n}T_k$ | Necessary condition<br><br>$-L^3+3L^2\left(1-\sum_{k=1}^{n}T_k\right)+$<br><br>$+6L\left(\sum_{k=1}^{n}T_k-\sum_{k\neq j}T_jT_k\right)$<br><br>$+6\sum_{k\neq j}T_jT_k-6\sum_{j\neq i,k\neq i,k\neq j}T_iT_jT_k>0$<br><br>Sufficient condition<br><br>$\lvert\alpha\rvert<\sqrt{1+\left(\sum_{k=1}^{n}T_k^2\right)-\min(T_k^2,1)},$<br><br>$L<\sqrt{1+\left(\sum_{k=1}^{n}T_k^2\right)-\beta^2}+\alpha-\sum_{k=1}^{n}T_k+1,$<br><br>$\beta^2\triangleq\min\{\sum_{i=1}^{p}\delta_i^2\mid \delta_i\in(T_k,1),p\leq n,\beta^2\geq\alpha^2\}.$ |

In the view of the above observations, we are motivated to address in this thesis the stabilization of a general delay process by proportional controller and to provide a complete solution in first for a strictly proper process and

then for a bi-proper process.

Even though bi-proper processes are less popular in industry, such processes may be found in practices such as missiles [35] and robotic processes [36]. Thus, they should be addressed for general applicability and completion of the method. Such extension of method occurred to complementary root locus method [37] which solely studied root locus for a bi-proper process. Note that the generalization from a strict proper case to a bi-proper case is not trivial for our method that is developed for strictly proper processes.

If $G_0(s)$ is a strict proper transfer function, its gain eventually reduces to zero, i.e. $\lim_{\omega \to \infty} |G_0(j\omega)| = 0$, and its Nyquist plot ends at the origin. $kG_0(s)e^{-Ls}$ will always go to the origin at $\omega = \infty$ for any finite value of $k$, regardless of $L$.

The point at $\omega = \infty$, therefore, does not affect closed-loop stability, and can be excluded from stability analysis. This will significantly simplify technical development of the method developed in Chapter 3.

On the other hand, bi-proper process has a non-zero finite gain at infinity frequency. As a result, this will create more new scenarios to consider, such as monotonic gain increase, and infinite encirclements of the critical point by Nyquist curve of a delay process. The most challenging issue is that there are infinite boundary functions within a limited delay range. It is impossible to draw and thus infer stability regions, whereas it is shown that finite boundary functions are sufficient to determine stability region for a strictly proper case.

An industrial control problem could involve a single-input single-output (SISO) process or multi-input multi-output (MIMO) process. Thus, we are

motivated to extend the stabilizing results to MIMO processes. Determining loop stability margins for a two-input two-output (TITO) process is one of the challenging problem that we will investigate in this thesis. Stability margin problem for SISO and MIMO processes have been studied extensively in [38]–[42]. However, these methods are either not applicable for independent and simultaneous gain changes of decentralized controller or conservative in estimating these ranges. Recently, Wang et al. [43] employed a quasi-LMI technique to compute the stabilizing parameter ranges of a decentralized proportional controller for a MIMO process. Wang used rectangular subset of these controller gain regions to form the suitable gain margins. However, that region did not reflect the exact or maximum region available due to the conservativeness of LMI framework. Besides, the method could not be applied directly without rational approximation to time delay if the process has time delay. To relax the conservativeness, Nie et al. [44] presented a frequency approach to compute exact stabilizing gain margins of a MIMO process, where they converted stability condition in frequency domain to some constrained optimization using vector mapping method. An algorithm which implements the Lagrange multiplier and Newton-Raphson iteration was then developed to solve the optimization problem. This approach proposed the nominal stabilization for unity gain so that the algorithm would stop when the gain solutions form a closed region including unity gain. This method required many iterations for each frequency to find the stability boundaries. For a TITO process, Nie et al. [45] showed that each point on stability boundaries was the intersection of some constructed curves. Thus, to reduce the computational effort, they employed the geometric analysis to find those points. In [46],

Gryazina and Polyak extended D-decomposition method [47] to TITO process to find the stable region in the controller's parameter space with the state space method for delay-free processes. In this thesis, we will develop a graphical method to compute the stabilizing gain ranges of a decentralized proportional controller for a linear time invariant TITO process. The problem of finding stabilizing loop gain and delay is also extended to TITO process with varying common delay.

## 1.2.  Contributions

In this thesis, stabilizing parameterizations for uncertain delay processes are investigated. A method is developed by using stability boundary bands to find PID stabilizing parameterization. For strictly proper processes with uncertain time delay in feedback configuration, we present an approach to determine the stabilizing controller gain and process delay ranges. The work is then extended to bi-proper processes. Finally, we show the application of our stabilizing parameterization method to MIMO processes. In particular, the thesis has investigated the following areas:

**A. Parametric Approach to Computing Stabilizing PID Regions**

For a general process with/without time delay, a method is presented to obtain stabilizing PID parameter ranges. By extending the stability boundary concept to the parameterized stability boundary band, the stabilizing region in $(K_p, K_i)$ plane while $K_d$ varies in a range is obtained. For a process with monotonic $\lambda(\omega)$, the entire stabilizing ranges of three parameters of PID controller are given. For process with non-monotonic $\lambda(\omega)$, root locus for $K_d$ is used to find stabilizing range of $K_d$ in all possible conditionally stable

regions.

**B. Stabilizing Loop Gain and Delay for Strictly Proper Processes**

A graphical method is developed to compute the exact stabilizing gain and delay ranges for a strictly proper process. This is achieved by determining the boundary functions which may change system's stability. To effectively reduce the infinite number of boundary curves due to the delay, properties of these curves are investigated thoroughly. It will greatly helps to simplify the stability determination of the resulting regions. As a result, all stable regions can be identified and stabilizing gain ranges can also be obtained in term of delay.

**C.   Stabilizing Loop Gain and Delay for Bi-proper Processes**

The D-decomposition method for computing stabilizing loop gain and delay ranges is extended to the case of bi-proper processes. Properties of boundary functions from such processes will be investigated in great details. It has been shown that finite boundary functions are sufficient to determine all stable regions for finite parameter intervals. The formula is given for calculating this number. Moreover, the algorithms are established to find exact stabilizing gain and delay ranges, and they are illustrated by many kinds of processes including stable/unstable poles and minimum/non-minimum zeros. These new results, together with those for strictly proper processes, provide a complete solution for numerical parameterization of stabilizing loop gain and delay for a general delay SISO process.

**D.   Stabilizing Loop Gain and Delay for MIMO Processes**

For a TITO process with fixed time delay, we propose a method to

compute the stabilizing gain ranges of a decentralized proportional controller for a linear time invariant (LTI) two-input and two-output (TITO) system. Firstly, this method will determine all possible stability boundaries. These boundaries divide the gain plane to regions and the stability of each region is checked to identify the stable ones. Subsequently, the loop gain margins as well as controller integrity are obtained from these stable regions. The proposed method is simple and easy to apply and no iteration is required for computing stability boundaries. For MIMO processes that are represented by square transfer functions that with common varying time delay, and by employing the characteristic locos approach, the common gain stabilizer is given in term of the delay.

## 1.3. Organization of the thesis

This thesis is organized as follows. Chapter 2 presents a method to find PID stabilizing region in controller parameters plane. Chapter 3 deals with the problem of determining the stabilizing controller gain and process delay ranges for a general delay process in feedback configuration. In Chapter 4, the aforementioned problem for a bi-proper process is investigated. Finally, the graphical method is also extended to two-input two-output processes with time delay in Chapter 5. In Chapter 6, general conclusions are drawn and expectations for further works are suggested.

# Chapter 2

# Parametric Approach to Computing Stabilizing PID Regions

## 2.1. Introduction

The Proportional-Integral-Derivative (PID) controllers are widely implemented in industrial application because of their simple structure and reasonable robustness to system uncertainty [1]. Despite its popularity in application as well as in theory studies, the problem of determining the stabilizing region in PID parameters space is still a difficult topic that still gets a lot of attention. D-decomposition technique [2], [3] is one of the most popular tool to obtain stability boundary in controller parameter plane. In [4]–[6], this technique was applied to determine the stability boundary in the 3D space $(K_p, K_i, K_d)$ and find the stable regions of such space. However, the stabilizing graph produced by this approach is difficult to visualize. Another approach in employing D-decomposition technique is to fix one parameter of the controller and consider the stabilizing problem with the other two variable gains [7], [8]. This approach produces a 2D stabilizing graph with stability boundary curves which are easy to display. Obviously, the limitation of this method is the fixed parameter which reduces the size of stabilizing controller gain set.

In this chapter, we eliminate this restriction while maintaining the advantage of the 2D method. We extend the stability boundary concept to the

parameterized stability boundary, which is a band, when one of the controller gains varies in a range. The rest of the chapter is organized as follows. Section 2.2 presents our problem formulation and preliminaries about the D-decomposition method for the normal case of 2 controller parameters. The general approach for simple processes is studied in Section 2.3. In Section 2.4, a solution for a complicated process is given. Finally, Section 2.5 draws the conclusions.

## 2.2. Problem Formulation and Preliminaries

Consider the unity output feedback system shown in Figure 1.1, where $G(s)$ is the process with the transfer function,

$$
\begin{aligned}
G(s) &= \frac{N(s)}{D(s)} e^{-Ls} \\
&= \frac{b_m s^m + b_{m-1} s^{m-1} + \ldots + b_1 s + b_0}{a_n s^n + a_{n-1} s^{n-1} + \ldots + a_1 s + a_0} e^{-Ls},
\end{aligned}
\tag{2.1}
$$

where $n > m$; and $K(s)$ is the analytical PID controller,

$$
K(s) = K_p + \frac{K_i}{s} + K_d s \quad,
\tag{2.2}
$$

where $K_p$ and $K_i$ and $K_d$ are real numbers and stand for the integral, proportional and derivative gains, respectively. Our objective here is to determine the gain ranges of all the three controller parameters, $K_p$ and $K_i$ and $K_d$, such that, when $K_p$ and $K_i$ and $K_d$ varies simultaneously within these ranges, the closed-loop system is stable.

The characteristic quasi-polynomial of the PID feedback control system is

$$
1 + K(s)G(s) = 0.
\tag{2.3}
$$

or

$$s\left(a_n s^n + a_{n-1} s^{n-1} + \ldots + a_1 s + a_0\right) +$$
$$+\left(K_p s + K_i + K_d s^2\right)\left(b_m s^m + b_{m-1} s^{m-1} + \ldots + b_1 s + b_0\right)e^{-Ls} = 0 \tag{2.4}$$

The roots of the above polynomial, or the poles of the closed-loop, are functions of gains, $K_p$, $K_i$ and $K_d$. According to the D-decomposition technique [2], the following three conditions characterize the stability boundaries in term of $K_p$, $K_i$ and $K_d$.

1) The characteristic equation has roots that cross the imaginary axis at infinity. This condition determines the infinity roots boundary (IRB). It follows from [2] that this boundary exits if and only if $m = n-1$ and $K_d = -b_n / a_m$.

2) The characteristic equation has roots that cross the imaginary axis at zero. This condition determines the real root boundary (RRB) which is the straight line $K_i = 0$ [2]. From [5], for $K_p > -a_0 / b_0$, the regions above the line $K_i = 0$ have one more stable pole than their neighbors that are below the line $K_i = 0$; for $K_p < -a_0 / b_0$, the regions above the line $K_i = 0$ have one less stable pole than their neighbors that are below the line $K_i = 0$.

3) The characteristic equation has roots that cross the imaginary axis at finite frequency $s = j\omega$ where $\omega \neq 0$. This condition determines the complex root boundaries (CRB).

Obviously, the above cases 1) and 2) are trivial, and our focus will be on 3) from now on. The complex root boundaries are obtained by solving the characteristic equation with $s = j\omega$, where $\omega \neq 0$, that is,

$$1 + K(j\omega)G(j\omega) = 0,$$

which can be rewritten as

$$K_p + \frac{K_i}{j\omega} + j\omega K_d = -G^{-1}(j\omega).$$  (2.5)

With $K_d$ as a parameter, (2.5) is solved for $K_p$ and $K_i$ as:

$$
\begin{aligned}
K_p &= -\mathrm{Re}\left[G^{-1}(j\omega)\right], \\
K_i &= K_d\omega^2 + \omega\,\mathrm{Im}\left[G^{-1}(j\omega)\right],
\end{aligned}
$$  (2.6)

where $\mathrm{Re}\left[G^{-1}(j\omega)\right]$ and $\mathrm{Im}\left[G^{-1}(j\omega)\right]$ are, the real part and imaginary part of $G^{-1}(j\omega)$, respectively.

Suppose that $K_d$ is fixed, and the stability boundaries have only two parameters $K_p$ and $K_i$ only, then this case becomes a problem of stabilization using PI controller, a standard 2D case. In such a case, one can plot all the stability boundaries in the parameter space and then determine the number of unstable poles in each resulting regions to find the stabilizing one [2].

For efficiently determining the number of unstable poles in each region, the Jacobian of the characteristic function is employed to establish which side of the stability boundaries has more unstable poles. Jacobian, $J$, is the determinant of the matrix of all first-order partial derivatives of the characteristic function and given by

$$
J = \begin{vmatrix}
\mathrm{Re}\dfrac{\partial f(\omega)}{\partial K_p} & \mathrm{Im}\dfrac{\partial f(\omega)}{\partial K_p} \\
\mathrm{Re}\dfrac{\partial f(\omega)}{\partial K_i} & \mathrm{Im}\dfrac{\partial f(\omega)}{\partial K_i}
\end{vmatrix},
$$

where

$$f(s) = s + \left(K_p s + K_i + K_d s^2\right)G(s),$$  (2.7)

It describes the amount of rotating to transform from the complex plane to the $(K_p, K_i)$ plane. Thus, the sign of its determinant dictates which side of the boundary curves corresponds to the left half plane. To determine the stable regions, the side corresponding to the left half plane of all boundary curves will be shaded. If $J < 0$, the region on right side of the boundary curve, facing direction in which $\omega$ increases, corresponds to the left half plane of the complex plane, and thus, has fewer unstable poles. If $J > 0$, the region on right side of the boundary curve, facing direction in which $\omega$ increases, corresponds to the right half plane of the complex plane, and thus, has more unstable poles. It follows from [48] that when $J = 0$, there may be a line to be plotted on the parameter space. Such a line is shaded so that it can be consistent with the boundary curve for which $J$ changes sign. Since the coefficients of the characteristic equation are real numbers, if $j\omega$ is a root, then $-j\omega$ is also a root of the characteristic number. Thus, when one moves from one side of the CBR to another side, the number of unstable poles increases or decreases by 2.

In our case (2.5), the determinant of the Jacobian is calculated as follows:

$$J = \begin{vmatrix} -\omega \operatorname{Im}[G(j\omega)] & \omega \operatorname{Re}[G(j\omega)] \\ \operatorname{Re}[G(j\omega)] & \operatorname{Im}[G(j\omega)] \end{vmatrix} = -\omega |G(j\omega)|^2$$

For $\omega > 0$, $J < 0$ so in the plane $(K_p, K_i)$, the regions on the right of the boundary curve defined by (2.6) in direction of increasing $\omega$ have two fewer RHP poles than the region on the left. We shade the right hand side of the boundary curve. Since the curve defined by (2.6) decomposes the plane

$(K_p, K_i)$ into several regions with invariant number of RHP poles [2], [3], and with help from the shading rules above, if the number of RHP poles in one region is known, the number of RHP poles of other regions can also be found by inspection. Let the reference region to be the most left region to the point $(-b_0 / a_0, 0)$ and the number of RHP poles of the reference region be $P^+$, we are able to display the number of RHP poles of all other regions. The stable regions (if any) must be with the fewest number of RHP poles. Therefore, to find the stable regions, we only need to verify if the fewest number of RHP poles is zero.

**Example 2.1**. For illustration, consider the hydro-turbine governing system [7] which has the transfer function as follows,

$$G(s) = \frac{1.313 - 0.2935s}{2.79s^3 + 20.7949s^2 + 6.52s + 0.5} . \tag{2.8}$$

For a fixed $K_d = 0$, there is one single CRB curve as seen in Figure 2.1. The arrow along the boundary curve indicates the direction in which $\omega$ increases. This curve and the line $K_i = 0$ divide the plane into 4 regions. Next, we shade these regions using shading rule and show the number of unstable poles on them, respectively, as in Figure 2.1.
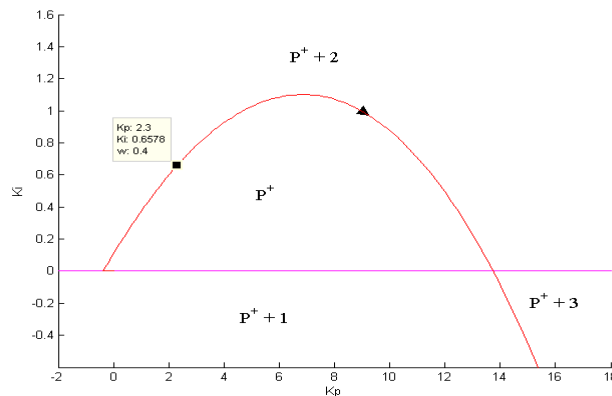


Figure 2.1: D-graph for Example 2.1 with $K_d = 0$

It is seen that the region with $P^+$ number of unstable poles has the fewest number of unstable poles. It follows from the Nyquist criteria for stability test that $P^+ = 0$. Thus, this region is stable.

## 2.3. The Proposed Method

Suppose that $K_d$ varies, and now we are facing a 3D problem essentially. Note that $K_d$ is always upper-bounded in practice due to engineering and implementation constraints. A high value of $K_d$ may damage the actuator and shorten its life if there is significant measurement noise [49]. Thus, $K_d$ usually ranges in $\left[ 0, \bar{K}_d \right]$, where $\bar{K}_d$ should be given based on engineering consideration. For the generality of our method, let $K_d$ be in the range of $\left[ \underline{K}_d, \bar{K}_d \right]$.

Taking a frequency $\omega$ for consideration, this $\omega$ corresponds to a fixed point in the boundary curve when $K_d$ is fixed. When $K_d$ varies in the range of $\left[ \underline{K}_d, \bar{K}_d \right]$, this point sweeps a vertical straight line between two ending points which correspond to $\underline{K}_d$ and $\bar{K}_d$ according to (2.6). For the process in **Example 2.1**, when $K_d$ varies in $\left[ 0,1 \right]$, the point corresponding to $\omega = 0.4$ maps to the straight line with two ending points $(K_p, K_i) = (2.3, 0.6578)$ and $(K_p, K_i) = (2.3, 0.8178)$ as shown in Figure 2.2. When frequency $\omega$ varies, such a vertical straight line moves with two ending points corresponding to $K_d = \underline{K}_d$ and $K_d = \bar{K}_d$, respectively. See Figure 2.2 for a few discrete frequencies. All other boundary curves with other values of $K_d$ are neatly laid one after another inside two extreme curves.

Note that the closer $K_{d1}$ is to $K_{d2}$, the closer the corresponding curves to each other; but they are always different at each frequency unless $K_{d1} = K_{d2}$. This can be easily verified by (2.6) as $K_d$ appears there linearly. Please note that here we compare $K_d$-curves pointwise in terms of the same frequency; that means for those ones with the same frequency, the curves with different $K_d$ are different and they sit neatly next to each other. It should not be confused with our later discussion on intersection of curves at different frequencies, where it is shown that one $K_d$-curve may intersect with itself or others at two different frequencies.
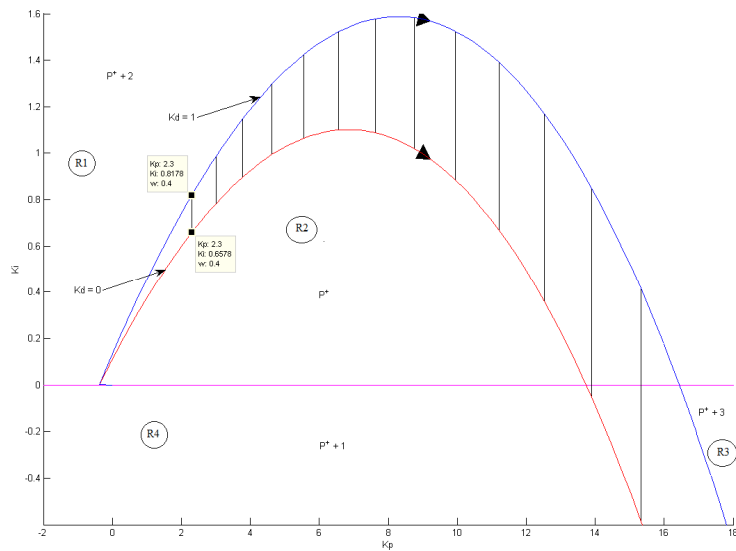


Figure 2.2: D-graph for Example 2.1c with $K_d$ in $[0,1]$

For the entire $\omega \in (0, \infty)$, the above vertical line sweeps a band. It is upper and lower bounded by two extreme boundary curves in the normal 2D sense with regard to $K_p$ and $K_i$, where $K_d$ is fixed at $K_d = \underline{K}_d$ and $K_d = \overline{K}_d$, respectively. We call such a band a boundary band. Drawing a

boundary band is to draw the following two extreme boundary curves, firstly

$$K_p = -\mathrm{Re}\left[ G^{-1}(j\omega) \right],$$
$$K_i = \underline{K}_d \omega^2 + \omega \mathrm{Im}\left[ G^{-1}(j\omega) \right],$$
(2.9)

and secondly,

$$K_p = -\mathrm{Re}\left[ G^{-1}(j\omega) \right],$$
$$K_i = \overline{K}_d \omega^2 + \omega \mathrm{Im}\left[ G^{-1}(j\omega) \right].$$
(2.10)

The band characteristics can vary with the process properties and $K_d$ range, and they cause a great difference in our stability analysis. We first consider the simple case of no band intersection in the rest of this section, while the intersection case is very complex and will be addressed in the next section. The band is said to have no intersection if any two boundary curves in the band corresponding to $K_{d1} \in \left[ \underline{K}_d, \overline{K}_d \right]$ and $K_{d2} \in \left[ \underline{K}_d, \overline{K}_d \right]$, respectively, do not intersect (neither self-intersection nor cross-intersection). The mathematical condition for no band intersection will be given in the next section and can be checked before the relevant technique for stability analysis in this section is applied.

For the rest of this section, we only discuss about the case of no band intersection, where each boundary curve inside the band moves in the same way as any other boundary curve inside it. We can view the band like a normal boundary curve when it is from outside of the band. Thus, like a fixed $K_d$ case, the boundary band cuts the plane $(K_p, K_i)$ into several regions. Note that in our definition, these regions are formed from the band excluding the boundary band itself. We will discuss stability of regions and bands separately.

**Example 2.2**. For illustration of the simple case, we consider a process

with the transfer function,

$$G(s) = \frac{1}{(s-1)(s+2)}.$$

The D-graph with $K_d$ varies in $[0,10]$ is showed in Figure 2.3. From Figure 2.3, the boundary band cuts the plane $(K_p, K_i)$ into $R1$, $R2$ and $R3$.

To investigate stability of the regions, the shading rules for a fixed $K_d$ with a boundary curve is adapted for the boundary band case as follows: instead of shading the right hand side of the boundary curve in direction of $\omega$ increase, we shade the right of the boundary band. If the line $K_i = 0$ is not inside the band, the region on the shaded side of the band has two fewer unstable poles than its neighbor on the other side. To search for the stable regions, we again count the number of RHP poles of all the regions, to find the regions with the fewest number of RHP poles, and verify if this number is zero. Since the boundary band does not overlap with any other band, a region is either stable or unstable for any value of $K_d$ in $\left[\underline{K}_d, \overline{K}_d\right]$. Thus, if a region of $(K_p, K_i)$ is stable based on the above procedure, it is stable for any $(K_p, K_i)$ in this region, when $K_d$ ranges in $\left[\underline{K}_d, \overline{K}_d\right]$. In Example 2.2, region $R2$ has the fewest number of unstable poles $P^+$; moreover, with $P^+ = 0$, this region is stable for $K_d \in [0,10]$. This means that for any $(K_p, K_i, K_d)$ where $(K_p, K_i) \in R2$ and $K_d \in [0,10]$, the corresponding PID controller can stabilize the process.

We now study stability of the boundary band based on the number of unstable poles of its two neighbor regions as following: Suppose the neighbor region on the right side of the band is stable. Without loss of generality, we

may consider any stable region and let the boundary curve for $\underline{K}_d$ be a boundary for this region (implying that the boundary curve for $\bar{K}_d$ does not touch this region). Note that for each interior point in the band, there are explicitly a pair of $(K_p^*, K_i^*)$ from the readings of coordinates and implicitly a value $K_d^* \in \left[ \underline{K}_d, \bar{K}_d \right]$, which is found by inverting (2.6) as

$$K_d^* = \frac{-\omega^* \operatorname{Im}\left[ G^{-1}(j\omega^*) \right] + K_i^*}{(\omega^*)^2}. \tag{2.11}$$

For this value of $K_d^*$, there would be a corresponding boundary curve if we draw for this $K_d^*$. Then, the contracted band is bounded by this new boundary curve for $K_d^*$ in place of the previous $\underline{K}_d$ and the one for $\bar{K}_d$ is the same as before. The region previously touching $\underline{K}_d$-curve now extends to those touching $K_d^*$-curve. The new band acts in the same way as the previous band in terms of stability analysis. It follows from the same argument like before that the region touching $K_d^*$-curve is stable with regard to the new range of $K_d$, $\left[ K_d^*, \bar{K}_d \right]$, implying that any point in this region with their PI values will stabilize the process for the sub-range of $\left[ K_d^*, \bar{K}_d \right]$. Therefore, we conclude that for each interior point at $(K_p^*, K_i^*)$ in the band next to a stable region, the underlying closed-loop system is conditionally stable for a sub-range, either $\left[ K_d^*, \bar{K}_d \right]$ when the curve $\underline{K}_d$ touches the stable region, or $\left[ \underline{K}_d, K_d^* \right]$ when otherwise. We call such a boundary band a conditionally stable region. Now, suppose the neighbor region on the left side of the band has exact two unstable poles, then with similar analysis as above, portion of band that is next

to it is also conditionally stable. The range of stabilizing $K_d$ is $\left[\underline{K}_d, K_d^*\right]$ when the curve $\underline{K}_d$ touches the left side region, or $\left[K_d^*, \bar{K}_d\right]$ if otherwise. In any other case, i.e. the neighbor region on the left has more or less than two RHP pole or the neighbor region on the right has more than zero RHP poles, the portions of boundary band next to them are unstable. Look at the Example 2.2, the boundary band that is next to region $R2$ and $R1$ is conditionally stable. In Figure 2.3, the stable region is marked in green and the conditionally stable region grey.

Please note our terms of stability and conditional stability. In our context of PID stabilization, a $K_d$ range is prescribed based on practical consideration. We study stabilization of the process by such a PID with $K_d$ in that range. Thus, regions are stable or unstable, or unconditionally stable, for all values of $K_d$ in this range. On the other hand, some band is conditionally stable or unstable only for some subsets of $K_d$.
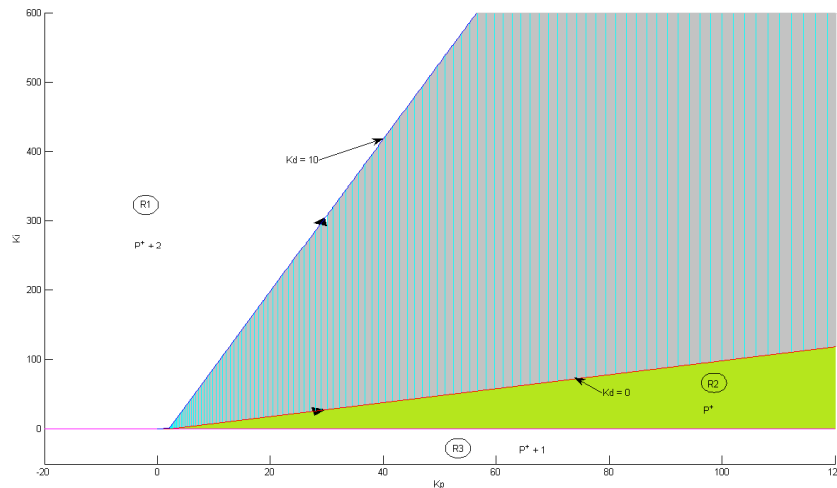


Figure 2.3: D-graph for Example 2.2 with $K_d$ in $[0,10]$

The above analysis is summarized as follows.

**Procedure 2.1 .** Determine the stabilizing PID regions in the case of no band intersection.

Step 1. Plot the straight line $K_i = 0$ on the plane $(K_p, K_i)$, then shade the region above the line for $K_p > -a_0 / b_0$ and the region below the line for $K_p < -a_0 / b_0$.

Step 2. Plot the boundary band with (2.9) and (2.10), and shade the region on the right of the boundary band.

Step 3. Count the number of RHP poles of regions.

Step 4. Look for the regions with the fewest number of RHP poles (they are only possibly stable regions). Check their stability (check stability of one point for each region).

Step 5. The portions of boundary band on the left of the stable regions and on the right of regions with two RHP poles are conditionally stable regions.

**Example 2.2c.** Consider the PID control of the process with transfer function,

$$G(s) = \frac{1}{(s-1)(s+2)},$$

if $K_d$ lies in $[0,10]$, this process is unstable with 1 RHP pole at $s=1$. Step 1 yields the straight line $K_i = 0$ in the plane $(K_p, K_i)$ (Figure 2.3). In Step 2, the boundary band is plotted and shaded on the right side. In Step 3, the number of unstable poles of all resulting region with regard to the reference regions are counted. These number is displayed in Figure 2.3. In Step 4, it turns out that region shaded in green has the fewest number of RHP poles which is $P^+$. Subsequently, a point in the green region which has coordinate

as $(K_p, K_i, K_d) = (3, 0.1, 0.5)$ is selected to check the region stability. The corresponding Nyquist plot has one counter-clockwise encirclement of the critical point, which means the closed-loop system is stable (Figure 2.4). Thus, the region marked in green is the stable region for $K_d \in [0,1]$ (Figure 2.3). The region marked in grey is the conditionally stable region, that is, for any point in such region, the range of stable $K_d$ must be calculated with (2.11). For example, for $(K_p, K_i) = (10, 10)$, $K_d^*$ is calculated to be $K_d^* = 0.255$. The stable range of $K_d$ for $(K_p, K_i) = (10, 10)$ is $K_d \in [0.255, 10]$.
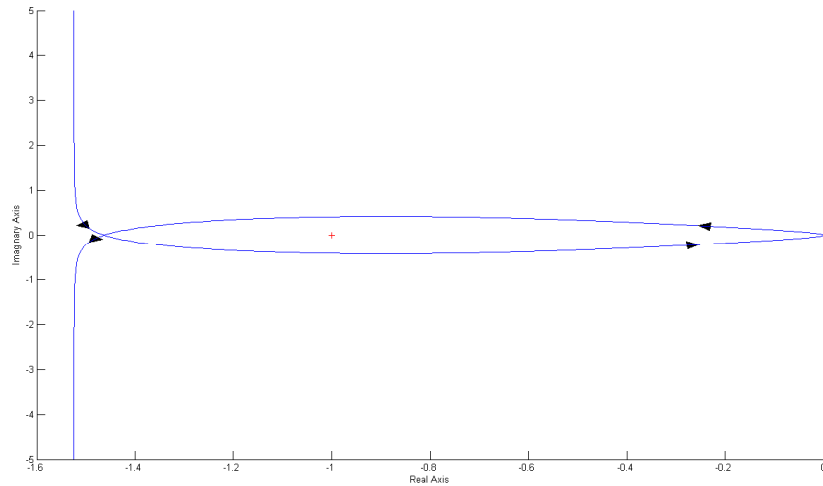


Figure 2.4: Nyquist plot for Example 2.2c.

**Example 2.3.** Consider PID control of the following process [5]

$$G(s) = -\frac{s+2}{(s-1)(s-2)}$$

Suppose $K_d$ in $[0,5]$, this process has 2 unstable poles at $s = 1$ and $s = 2$. Note $m = n - 1$, so there is IRB at $K_d = 1$. Thus, we can divide the range of $K_d$ into two intervals. Consider the first interval, $[0,1)$, the D-graph is given in Figure 2.5, which has no band intersection. It follows from Procedure 2.1

that the stable region is obtained and marked in green and the conditionally stable region in grey. For the second interval, $[1,5]$, Procedure 2.1 produces Figure 2.6.
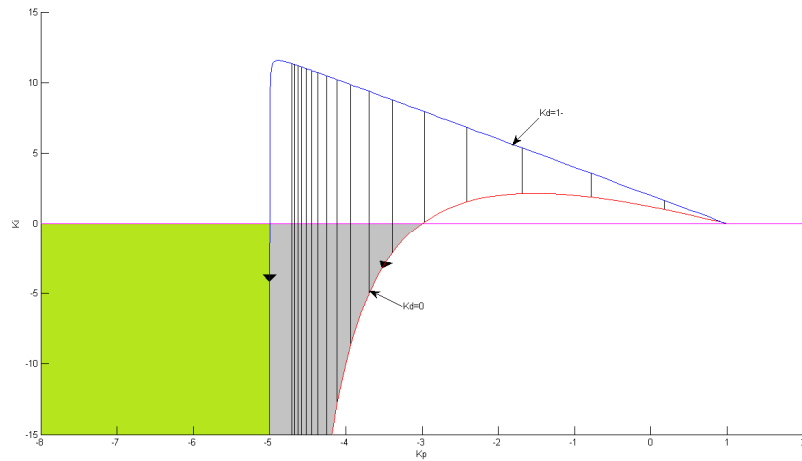


Figure 2.5: D-graph for Example 2.3 with $K_d$ in $[0,1)$.
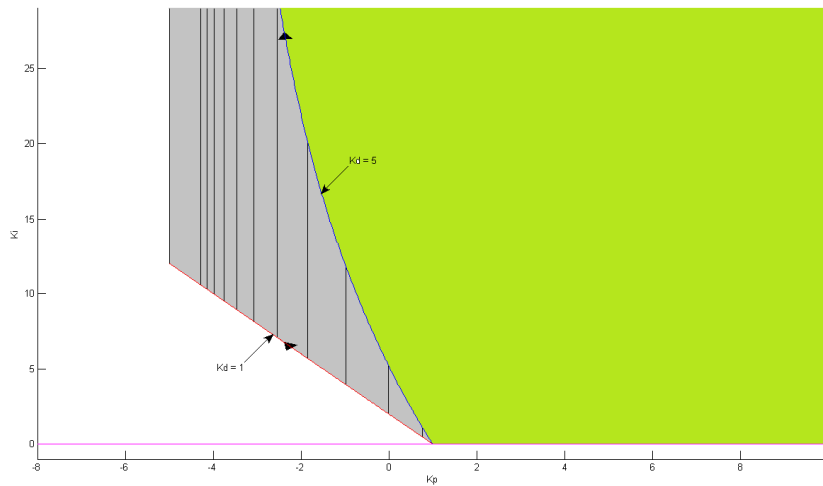


Figure 2.6: D-graph for Example 2.3 with $K_d$ in $[1,5]$.

## 2.4. Band Intersections

Complications occur when the boundary band intersects with itself causing difficulty in stability analysis. This will be illustrated as following:

**Example 2.1c,** we continue **Example 2.1** with the range of $K_d$ in $[0,100]$. Take a look at three cases of $K_d$ with ranges of $[0,1]$, $[0,50]$ and $[0,100]$, for which the boundary bands are exhibited in Figures 2.2, 2.7 and 2.8, respectively. Let the first part of the boundary band to be a part corresponding to $\omega \in [0,3.68)$ and the second part to be the part corresponding to $\omega \in [3.68, \infty)$. These cases show band intersections, as soon as $\bar{K}_d$ increases, the second part of the boundary band covers the first part of the band. The reason is: for $K_d > 70.85$, the $K_d$-boundary curve no longer moves in clockwise direction but in counter clockwise direction. This makes the second part of the band totally covering the first part of the band and the regions that are neighbor to the first part of the band become a part of the band. Thus, if the range of $K_d$ contain the value $K_d = 70.85$, when it moves from one side of the first part of the band to another side, the number of unstable poles is not simply change to two fewer or two more unstable poles.
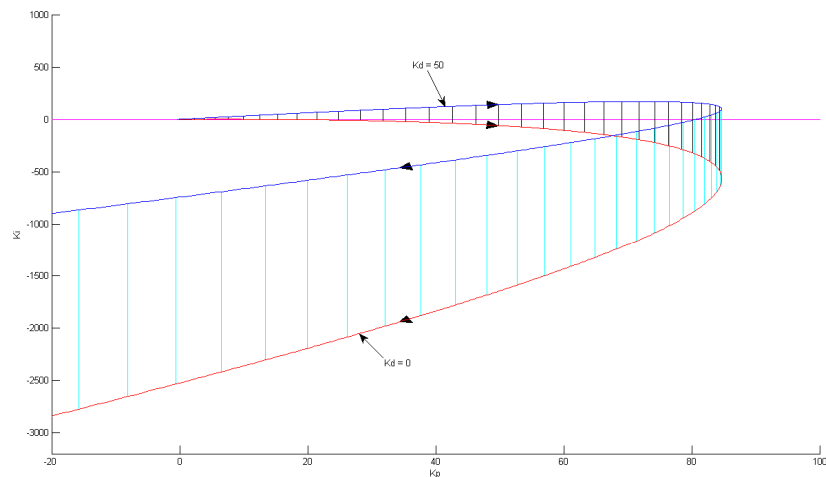


Figure 2.7: D-graph of Example 2.1cc with $K_d$ in $[0,50]$.
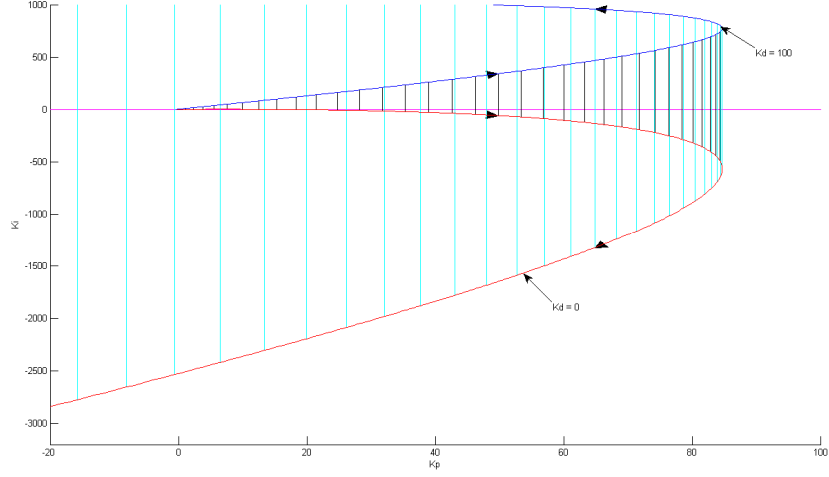
Figure 2.8: D-graph of Example 2.1cc with $K_d$ in [0,100].

The boundary band intersects if and only if two boundary curves in the band corresponding to two $K_{d1}$ and $K_{d2}$ which may or may not be equal, intersect with each other (which must be at two different $\omega_1$ and $\omega_2$). That means:

$$K_p(\omega_1) = K_p(\omega_2) \tag{2.12}$$

$$K_i(\omega_1, K_{d1}) = K_i(\omega_2, K_{d2}) \tag{2.13}$$

where $K_{d1} \in \left[ \underline{K}_d, \bar{K}_d \right]$, $K_{d2} \in \left[ \underline{K}_d, \bar{K}_d \right]$, $\omega_1$ not equal $\omega_2$ In view of (2.6), we define

$$K_p = -\text{Re}\left[ G^{-1}(j\omega) \right] = \frac{-\text{Re}\left[ G(j\omega) \right]}{\left| G(j\omega) \right|^2} =: \lambda(\omega) \tag{2.14}$$

Obviously, (2.12) cannot hold and no intersection of the boundary band can occur if $\lambda(\omega)$ is globally monotonic. The following lemma follows.

**Lemma 2.1**. A necessary condition for the band intersection is that $\lambda(\omega)$ is not monotonic.

In view of (2.7), we define

26

$$K_i = K_d \omega^2 + \omega \, \mathrm{Im}\left[ G^{-1}(j\omega) \right] := h(\omega, K_d) \tag{2.15}$$

Equations (2.12) and (2.13) are equivalent to

$$\lambda(\omega_1) = \lambda(\omega_2) \tag{2.16}$$

$$h(\omega_1, K_{d1}) = h(\omega_2, K_{d2}) \tag{2.17}$$

which involve 4 unknowns. Letting $K_{d1} = K_{d2} = K_d$ means that a single $K_d$-curve intersects with itself but not with other curves, and yields

$$\lambda(\omega_1) = \lambda(\omega_2) \tag{2.18}$$

$$h(\omega_1, K_d) = h(\omega_2, K_d) \tag{2.19}$$

with 3 unknowns, which have finite and usually few solutions only for each $K_d$. Such solutions give self intersection points of a particular curve corresponding to this $K_d$.

**Lemma 2.2**. A sufficient condition for band intersection is that (2.19) admits a solution for $K_d \in \left[ \underline{K}_d, \overline{K}_d \right]$.

It is crucial to find when there is band intersection. We want to reduce work of solving set of equations (2.16) and (2.17). Observe that by **Lemma 2.1**, or equation (2.16), we can plot $\lambda(\omega)$, and find possible range $\omega$ for which this equation holds, and denote it by $Q_1$. Moreover, in a real practice, physical processes likely restrict the controller parameters, for which the consideration range of $\omega$ can be upper-limited. Indeed, it follows from the very first equation, characteristic equation, (2.3), that

$$\left| G(j\omega) K(j\omega) \right| = 1,$$

which is violated by $\left| G(j\omega) K(j\omega) \right| < 1$, or by

$$\left| G(j\omega) K(j\omega) \right| \le \left| G(j\omega) \right| \left| K(j\omega) \right| \le \left| G(j\omega) \right| \sqrt{ \overline{K}_p^2 + \frac{\overline{K}_i^2}{\omega^2} + \overline{K}_d^2 \omega^2 + 2 \overline{K}_p \overline{K}_i } < 1.$$

where

$$A = \sqrt{\overline{K}_p^2 + \frac{\overline{K}_i^2}{\omega^2} + \overline{K}_d^2 \omega^2 + 2\overline{K}_p \overline{K}_i} \; ;$$

and $\overline{K}_p$, $\overline{K}_i$ are the maximum absolute values of $K_p$ and $K_i$, respectively.

Let

$$\alpha(\omega) = |G(j\omega)| A, \qquad\qquad (2.20)$$

observe that

$$\lim_{\omega \to \infty} \alpha(\omega) = 0,$$

thus, from some frequency $\overline{\omega}$, for $\omega > \overline{\omega}$ we have $\alpha(\omega) < 1$. Apparently, $\omega > \overline{\omega}$ is not in solution set of (2.16). This $\overline{\omega}$ can be obtained by graphical method by from plotting function $\alpha(\omega)$. This analysis gives the admissible set of frequencies denoted by $Q_2$. Because both conditions which we considered so far to get $Q_1$ and $Q_2$ are necessary, we can reduce search range for frequency to $Q_a = Q_1 \cap Q_2$. We can mark it on the plot of $\lambda(\omega)$.

Now, take a look at one interval of $Q_a$ at a time. Without loss of generality, suppose it is in $[\underline{\omega}_1, \overline{\omega}_1]$ where $\lambda(\omega)$ increases to $\omega_1^* \in [\underline{\omega}_1, \overline{\omega}_1]$ which reaches maximum $\lambda(\omega)$ and then decrease. Observe that for a fixed pair of $\omega_1 \in [\underline{\omega}_1, \omega_1^*]$ and $\omega_2 \in [\omega_1^*, \overline{\omega}_1, ]$, which forms a solution of (2.16), it follows from (2.17) that

$$K_{d2} = \frac{\omega_1^2}{\omega_2^2} K_{d1} + \frac{\omega_1 \operatorname{Im} G(j\omega_1)^{-1} - \omega_2 \operatorname{Im} G(j\omega_2)^{-1}}{\omega_2^2}, \qquad (2.21)$$

which represents a line in plane $(K_{d1}, K_{d2})$. Thus, solution of (2.17) can be found by drawing this line for $K_{d1} \in \left[ \underline{K}_d, \overline{K}_d \right]$ and find the intersection segment of it with square $K_{d1} \in \left[ \underline{K}_d, \overline{K}_d \right]$ and $K_{d2} \in \left[ \underline{K}_d, \overline{K}_d \right]$. Each point $(K_{d1}, K_{d2})$ that lies on the intersection segment is a solution of (2.17) for the corresponding $(\omega_1, \omega_2)$. This holds for any $\omega_1 \in [\underline{\omega}_1, \omega_1^*]$, hence, the complete solution of (2.16) and (2.17) are obtained by drawing all the lines corresponding to the range $[\underline{\omega}_1, \omega_1^*]$.

Note that if there is a sub-range $\left[ \underline{K}_d^{c1}, \overline{K}_d^{c1} \right]$ of $\left[ \underline{K}_d, \overline{K}_d \right]$ in which

there is no band intersection, the corresponding inner square $K_{d1} \in \left[ \underline{K}_d^{c1}, \overline{K}_d^{c1} \right]$

and $K_{d2} \in \left[ \underline{K}_d^{c1}, \overline{K}_d^{c1} \right]$ does not intersect with any of solution lines, and vice

versa. Let denote the set of all such sub-ranges $K_D^c$ and the complement of

$K_D^c$ in the $K_d$-range $K_D^s$. Please note that $K_D^s$ and $K_D^c$ may consist of

disjoint subsets. For $K_D^c$, we can use **Procedure 2.1** to find stable regions and

conditionally stable region. The main issue here is to study stability for $K_D^s$.

To this, there is further room for reduction. The band for such $K_D^s$ may not

intersect everywhere but only parts of it. When we solve (2.16) above, we also

get $\omega$ range, $Q_1$, which give $K_D^s$. In the band for $K_D^s$, the only portion of

intersection corresponds to $Q_1$. The other portions get no intersection and act

as band with no intersection.

Consider now the real complex case of intersecting portion of the band.

The band still cuts the plane to regions. We need to check stability of each

region to find stable ones. As for stability of band, for some intersection

portions corresponding to the range of frequency in $Q_a$, if the neighbor

regions $R_1$, $R_2$ are both unstable and all the portions has the same shaded

size toward $R_1$ or $R_2$, then these portions are impossible to be conditionally

stable. This further reduces the intersecting portions of the band to check for

stability. For other possible stable band portion, for any point in band, which

means a pair of fixed value $K_p$ and $K_i$, we can draw root locus for $K_d$ to

find the stabilizing range of $K_d$. From the characteristic equation (2.3) we

have:

$$1 + K_d \frac{sG(s)}{1 + \left( K_p + \dfrac{K_i}{s} \right) G(s)} = 0 .$$

Observe that the stabilizing range of $K_d$ can be obtained from drawing the

root locus corresponding to the modified process $\dfrac{sG(s)}{1+\left(K_p+\dfrac{K_i}{s}\right)G(s)}$. Notice

that our application is much simpler as the parameter range is limited to a

interval in $K_D^s$, not from 0 to infinity.

The above analysis is summarized as follows.

**Procedure 2.2 .** Determine the stabilizing PID regions in the case of band

intersection.

Step 1. Plot $\alpha(\omega)$ and $\lambda(\omega)$. Compute $Q_1$ from $\lambda(\omega)$ and $Q_2$ from

$\alpha(\omega)$. Compute $Q_a = Q_1 \cap Q_2$.

Step 2. Determine $K_D^s$ and $K_D^c$.

Step 3. For each interval in $K_D^c$ with no intersection, apply Procedure 2.1

to find stable regions and conditionally stable band.

Step 4. For each interval in $K_D^s$, draw D-graph to divide the space to

regions and find stable regions. For the band, use Procedure 2.1 to find

conditionally stability for its portion with no intersection, and use root locus to

determine stable sub-intervals of $K_D^s$ for the band with intersection.

**Example 2.1cc.** Consider Example 2.1 when $K_d$ varies in $[0,1]$ with

$\bar{K}_i = 100$ and $\bar{K}_p = 100$. Step 1 produces Figure 2.9 and Figure 2.10. From

Figure 2.9, we compute $Q_1 = [0,5977]$ while Figure 2.10 gives

$Q_2 = [0,2.77]$. As $Q_a = Q_1 \cap Q_2$, we obtain $Q_a = [0,2.77]$. In Step 2, in order

to compute $K_D^s$ and $K_D^c$, we solve (2.16) for $Q_a = [0,2.77]$, which does not

has any solution. Thus $K_D^s$ is null and $K_D^c$ is $[0,1]$. In Step 3 we apply

Procedure 2.1 for $K_d$ varies in $[0,1]$, this gives Figure 2.11 with the stable

region marked in green and the conditionally stable region mark in grey. Since

$K_D^s$ is null, Step 4 is bypassed.
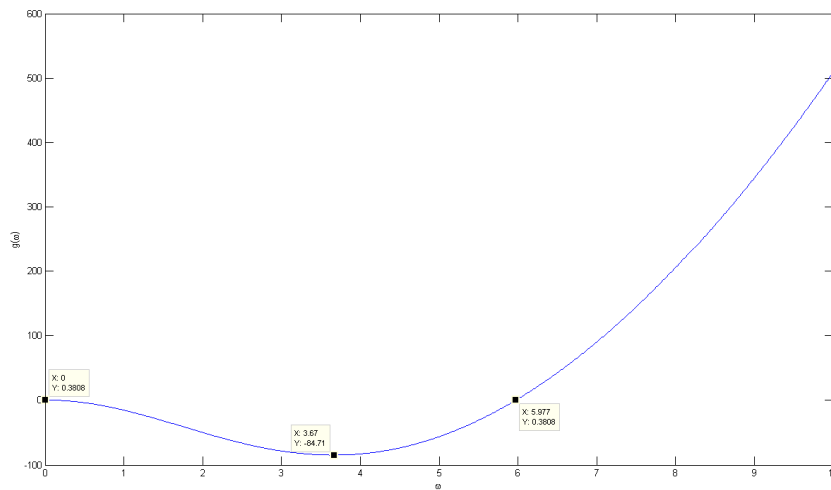


Figure 2.9. Plot of $\lambda(\omega)$ of Example 2.1cc
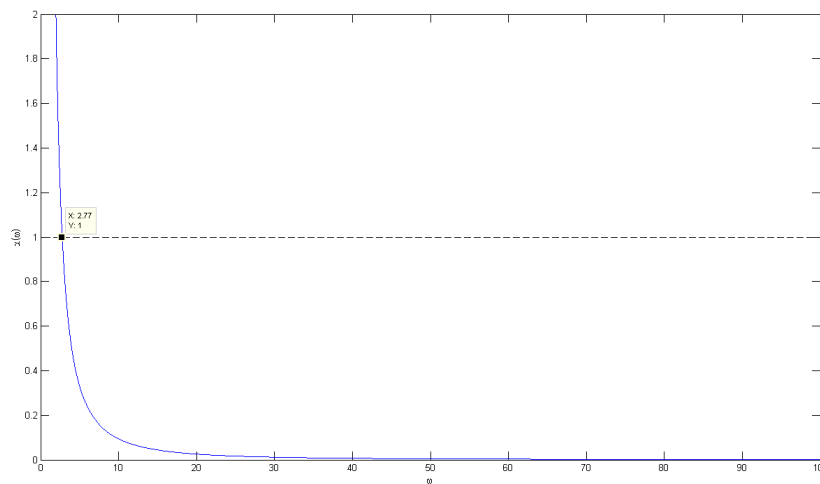


Figure 2.10: Plot of $\alpha(\omega)$ of Example 2.1cc
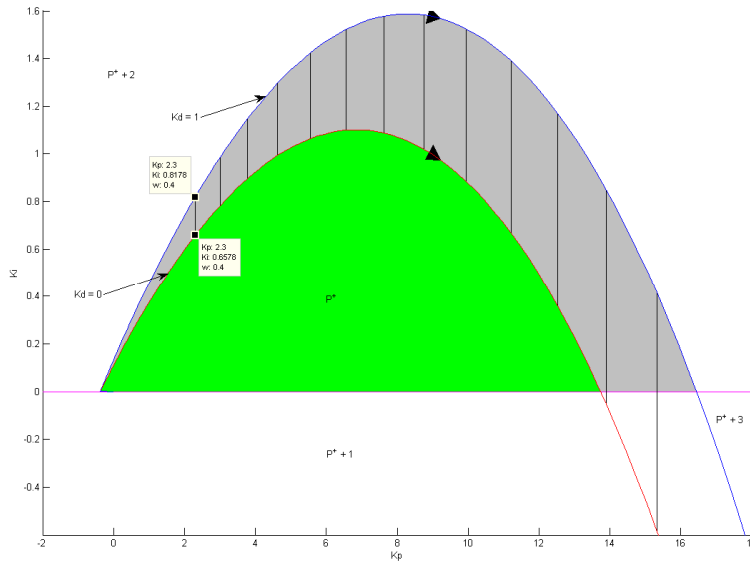
Figure 2.11: D-graph for Example 2.1cc with $K_d$ in $[0,1]$

**Example** 2.**1ccc.** Consider Example 2.1 when $K_d$ varies in $[0,100]$. Step 1 produces Figure 2.9 and Figure 2.10. From Figure 2.9, we compute $Q_1 = [0,5977]$ while Figure 2.12 gives $Q_2 = [0,9.44]$. As $Q_a = Q_1 \cap Q_2$, we obtain $Q_a = [0,5977]$. In Step 2, in order to compute $K_D^s$ and $K_D^c$, we compute the slope and Y-intercept of equation (2.21) for $\omega \in [0,3.659]$. These values are plotted in Figure 2.13. All solution lines of (2.16) and (2.17) are plotted in Figure 2.14, which shows that $K_D^c$ is null. Thus Step 3 is bypassed. Step 4 gives the D-graph in Figure 2.8 with boundary band and the line $K_i = 0$. From checking region stability, the region above the RRB has two RHP poles while the region below the RRB has three RHP. Thus, there is no stable region in this example. In step 5, the portion with possible conditionally stable region is the band for $\omega = [0,5977]$. Take one point in this portion as $(K_p, K_i) = (200,60)$, the root locus for $K_d$ can be seen in

Figure 2.15. The stabilizing range of $K_d$ for $(K_p, K_i) = (200, 60)$ is $[57.6, 67.8]$. Figure 2.14 shows that there is only one solution for the set of equations (2.18) and (2.19) which is $K_d = 70.85$. In this example, such solution can help to find the conditionally stable region, which is the grey region in Figure 2.16.
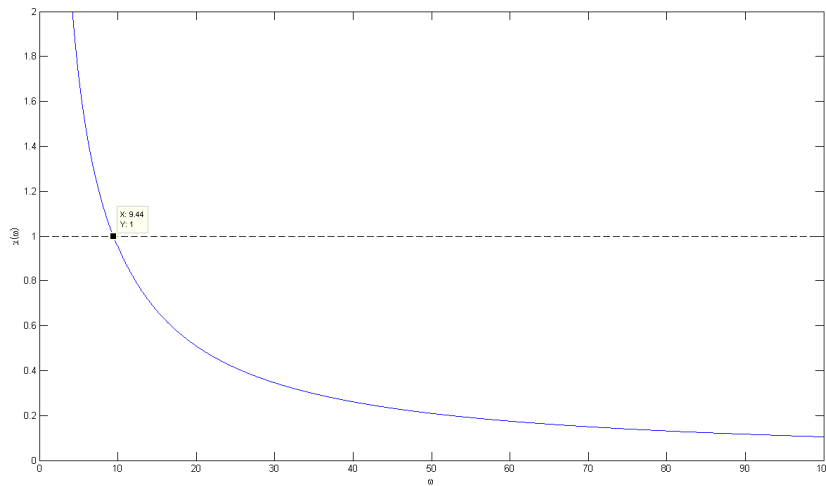


Figure 2.12: Plot of $\alpha(\omega)$ of Example 2.1cc
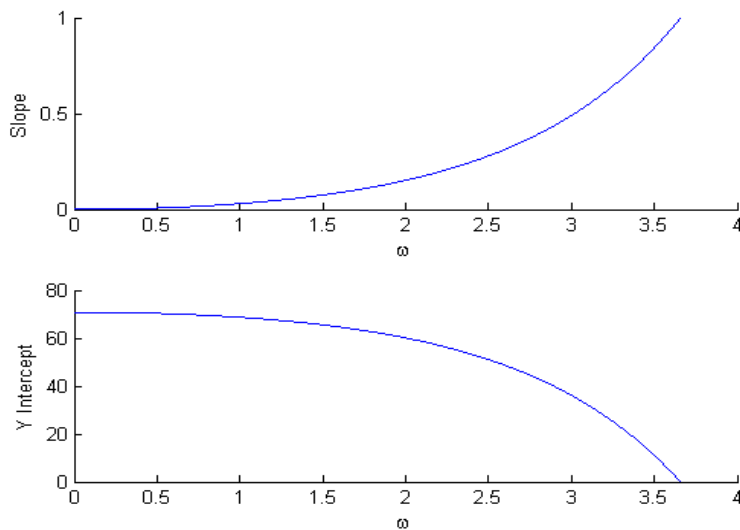


Figure 2.13: Plot of Slope and Y-Intercept of Equation (2.21) of Example 2.1cc
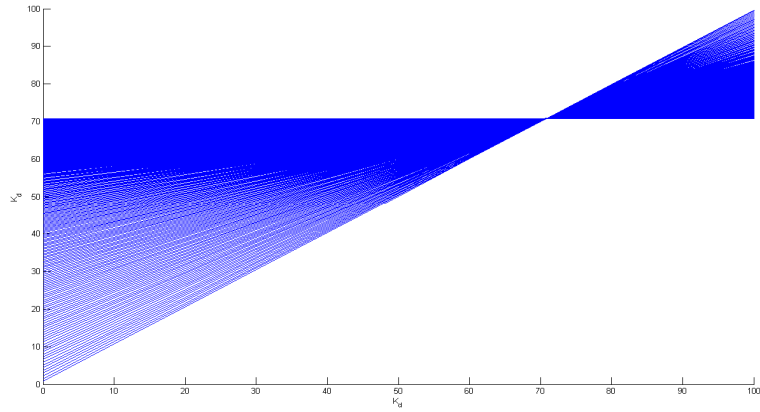
Figure 2.14: Plot of   Equation  (2.21)  of Example 2.1cc
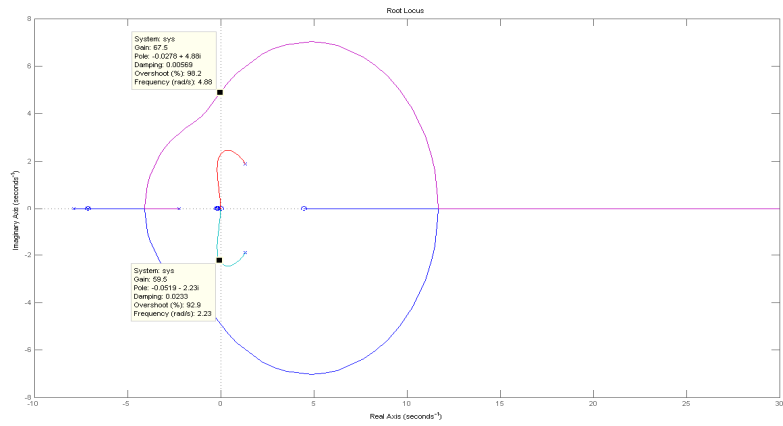


Figure 2.15: Root Locus for   $K_d$   of Example 2.1cc with   $K_i = 200$   and

$$K_p = 60$$
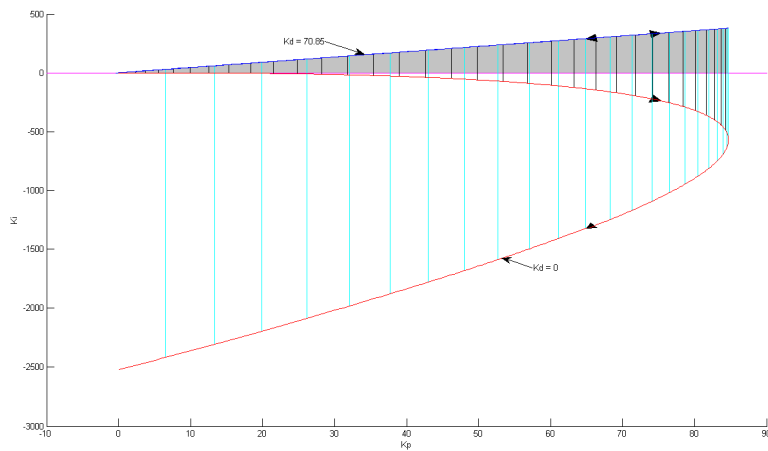


Figure 2.16: D-graph of Example 2.1cc with $K_d$   in [0,70.85].

**Example 2.4.** Consider PID control of the following process [4]

$$G(s) = \frac{1}{s^3 + s^2 + s} e^{-s}$$

In this example, with $[\underline{K}_d, \overline{K}_d] = [0, 20]$, $\overline{K}_i = 100$ and $\overline{K}_p = 100$, we plots $\lambda(\omega)$ and $\alpha(\omega)$ to give $Q_1 = [0, \infty)$ and $Q_2 = [0, 6.05]$ (Figure 2.17, Figure 2.18). This will result in $Q_a = [0, 6.05]$ and $Q_a$ can be further divided into 3 ranges $[0, 1.206]$, $[1.206, 3.448]$ and $[4.553, 6.05]$ (Figure 2.19). Solution lines for the first range of $Q_a$, which is $[0, 1.206]$ are plotted in the $K_d$-plane in Figure 2.20. This shows $K_D^c$ is null. The D-graph for the range of frequency $Q_a = [0, 6.05]$ is given in Figure 2.21. In Figure 2.22 a zoom into a possible stable region and a possible conditionally stable region of D-graph. Verifying the RHP of region with the fewest RHP reveals that it is a stable region and it is marked in green in Figure 2.22. The portion of boundary band next to it with no intersection of band is the conditionally stable region and is marked in grey. For other portion of band in Figure 2.22, the root locus of $K_d$ is needed for finding stabilizing range.
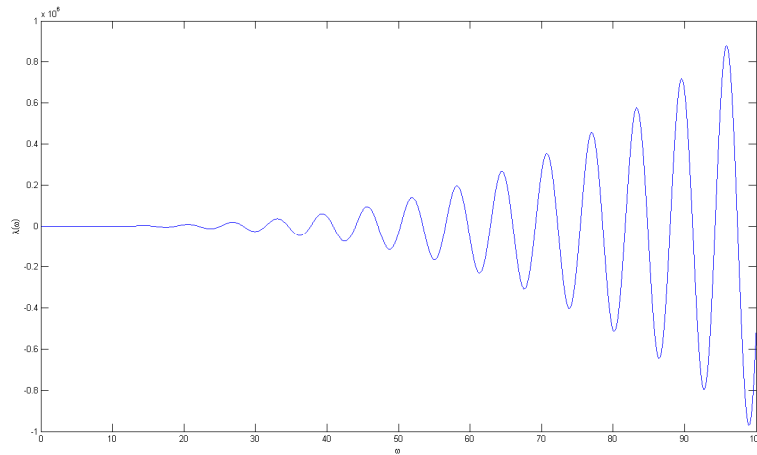


Figure 2.17: Plot of $\lambda(\omega)$ of Example 2.4
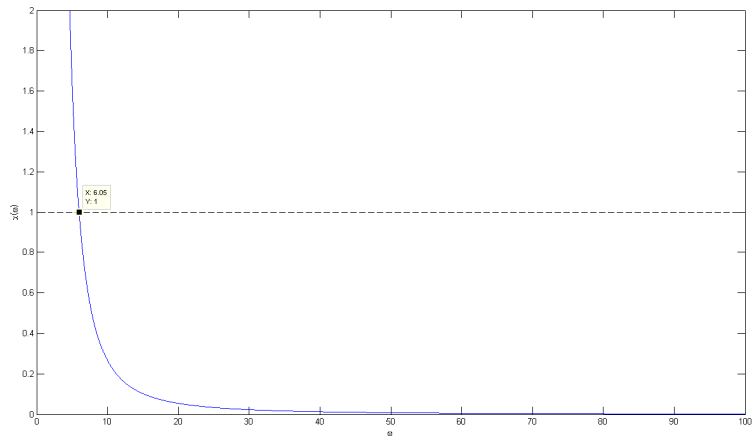
Figure 2.18: Plot of $\alpha(\omega)$ of Example 2.4.
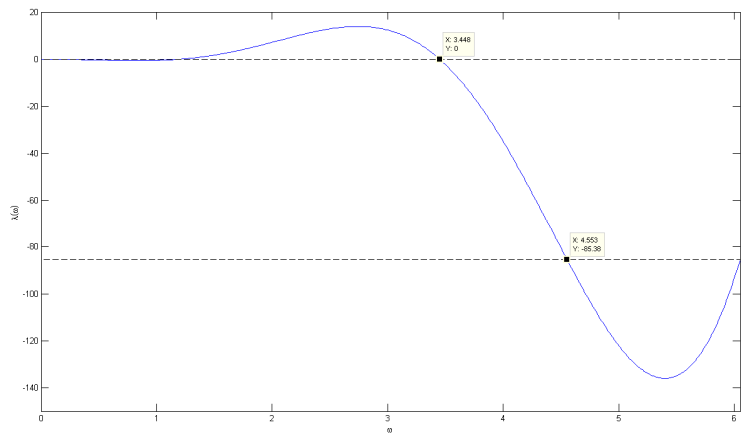


Figure 2.19: Plot of $\lambda(\omega)$ for $\omega \in [0, 6.05]$ of Example 2.4
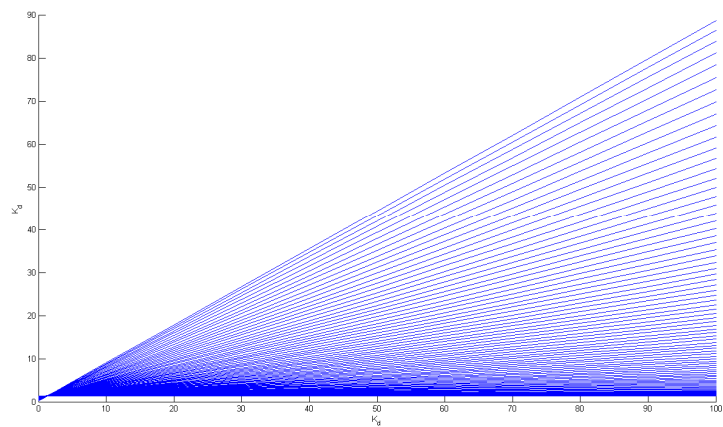


Figure 2.20: Plot of Equation (2.21) of Example 2.4
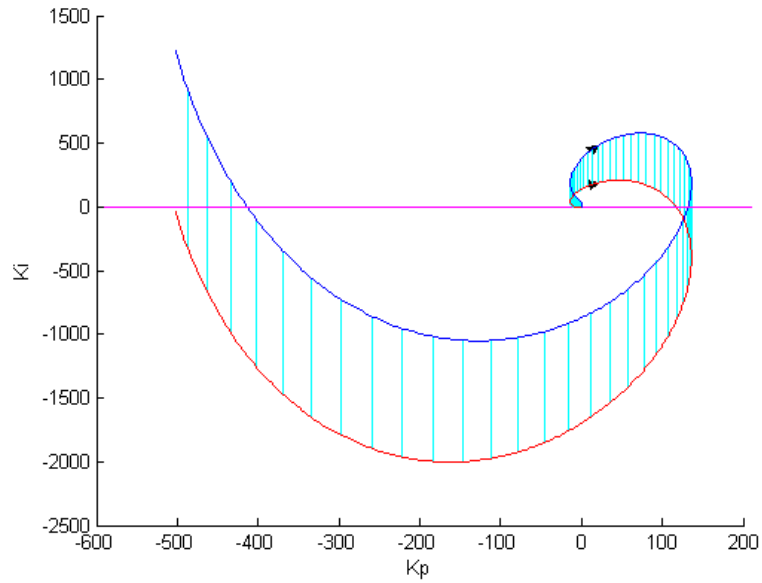
Figure 2.21: D-graph of Example 2.4
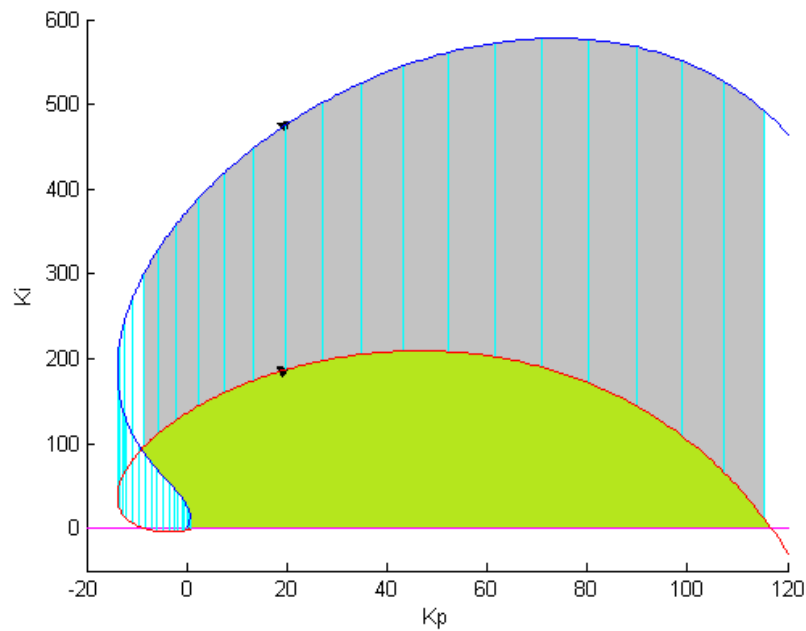

Figure 2.22: Zoom-in D-graph of Example 2.4

## 2.5. Conclusion

The chapter represents a method to compute stabilizing region in $(K_p, K_i)$ plane while $K_d$ varies in a range by extending the stability boundary concept to the parameterized stability boundary band. This approach is applicable for a general process with/without time delay. For process with monotonic $\lambda(\omega)$,

the entire stabilizing range with three parameters of PID controller are given.

For process with non-monotonic $\lambda(\omega)$, root locus of $K_d$ is needed to find

stabilizing range of $K_d$ in the possible conditionally stable region.

# Chapter 3

# Stabilizing Loop Gain and Delay for Strictly Proper Processes

## 3.1. Introduction

The problem under consideration in this chapter is to compute the exact stabilizing gain ranges for a general SISO process with uncertain time delay. Note that this problem is highly nonlinear and analytical solution seems to be difficult to derive. Thus, we present an effective graphical method to exactly compute stabilizing gain and delay ranges for any process. First, all the critical gains and delays at which the feedback control system may change stability are determined. These gains and delays are computed when the process's Nyquist curve intersects with the critical point. Then, the delay-gain plane is divided into regions and the stable ones are easily identified with our novel perturbation analysis. The stabilizing ranges of the gain controller are given in terms of the delay. The method requires no iterations, and can be applied to any process with possible unstable poles/zeros and large delay. It is simple in computation (no equation to be solved) and extremely powerful when it generates the boundary functions in the 2D space of $(L, k)$, which encloses the complete set of stabilizing parameters.

It should be pointed out that although Nyquist analysis is employed in this chapter as well as in [34], there are great deal of differences exist between them. This thesis looks only at local behavior of the Nyquist curve near the

critical point to find out how a delay perturbation changes the number of the curve's encirclements with regard to the critical point, without considering the entire curve, telling how a delay change affects stability change. On the other hand, [34] looked at the entire Nyquist curve and figured out the total number of the curve's encirclements with regard to the critical point for each pair of specific process and controller, which can be imagined to be too difficult to use when the process is general and can create a highly complex Nyquist curve and encirclements.

Even though our method and the traditional D-decomposition method share the same fundamental principles, our method has the following essential differences and significant advantages. The traditional D-decomposition method starts from the characteristic equation no matter where it comes from. The idea behind this method is to solve this equation for all its roots. In particular, the characteristic equation is separated into two equations of real and imaginary parts, respectively, and then two equations are solved simultaneously to find the common roots. On the other hand, our method also starts from the characteristic equation, we base our analysis on the Nyquist stability criteria. In particular, we transform the characteristic equation into magnitude and phase equations. These equations enable us to use Nyquist plot argument easily and see the effect of the controller gain k and time delay L on the open loop Nyquist curve, where the former affects only the gain and the later affect only the phase. This leads to explicit solutions for k and L without the need of solving any equations. In this thesis, we are for the first time to develop such a new approach, specially designed for delay processes. Furthermore, our method provides effective techniques to reduce the number

of solution curves needed to be plotted, as much as possible by careful studying of the solution curve properties. It also greatly simplifies the stability region determination and is able to identify stable regions by inspection without any numerical checking in many cases.

The remainder of the chapter is organized as follows. Section 3.2 presents our general approach via the Nyquist analysis. The boundary functions are studied in details in Section 3.3. The simple solution for a process with monotonic gain reduction is given in Section 3.4. In Section 3.5, a solution for a general process is presented. Finally, Section 3.6 draws the conclusions.

## 3.2. The Problem Formulation and Proposed Approach

Consider the unity output feedback system depicted in Figure 1.1, where $G(s) = G_0(s)e^{-Ls}$ and $K(s) = k$ are the process and controller, respectively. $G_0(s)$ is a *fixed* transfer function with no delay. The goal here is to determine the gain ranges for $k$ which stabilize the process in terms of a variable delay $L$.

**Problem 3.1.** For a process, $G(s) = G_0(s)e^{-Ls}$, under the proportional controller, $K = k$, with $L > 0$ and $k > 0$, find the regions in the 2D space, $(L, k)$, such that their interior points give stable closed-loop while their boundary points produce unstable closed-loop (with poles in the closed right-half plane).

**Theorem 3.1** [50]**.** *Given open-loop transfer function G(s) with $P_o$ unstable poles, the feedback system with proportional controller $K(s) = k$ is stable if and only if the Nyquist plot of $kG(s)$ encircles the critical point, $(-1 + j0)$, $P_o$ times anticlockwise.*

Let the open-loop transfer function be $Q(s) = kG_0(s)e^{-sL}$. By Theorem 3.1, the closed-loop system may change its stability with regard to $L$ and/or $k$ only when the number of encirclements of the *Nyquist plot of* $Q(s)$ with respect to the critical point changes. To find a stabilizing region for $(L,k)$, we locate its boundary where $Q(j\omega)$ passes through the critical point at some frequency $\omega$. That case satisfies $Q(j\omega) = kG_0(j\omega)e^{-j\omega L} = (-1 + j0)$, which implies, for $\omega > 0$, that

$$k = \frac{1}{|G_0(j\omega)|}, \quad G_0(j\omega) \neq 0, \tag{3.1}$$

$$L_n = \frac{\arg[G_0(j\omega)] + (2n+1)\pi}{\omega}, \quad n \in \{...,-1,0,1,...\} \tag{3.2}$$

while for $\omega = 0$, $Q(0) = kG_0(0) = -1$ with $k > 0$ requires

$$\arg[G_0(0)] = -\pi, \tag{3.3}$$

under which,

$$k = \frac{1}{|G_0(0)|}. \tag{3.4}$$

By convention, let

$$\arg[G_0(0)] = \begin{cases} 0 \text{ if } G_0(0) > 0 \\ -\pi \text{ if } G_0(0) < 0 \end{cases}$$

Note that only positive delay is realistic, which requires (2) to meet

$$L_n = \frac{\arg[G_0(j\omega)] + (2n+1)\pi}{\omega} > 0.$$

This yields

$$n > \frac{-\Phi - \pi}{2\pi}, \tag{3.5}$$

where $\Phi$ is the maximum phase of $G_0(j\omega)$. Denote $n_{min}$ as the smallest integer number that satisfies (3.5). Thus, (3.2) is valid only for $n = n_{min}, n_{min} + 1, ...$, which is used in the rest of this chapter.

Equations (3.1) and (3.2) for each valid $n$ define a boundary function which is an implicit mapping from the delay, $L$, to the gain, $k$, which is parameterized in terms of the frequency, $\omega$. Equation (3.4) defines another boundary function, which is an explicit mapping from $L$ to $k$ and is actually a horizontal line in the plane of $(L, k)$. The boundary functions defined by (3.1), (3.2) and (3.4) based on the frequency response of the fixed part of the process, $G_0$, can be drawn in the 2D plane, $(L, k)$. They divide the plane into regions. Each interior point in a so-formed region will have the same number of encirclements of the critical point by the Nyquist curve of the corresponding open-loop as that of any other points in the region. Thus all the points in the same region produce either closed-loop stability or instability. There will be no stability difference among the points in one region. Therefore, one only needs to check stability of one region by looking at any single point inside that region. Single point stability test is simple and can be done in many ways. For instance, one may use Theorem 3.1 to test for stability.

In general, all the boundary functions $L_n$ need to be plotted on the plane of $(L, k)$ in order to determine the stability of regions. However, there are an infinite number of boundary functions $L_n$, and, an infinite number of the resulting regions. It is impossible to plot and check the stability of all these regions. To overcome this problem, we attempt to limit the number of boundary functions to a few only in the subsequent sections. First of these is to develop a

perturbation analysis, in the next section, which tells how a delay perturbation at the critical point changes the number of unstable poles of the resulting closed-loop.

## 3.3. Properties of Boundary Functions

This section will study how the boundary functions defined in the preceding section are related to stability of their neighbor regions. These properties will be used in the next two sections to dramatically reduce the number of boundary functions needed, and in particular, only one boundary function, $L_{n_{\min}}$, is needed to determine the entire stability parameter ranges if the process has monotonic gain reduction.

**Lemma 3.1.** *For* $m \neq n$ , *a boundary function* $L_m$ *intersects with another* $L_n$ *only if there are* $\omega_m$ *and* $\omega_n$ *with* $\omega_m \neq \omega_n$ *such that* $\left| G_0(j\omega_m) \right| = \left| G_0(j\omega_n) \right|$ .

**Proof.** Suppose that two different boundary functions, $L_m$ and $L_n$ , $m \neq n$ , intersect with each other at a point in the plane $(L, k)$ . Then, they have equal gains and delays, respectively,

$$\frac{1}{\left| G_0(j\omega_m) \right|} = \frac{1}{\left| G_0(j\omega_n) \right|} \tag{3.6}$$

$$\frac{\arg[G_0(j\omega_m)] + (2m+1)\pi}{\omega_m} = \frac{\arg[G_0(j\omega_n)] + (2n+1)\pi}{\omega_n} . \tag{3.7}$$

Since $m \neq n$ , (3.7) holds only if $\omega_m \neq \omega_n$ , in which case (3.6) gives $\left| G_0(j\omega_m) \right| = \left| G_0(j\omega_n) \right|$ for $\omega_m \neq \omega_n$ . The proof is complete.

It is implied by Lemma 3.1 that the boundary functions $L_n$ will not intersect with each other if the gain of $G_0(s)$ monotonically reduces to zero

44

over the entire frequency range, a case which is shown in Section 3.4 to have a simple solution to Problem 3.1. General case is more complex and will be discussed in Section 3.5.

It turns out in the next few lemmas that the change of stability of closed-loop with regard to delay depends on the local gain change direction of the open-loop at the critical point. Note that $d\left|kG_0(j\omega)e^{-j\omega L}\right|/d\omega = kd\left|G_0(j\omega)\right|/d\omega$. We use $d\left|kG_0(j\omega)e^{-j\omega L}\right|/d\omega$ in the following lemmas and their proofs for theoretical rigor whereas practically only the sign of $d\left|G_0(j\omega)\right|/d\omega$ matters when $k$ is a positive constant.

**Lemma 3.2.** *Let the Nyquist plot of the open-loop $kG_0(s)e^{-sL}$ for $\omega > 0$ has the unique intersection with the critical point of $(-1+j0)$ at a frequency $\omega = \omega^* \in (0,\infty)$. If the gain of its frequency response decreases at this frequency, that is, $d\left|kG_0(j\omega)e^{-j\omega L}\right|/d\omega\big|_{\omega=\omega^*} < 0$, then the closed-loop system with $kG_0(s)e^{-s(L+\varepsilon)}$ has two more unstable poles than the closed-loop system with $kG_0(s)e^{-s(L-\varepsilon)}$ for some $\varepsilon > 0$.*

**Proof.** We split the problem into three cases of decreasing, increasing and no change of phase. Suppose that the phase of the frequency response of $kG_0(s)e^{-sL}$ decreases at the frequency $\omega = \omega^* > 0$, that is, $d\arg[kG_0(j\omega)e^{-j\omega L}]/d\omega\big|_{\omega=\omega^*} < 0$. In such a case, its Nyquist plot is moving clockwise when it intersects with the real axis. Note that the phase of all the points on the Nyquist plot of the slightly perturbed loop $kG_0(s)e^{-s(L+\varepsilon)}$ with a delay increase will differ by $-\omega^*\varepsilon$ from that of $kG_0(s)e^{-sL}$. In other word, the Nyquist plot of the perturbed loop moves up by that phase, the point at

45

$\omega = \omega^*$ is now above the critical point. The new intersection point with the real axis is on the left hand side of the critical point with its phase cross-over frequency less than $\omega^*$ and its gain greater than 1 because of the assumed gain reduction at $\omega = \omega^*$. Note similarly that the phase of all the points on the Nyquist plot of the slightly perturbed loop $kG_0(s)e^{-s(L-\varepsilon)}$ with a delay decrease differs by $\omega^*\varepsilon$ from that *of* $kG_0(s)e^{-sL}$. In other word, Nyquist plot of the perturbed loop moves down by that phase, the point at $\omega = \omega^*$ is now below the critical point. The new intersection point with the real axis is on the right hand side of the critical point with its phase cross-over frequency greater than $\omega^*$ and its gain less than 1 because of the assumed gain reduction at $\omega = \omega^*$. Combination of these two delay change observations shows the intersection point shifts from the left to the right of the critical point when the delay changes from $L+\varepsilon$ to $L-\varepsilon$ on the loop $kG_0(s)e^{-s(L)}$. The above analysis is drawn for $\omega > 0$. The same shift occurs for $\omega < 0$, because the frequency response with real coefficients is symmetry. Since the Nyquist plot of a proper transfer function with real coefficients on the entire Nyquist curve including both positive and negative frequencies always forms a closed curves, the above two shifts will either add two more clockwise encirclements (Figure 3.1a), or reduce two more counter-clockwise encirclements (Figure 3.1b), when the open loop $kG_0(s)e^{-s(L+\varepsilon)}$ is compared with $kG_0(s)e^{-s(L-\varepsilon)}$, which causes the closed-loop system with $kG_0(s)e^{-s(L+\varepsilon)}$ to have two more unstable poles than the closed-loop system with $kG_0(s)e^{-s(L-\varepsilon)}$ for $\varepsilon > 0$.

Consider next the phase increase: $d\arg[kG_0(j\omega)e^{-j\omega L}]/d\omega\big|_{\omega=\omega^*} > 0$. In

such a case, its Nyquist plot is moving counter-clockwise when it intersects with the real axis. Note that the phase of all the points on the Nyquist plot of the slightly perturbed loop $kG_0(s)e^{-s(L+\varepsilon)}$ with a delay increase differs by $-\omega^*\varepsilon$ from that of $kG_0(s)e^{-sL}$. In other word, the Nyquist plot of the perturbed loop moves up by that phase, the point at $\omega=\omega^*$ is now above the critical point, and the new intersection point with the real axis is on the right hand side of the critical point with its phase cross-over frequency less than $\omega^*$ and its gain less than 1 because of the assumed gain reduction at $\omega=\omega^*$. Note similarly that the phase of all the points on the Nyquist plot of the slightly perturbed loop $kG_0(s)e^{-s(L-\varepsilon)}$ with a delay decrease differs by $\omega^*\varepsilon$ from that of $kG_0(s)e^{-sL}$. In other word, the Nyquist plot of the perturbed loop moves down by that phase, the point at $\omega=\omega^*$ is now below the critical point, and the new intersection point with the real axis is on the left hand side of the critical point with its phase cross-over frequency greater than $\omega^*$ and its gain less than 1 because of the assumed gain reduction at $\omega=\omega^*$. Combining these two observations on delay changes shows that the intersection point shifts from the right to the left of the critical point when the delay changes from $L+\varepsilon$ to $L-\varepsilon$ on the loop $kG_0(s)e^{-s(L)}$. The above analysis is drawn for $\omega>0$. The same shift occurs for $\omega<0$, because the frequency response with real coefficients is symmetry. Since the Nyquist plot of a proper transfer function with real coefficients on the entire Nyquist curve including both positive and negative frequencies always forms a closed curves, the above two shifts will either reduce two more counter-clockwise encirclements (Figure 3.2a), or add two more clockwise encirclements (Figure 3.2b), when the open

loop $kG_0(s)e^{-s(L+\varepsilon)}$ is compared with $kG_0(s)e^{-s(L-\varepsilon)}$, which causes the closed-loop system with $kG_0(s)e^{-s(L+\varepsilon)}$ to have two more unstable poles than the closed-loop system with $kG_0(s)e^{-s(L-\varepsilon)}$ for $\varepsilon > 0$.



a)                                         b)
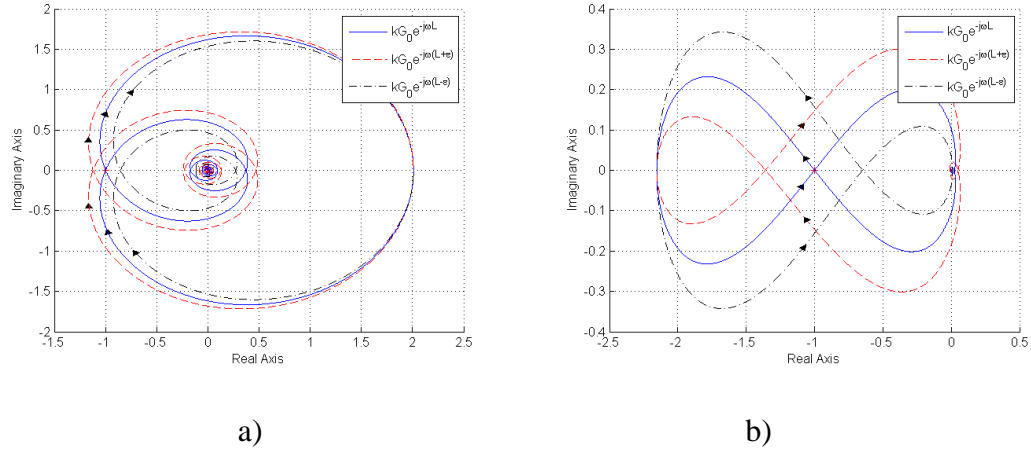
Figure 3.1: Open loop with local gain reduction and phase decrease.



a)                                         b)
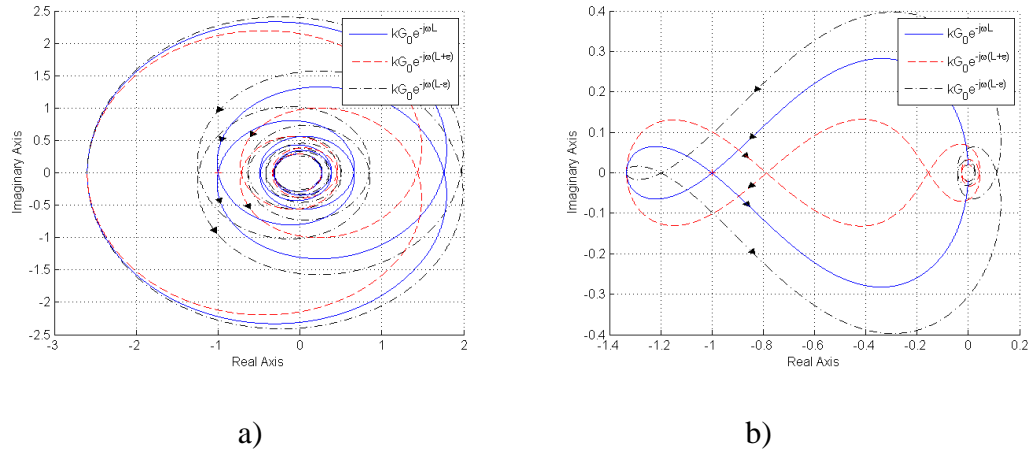
Figure 3.2: Open loop with local gain reduction and phase increase.

Consider finally zero phase rate: $d\arg[kG_0(j\omega)e^{-j\omega L}]/d\omega\big|_{\omega=\omega^*} = 0$. There are 4 possible cases:

- $d\arg[kG_0(j\omega)e^{-j\omega L}]/d\omega\big|_{\omega \in (\omega^*-\delta,\omega^*)\cup(\omega^*,\omega^*+\delta)} < 0$ : then the phase decreases over $\omega^* - \delta$ to $\omega^* + \delta$. This is the same as the above case of phase decrease.

- $d \arg[kG_0(j\omega)e^{-j\omega L})]/d\omega\big|_{\omega \in (\omega^*-\delta,\omega^*) \cup (\omega^*,\omega^*+\delta)} > 0$ : then the phase increases over $\omega^* - \delta$ to $\omega^* + \delta$. This is the same as the above case of phase increase.

- $d \arg[kG_0(j\omega)e^{-j\omega L})]/d\omega\big|_{\omega \in (\omega^*-\delta,\omega^*)} < 0$ ,

  $d \arg[kG_0(j\omega)e^{-j\omega L})]/d\omega\big|_{\omega \in (\omega^*,\omega^*+\delta)} > 0$: then the phase at $\omega = \omega^*$ has a local minimum. In the neighborhood of this point, the open loop $kG_0(s)e^{-s(L+\varepsilon)}$ moves above the critical point with clockwise direction whereas $kG_0(s)e^{-s(L-\varepsilon)}$ goes below it. It will either add two more clockwise encirclements, or reduce two more counter-clockwise encirclements, which causes the closed-loop system with $kG_0(s)e^{-s(L+\varepsilon)}$ to have two more unstable poles than the closed-loop system with $kG_0(s)e^{-s(L-\varepsilon)}$ for $\varepsilon > 0$. The net effect is the same as the above case of phase decrease.

- $d \arg[kG_0(j\omega)e^{-j\omega L})]/d\omega\big|_{\omega \in (\omega^*-\delta,\omega^*)} > 0$ ,

  $d \arg[kG_0(j\omega)e^{-j\omega L})]/d\omega\big|_{\omega \in (\omega^*,\omega^*+\delta)} < 0$: then the phase at $\omega = \omega^*$ has a local maximum. In the neighborhood of this point, the open loop $kG_0(s)e^{-s(L+\varepsilon)}$ moves above the critical point with counter-clockwise direction whereas $kG_0(s)e^{-s(L-\varepsilon)}$ goes below it. It will either add two more clockwise encirclements, or reduce two more counter-clockwise encirclements, which causes the closed-loop system with $kG_0(s)e^{-s(L+\varepsilon)}$ to have two more unstable poles than the closed-loop

system with $kG_0(s)e^{-s(L-\varepsilon)}$ for $\varepsilon > 0$. The net effect is the same as the above case of phase increase.

The proof of Lemma 3.2 is complete.

**Lemma 3.3.** *Let the Nyquist plot of the open-loop $kG_0(s)e^{-sL}$ for $\omega > 0$ has the unique intersection with the critical point of $(-1+j0)$ at a frequency $\omega = \omega^* \in (0, \infty)$. If the gain of its frequency response increases at this frequency, that is, $d\left|kG_0(j\omega)e^{-j\omega L}\right|/d\omega\Big|_{\omega=\omega^*} > 0$, then the closed-loop system with $kG_0(s)e^{-s(L+\varepsilon)}$ has two fewer unstable poles than the closed-loop system with $kG_0(s)e^{-s(L-\varepsilon)}$ for some $\varepsilon > 0$.*

**Proof.** Follow the proof of Lemma 3.2 with "greater", "gain reduction", "left" replaced with "less", "gain increase", "right", respectively.   □

**Lemma 3.4.** *Let the Nyquist plot of the open-loop $kG_0(s)e^{-sL}$ for $\omega > 0$ have the unique intersection with the critical point of $(-1+j0)$ at a frequency $\omega = \omega^* \in (0, \infty)$ and $d\left|kG_0(j\omega)e^{-j\omega L}\right|/d\omega\Big|_{\omega=\omega^*} = 0$. Then,*

i. *if $\quad d\left|kG_0(j\omega)e^{-j\omega L}\right|/d\omega\Big|_{\omega\in(\omega^*-\delta,\omega^*)\cup(\omega^*,\omega^*+\delta)} < 0$ for some $\delta > 0$, the closed-loop system with $kG_0(s)e^{-s(L+\varepsilon)}$ has two more unstable poles than the closed-loop system with $kG_0(s)e^{-s(L-\varepsilon)}$ for some $\varepsilon > 0$.*

ii. *if $\quad d\left|kG_0(j\omega)e^{-j\omega L}\right|/d\omega\Big|_{\omega\in(\omega^*-\delta,\omega^*)\cup(\omega^*,\omega^*+\delta)} > 0$ for some $\delta > 0$, the closed-loop system with $kG_0(s)e^{-s(L+\varepsilon)}$ has two fewer unstable poles than the closed-loop system with $kG_0(s)e^{-s(L-\varepsilon)}$ for some $\varepsilon > 0$.*

*iii. if*
$$d\left|kG_0(j\omega)e^{-j\omega L}\right|/d\omega\bigg|_{\omega\in(\omega^*-\delta,\omega^*)}<0 \qquad\qquad and$$

$$d\left|kG_0(j\omega)e^{-j\omega L}\right|/d\omega\bigg|_{\omega\in(\omega^*,\omega^*+\delta)}>0 \ \ for \ some \ \ \delta>0, \ the \ closed\text{-}loop$$

*system with* $kG_0(s)e^{-s(L+\varepsilon)}$ *has the same number of unstable poles with*

*the closed-loop system with* $kG_0(s)e^{-s(L-\varepsilon)}$ *for some* $\varepsilon>0$.

*iv. if*
$$d\left|kG_0(j\omega)e^{-j\omega L}\right|/d\omega\bigg|_{\omega\in(\omega^*-\delta,\omega^*)}>0 \qquad\qquad and$$

$$d\left|kG_0(j\omega)e^{-j\omega L}\right|/d\omega\bigg|_{\omega\in(\omega^*,\omega^*+\delta)}<0 \ \ for \ some \ \ \delta>0, \ the \ closed\text{-}loop$$

*system with* $kG_0(s)e^{-s(L+\varepsilon)}$ *has the same number of unstable poles with*

*the closed-loop system with* $kG_0(s)e^{-s(L-\varepsilon)}$ *for some* $\varepsilon>0$.

**Proof.** i) $d\left|kG_0(j\omega)e^{-j\omega L}\right|/d\omega\bigg|_{\omega\in(\omega^*-\delta,\omega^*)\cup(\omega^*,\omega^*+\delta)}<0$: The gain rate is

negative at both $\omega<\omega^*$ and $\omega>\omega^*$. The arguments in the proof of Lemma

3.2 can apply and the same statement as Lemma 3.2 thus carries to this case.

ii) $d\left|kG_0(j\omega)e^{-j\omega L}\right|/d\omega\bigg|_{\omega\in(\omega^*-\delta,\omega^*)\cup(\omega^*,\omega^*+\delta)}>0$: Similarly, this case is the

same as Lemma 3.3.

iii) 
$$d\left|kG_0(j\omega)e^{-j\omega L}\right|/d\omega\bigg|_{\omega\in(\omega^*-\delta,\omega^*)}<0 \qquad\qquad and$$

$d\left|kG_0(j\omega)e^{-j\omega L}\right|/d\omega\bigg|_{\omega\in(\omega^*,\omega^*+\delta)}>0$: the gain at $\omega=\omega^*$ has a local minimum.

In such a case, the phase of all the points on the Nyquist plot of the slightly

perturbed loop $kG_0(s)e^{-s(L+\varepsilon)}$ with an delay increase differs by $-\omega^*\varepsilon$ from

that of $kG_0(s)e^{-sL}$. In other word, the Nyquist plot of the perturbed loop

moves up by that phase, the point at $\omega=\omega^*$ is now above the critical point

and the new intersection point with the real axis is on the left hand side of the

critical point because of the assumed minimum gain at $\omega = \omega^*$. On the other hand, the phase of all the points on the Nyquist plot of the slightly perturbed loop $kG_0(s)e^{-s(L-\varepsilon)}$ with an delay decrease differs by $\omega^*\varepsilon$ from that *of* $kG_0(s)e^{-sL}$. In other word, the Nyquist plot of the perturbed loop moves down by that phase, the point at $\omega = \omega^*$ is now below the critical point, and the new intersection point with the real axis is on the left hand side of the critical point because of the assumed minimum gain at $\omega = \omega^*$. It follows that the intersection points of both $kG_0(s)e^{-s(L+\varepsilon)}$ and $kG_0(s)e^{-s(L-\varepsilon)}$ are on the left of the critical point when the delay changes from $L+\varepsilon$ to $L-\varepsilon$ on the loop $kG_0(s)e^{-s(L)}$ (Figure 3.3). Hence, there is no change of encirclements and unstable poles.



Figure 3.3: Open loop with local minimum gain.

iv) $\qquad d\left|kG_0(j\omega)e^{-j\omega L}\right|/d\omega\Big|_{\omega\in(\omega^*-\delta,\omega^*)} > 0 \qquad$ and

$d\left|kG_0(j\omega)e^{-j\omega L}\right|/d\omega\Big|_{\omega\in(\omega^*,\omega^*+\delta)} < 0$: the gain at $\omega=\omega^*$ has a local maximum.

In such a case, the phase of all the points on the Nyquist plot of the slightly perturbed loop $kG_0(s)e^{-s(L+\varepsilon)}$ with an delay increase differs by $-\omega^*\varepsilon$ from that of $kG_0(s)e^{-sL}$. In other word, the Nyquist plot of the perturbed loop moves up by that phase, the point at $\omega=\omega^*$ is now above the critical point and the new intersection point with the real axis is on the right hand side of the critical point because of the assumed maximum gain at $\omega=\omega^*$. On the other hand, the phase of all the points on the Nyquist plot of the slightly perturbed loop $kG_0(s)e^{-s(L-\varepsilon)}$ with an delay decrease differs by $\omega^*\varepsilon$ from that *of* $kG_0(s)e^{-sL}$. In other word, the Nyquist plot of the perturbed loop moves down by that phase, the point at $\omega=\omega^*$ is now below the critical point, and the new intersection point with the real axis is on the right hand side of the critical point because of the assumed maximum gain at $\omega=\omega^*$. It follows that the intersection points of both $kG_0(s)e^{-s(L+\varepsilon)}$ and $kG_0(s)e^{-s(L-\varepsilon)}$ are on the right of the critical point when the delay changes from $L+\varepsilon$ to $L-\varepsilon$ on the loop $kG_0(s)e^{-s(L)}$ (Figure 3.4). Hence, there is no change of encirclements and unstable poles.
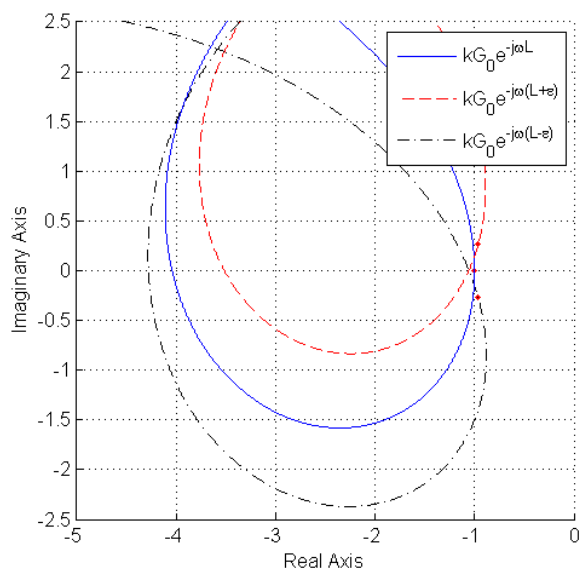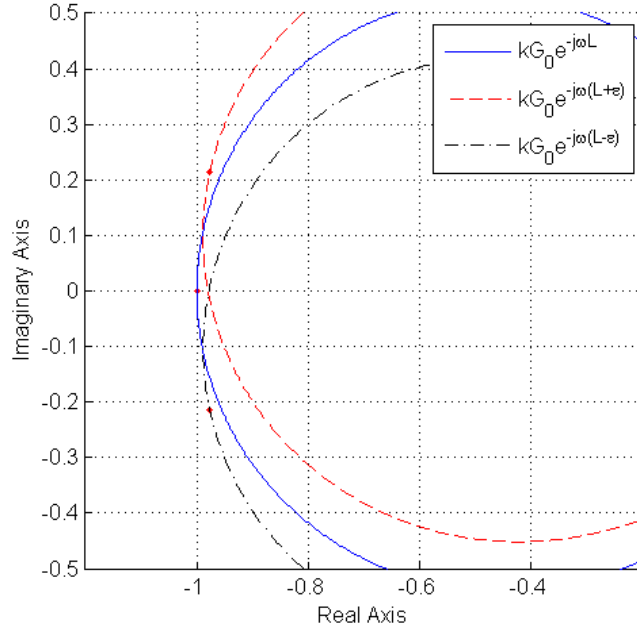
Figure 3.4: Open loop with local maximum gain.

The proof of Lemma 3.4 is complete. □

**Lemma 3.5.** *Let the Nyquist plot of the open-loop $kG_0(s)e^{-sL}$ for $\omega > 0$ have intersections with the critical point of $(-1+j0)$ at $\omega = \omega_i^* \in (0, \infty)$, $i = 1, 2, \ldots$ . Let $n_i$ and $n_d$ be the number of intersections with*

$$d \, | \, kG_0(j\omega)e^{-j\omega L}) | \, / d\omega |_{\omega=\omega_i^*} < 0 \qquad and \qquad d \, | \, kG_0(j\omega)e^{-j\omega L}) | \, / d\omega |_{\omega=\omega_i^*} > 0 \quad ,$$

*respectively. Then the closed-loop system with $kG_0(s)e^{-s(L-\varepsilon)}$ has $2(n_i - n_d)$ more unstable poles with the closed-loop system with $kG_0(s)e^{-s(L+\varepsilon)}$ for some $\varepsilon > 0$.*

**Proof.** Lemma 3.5 is proved by applying Lemma 3.2 or 3.3 to each *intersection and summing up individual numbers.* □

Obviously, one can include the case of zero gain rates in Lemma 3.4 into Lemma 3.5 but it was omitted for brevity.

## 3.4. Processes with Monotonic Gain Reduction

In what follows, we assume that $G_0(s)$ is a strictly proper transfer function. Thus, its gain eventually reduces to zero, i.e. $\lim_{\omega\to\infty} |G_0(j\omega)| = 0$, and its Nyquist plot ends at the origin. $kG_0(s)e^{-Ls}$ will all go to the origin at $\omega = \infty$ for any finite value of $k$, regardless of $L$. Therefore, the point at $\omega = \infty$ will not cause any change of encirclements of the loop in Nyquist plot with the critical point and does not affect closed-loop stability. It will be excluded from stability analysis in the rest of this paper. However, it should be pointed out here that this will not be the case if $G_0(s)$ is not strictly proper but bi-proper.

A transfer function $G_0(s)$ is said to have monotonic gain reduction if there holds $|G_0(j\omega_1)| > |G_0(j\omega_2)|$ for $0 \le \omega_1 < \omega_2$. For such a case, there are no two different frequencies with equal gain and from Lemma 3.1 the corresponding boundary functions do not intersect with each other. In addition, such a $G_0$ meets $d|G_0(j\omega)|/d\omega < 0$ for $\omega > 0$. It follows from Lemmas 3.2 that the closed-loop system with $kG_0(s)e^{-Ls}$ with $L > L_n$ has two more unstable poles than the closed-loop system with $kG_0(s)e^{-Ls}$ with $L < L_n$. Then, the region right to $L_n$ is impossible to be stable as the minimum number of unstable poles of a system is zero. For $\omega > 0$, this argument is true for each $n$. The induction on $n$ tells that the only possibly stable region is one left to $L_{n_{\min}}$, and its actual stability should be checked with one point inside it. Note that $L_{n_{\min}}$ is positive only for the frequency range with $\arg[G_0(j\omega)] \ge -(2n_{\min}+1)\pi$, and thus is computed there only to

plot $L_{n_{\min}}$ in the 2D plane.

For $\omega = 0$, it follows from (3.3) that the horizontal line $k = \dfrac{1}{|G_0(0)|}$ is

needed only if $G_0(0) < 0$. Since $G_0(s)$ has monotonic gain reduction, it

has the maximum gain at $\omega = 0$, and the corresponding $k = \dfrac{1}{|G_0(0)|}$ is

strictly smaller than $k = \dfrac{1}{|G_0(\omega)|}$ for $\omega > 0$ on $L_{n_{\min}}$. Thus, the line

$k = \dfrac{1}{|G_0(0)|}$ does not intersect with $L_{n_{\min}}$. These two boundary functions

divide the first quadrant of the plane $(L, k)$ into three regions, one below the

line $k = \dfrac{1}{|G_0(0)|}$, one above the line and left to $L_{n_{\min}}$, one above the line and

right to $L_{n_{\min}}$, with the last being unstable as shown above. The first region

meets $k < \dfrac{1}{\|G_0(j\omega)\|_{\omega=0}}$, or $\left| k G_0(j\omega) e^{-Ls} \right| < 1$, implying that its Nyquist plot

is impossible to have any encirclement of the critical point. It follows that a

stable $G_0(s)$ will yield stability of this region, while an unstable $G_0(s)$ will

yield instability of this region.

If $G_0(0) > 0$, there is no horizontal line. A point on the left hand side of $L_0$

and near the origin on $(L, k)$ is close to the corresponding open-loop system.

Thus, the region on the left hand side of $L_{n_{\min}}$ is stable (or unstable) if $G_0$ is

stable (or unstable).

The above analysis is summarized in Algorithm 3.1 for finding the

stabilizing gain ranges for a process with monotonic gain reduction as follows.

**Algorithm 3.1.** Consider a process with monotonic gain reduction.

Step 1. For $\omega = 0$, if $\arg[G_0(0)] = -\pi$, plot the horizontal

line, $k = \dfrac{1}{|G_0(0)|}$, on the plane $(L, k)$. The region below this line

is stable (or unstable) if $G_0$ is stable (or unstable).

Step 2. For $\omega \neq 0$, plot $L_{n_{\min}}$ with (3.1) and (3.2) on the plane $(L, k)$.

If $G_0(0) > 0$, the region on the left hand side of $L_{n_{\min}}$ is stable

(or unstable) if $G_0(s)$ is stable (or unstable). If $G_0(0) < 0$,

check stability of the region on the left hand side of $L_{n_{\min}}$.

**Remark 3.1.** If $G_0(0) < 0$ and $G_0$ is stable, the region on the left hand

side of $L_0$ is unstable. In such a case, there is the horizontal line $k = \dfrac{1}{|G_0(0)|}$

and the region below the line is stable based on Step 1 of Algorithm 3.1. A point

slightly above the line has the gain greater than $\dfrac{1}{|G_0(0)|}$. And the corresponding

open-loop Nyquist plot crosses the critical point and causes clockwise

encirclement due to monotonic gain reduction of the loop, and thus closed-loop

instability.

**Example 3.1.** Consider the following delay process,

$$G(s) = G_0(s)e^{-Ls} = \frac{-0.1s + 1}{0.16(s - 1)(s^2 + 5s + 7.8125)} e^{-Ls}.$$

This process has one unstable pole at $s = 1$, two complex poles at

$s = -1 \pm j0.5$ and one non-minimum-phase zero at $s = 10$. One can see from

the gain plot of $G_0(s)$ in Figure 3.5 that the process has monotonic gain

reduction, so Algorithm 3.1 is applicable. The maximum phase of $G_0(j\omega)$ is

$\Phi = -3.044$. It follows from (5) that $n > -0.0155$ so $n_{min} = 0$. For Step 1, $G_0(0) = -0.8$ meets (3.3) and yields the black line $k = 1.25$. The region below this line is unstable since $G_0$ is unstable. Step 2 gives the curve $L_0$ marked in blue. Since the open-loop system is unstable and $G_0(0) < 0$, we need to check stability of the region in the left hand side of $L_0$. We select one point as $(L, k) = (0.1, 1.6)$ in this region. The corresponding Nyquist plot of $kG_0(s)e^{-Ls}$ has one counter-clockwise encirclement, see Figure 3.7. So, this region is the stable region and shaded in green. Note that the presence of unstable zero limits the stabilizing gain to 2.179, while the presence of unstable poles limits the delay to 0.26. For this example, the method in [34] cannot be applied because of complex poles.
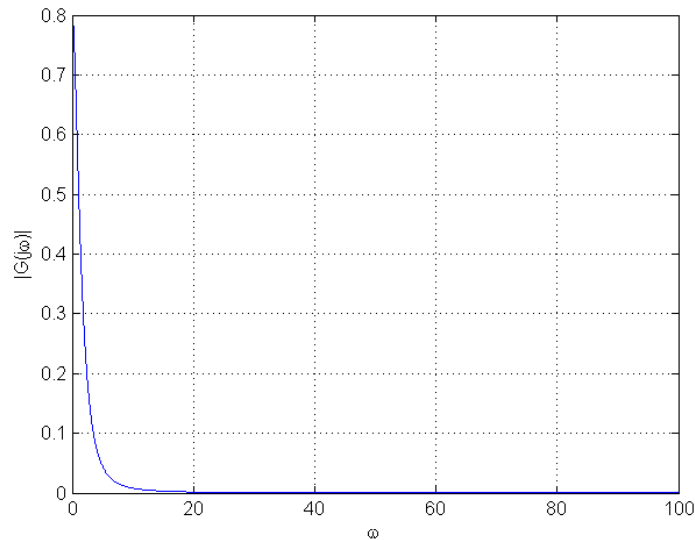


Figure 3.5: Gain plot of $G_0(s)$ of Example 3.1
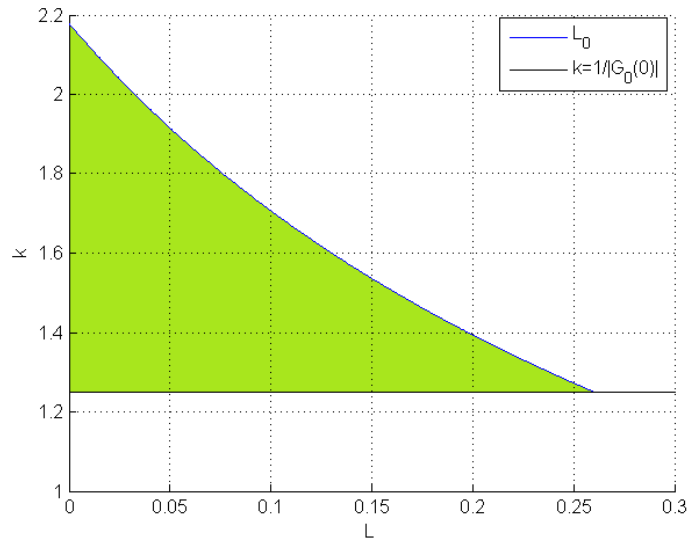
Figure 3.6: Stabilizing region of $(L, k)$ for Example 3.1
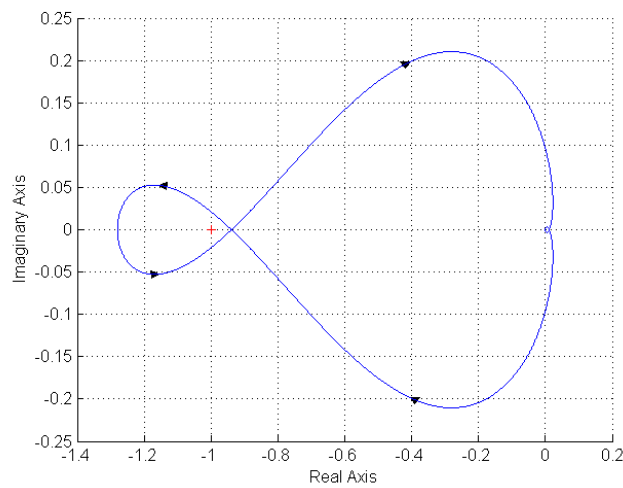


Figure 3.7: Nyquist plot of Example 3.1 with $k = 1.6; L = 0.1$

## 3.5. Processes with Non-monotonic Gain

In this section, we consider a process that does not have monotonic gain reduction. For such a process, there are two frequencies with the same gain, and from Lemma 3.1, the corresponding boundary functions $L_n$ may intersect with each other. Such frequencies and their ranges are crucial to determine how many $L_n$ are needed for the solution of Problem 3.1 and thus

59

discussed first.
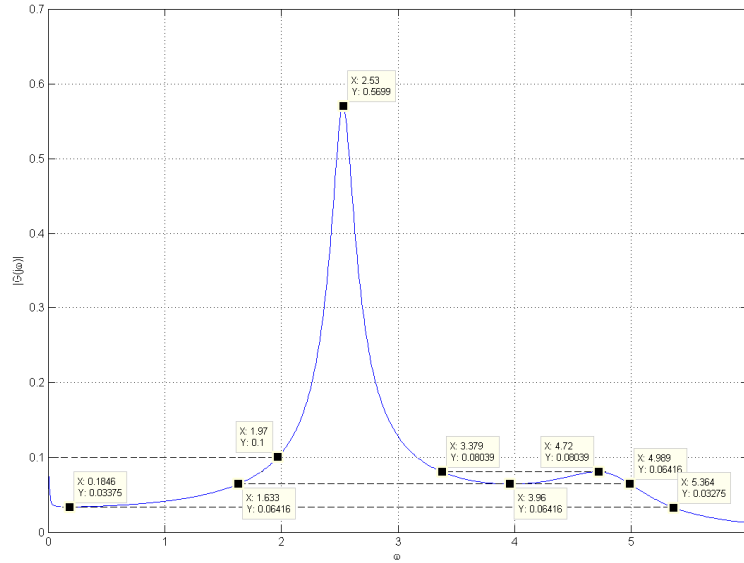


Figure 3.8: Gain plot of $G_0(j\omega)$

We draw the Bode gain plot, $\left|G_0(j\omega)\right|$. For illustration, consider

$$G_0(s) = \frac{5s+0.1}{s^5 + s^4 + 30s^3 + 10s^2 + 150s + 1},$$

with its gain plot shown in Figure 3.8. We proceed as following:

- Take $\omega_1 = 0$ as the first point of local minimum or local maximum of

  $\left|G_0(j\omega)\right|$. Draw the horizontal line of the gain equal to $\left\|G_0(j\omega_1)\right\|_{\omega_1=0}$.

  This line may intersect on its right with the gain plot at some frequency,

  $\bar{\omega}_1 > \omega_1$. If there does not exist $\bar{\omega}_1$, then $\omega_1$ is not needed for our

  calculations and is discarded. Form one frequency range as $[\underline{\omega}_1, \bar{\omega}_1]$,

  where $\underline{\omega}_1 = \omega_1$. For the above example, $G_0(0) = 0.1$, and this line

  intersects with the gain plot at $\omega = 1.97$. Then, we have $\omega_1 = 0$ with

  $[\underline{\omega}_1, \bar{\omega}_1] = [0, 1.97]$. See Figure 3.8.

- Find all the frequencies at which the gain has local minimum or local maximum, i.e. $d|G_0(j\omega)|/d\omega = 0$. Denote these frequencies as $\omega_2,\ldots,$ $\omega_m$ with $\omega_1 < \omega_2 < \ldots < \omega_m$. The example gives $\omega_2 = 0.1846$, $\omega_3 = 2.53$, $\omega_4 = 3.96$ and $\omega_5 = 4.72$. For each $\omega_i$, $i = 2,3,\ldots,m$, draw the horizontal line with gain equal to $|G_0(j\omega_i)|$. Find the nearest left and right intersections with the gain plot and assign the corresponding frequencies as $\underline{\omega}_i < \omega_i$ and $\bar{\omega}_i > \omega_i$, respectively. If there does not exist $\underline{\omega}_i$ or $\bar{\omega}_i$, then $\underline{\omega}_i = \omega_i$ or $\bar{\omega}_i = \omega_i$. Form one frequency range $[\underline{\omega}_i, \bar{\omega}_i]$ for each $i$. If $\underline{\omega}_i = \bar{\omega}_i$, the range $[\underline{\omega}_i, \bar{\omega}_i]$ has only one frequency and is not needed for our calculation and $\omega_i$ is excluded. The above example has $\omega_2 = 0.1846$ with $[\underline{\omega}_2, \bar{\omega}_2] = [0.1846, 5.364]$, $\omega_3 = 2.53$ with $[\underline{\omega}_3, \bar{\omega}_3] = \omega_3 = 2.53$, $\omega_4 = 3.96$ with $[\underline{\omega}_4, \bar{\omega}_4] = [1.633, 4.989]$, and $\omega_5 = 4.72$ with $[\underline{\omega}_5, \bar{\omega}_5] = [3.379, 4.72]$. Since $\underline{\omega}_3 = \bar{\omega}_3$, this range is discarded. See Figure 3.8.

- Take $\omega_{m+1} = \infty$ as the last point of local minimum or local maximum of $|G_0(j\omega)|$. Draw the horizontal line of the gain equal to $\lim_{\omega_{m+1} \to \infty} |G_0(j\omega_{m+1})|$. This line may intersect on its left with the gain plot at some frequency, $\underline{\omega}_{m+1} < \omega_{m+1}$. If there does not exist $\underline{\omega}_{m+1}$, then $\omega_{m+1}$ is not needed for our calculations and is discarded. Form one frequency range as $[\underline{\omega}_{m+1}, \bar{\omega}_{m+1}]$, where $\bar{\omega}_{m+1} = \omega_{m+1}$. For the above

example, $\lim_{\omega_6 \to \infty} |G_0(j\omega_6)| = 0$, and this line does not intersect with the

gain plot. Thus, $\omega_6$ is discarded.

It should be pointed out that in a real practice, physical systems restrict

delay and gain ranges. Thus, we suppose that $0 \le L \le L_{max}$ and $0 \le K \le K_{max}$

are of interests for our calculations. The key issue is how many $L_n$ are

necessary to determine the stabilizing ranges.

**Lemma 3.6.** *Let $\phi_i$ be the minimum phase of $G_0(j\omega)$ in $[\underline{\omega}_i, \overline{\omega}_i]$. Then,*

*there holds*

$$L_n(\omega)\big|_{\omega \in [\underline{\omega}_i, \overline{\omega}_i]} > L_{max} \quad for \quad n > n_i ,$$

*where*

$$n_i = \frac{\overline{\omega}_i L_{max} - \phi_i - \pi}{2\pi}. \qquad (3.8)$$

**Proof.** It follows from (3.2) that for $n > n_i$,

$$
\begin{aligned}
L_n &= \frac{\arg[G_0(j\omega)] + (2n+1)\pi}{\omega} \\
&> \frac{\phi_i + (2n_i + 1)\pi}{\omega} > \frac{\phi_i + (2n_i + 1)\pi}{\overline{\omega}_i} > L_{max}
\end{aligned}.
$$

This completes the proof. □

Since $L_n(\omega)\big|_{\omega \in [\underline{\omega}_i, \overline{\omega}_i]} > L_{max}$ with $n > n_i$, $L_n$ with $n > n_i$ is not in the

interesting domain of $0 \le L \le L_{max}$ and will not be needed. This is the case

for each $i$. Thus, the number of boundary functions needed to plot is

$$n_{max} = \max\{\overline{n}_i\} , \qquad (3.9)$$

where $\overline{n}_i$ is the smallest integer such as $\overline{n}_i > n_i$. We draw $L_n$,

$n = 0, 1, ..., n_{max}$, on the plane $(L, k)$ and the resulting curves divide the

rectangular area bounded by $0 \leq L \leq L_{\max}$ and $0 \leq K \leq K_{\max}$ into finite regions. We need an effective way to decide stability of each resulting region.

In the plane $(L, k)$, we can indicate direction of frequency increase with an arrow on a boundary function. The upward arrow indicates increasing controller gain $k$, which corresponds to decreasing process gain $|G_0(j\omega)|$, whereas the downward arrow indicates decreasing controller gain $k$, which corresponds to increasing process gain $|G_0(j\omega)|$. It follows from Lemma 3.2 that if the arrow of $L_n$ is upward, the closed-loop system with $(L, k)$ in the region on the left of $L_n$ has two fewer unstable poles than the closed-loop system with $(L, k)$ in the region on the right of $L_n$. On the other hand, it follows from Lemma 3.3 that if the arrow of $L_n$ is downward, the closed-loop system with $(L, k)$ in the region on the left of $L_n$ has two more unstable poles than the closed-loop system with $(L, k)$ in the region on the right of $L_n$. This fact is stated in the following Corollary 3.1 for easy reference later.

**Corollary 3.1.** *On the plane of* $(L, k)$,

- *if the arrow of $L_n$ is upward, the region on the left hand side of $L_n$ has two fewer unstable pole the region on the right hand side of $L_n$.*

- *if the arrow of $L_n$ is down ward, the region on the left hand side of $L_n$ has two more unstable pole the region on the right hand side of $L_n$.*

If $G_0(0) < 0$, there is the horizontal line $k = \dfrac{1}{|G_0(0)|}$ in the plane $(L, k)$.

This line divides the plane $(L, k)$ into two portions. Firstly, consider the lower portion. Start with the left-most region, that is, the nearest one to the origin. We can determine the number of unstable poles for the system corresponding to each point in this region by looking at only one point inside it. Then, we can infer from Corollary 3.1, the number of unstable poles of each region on its right, one region after another, from left to right. A region is stable if this number is zero. Note that the region near the origin has the same number of unstable poles as that of $G_0(s)$, because, for $(L, k)$ near the origin, the closed-loop system with $kG_0(s)e^{-Ls}$ is close to the open loop $G_0(s)$. Finally, one can repeat the above procedure for the upper portion.

Now, we are ready to propose Algorithm 3.2 to obtain stabilizing gain ranges with respect to delay of a process with non-monotonic gain.

**Algorithm 3.2.** Consider a process with non-monotonic gain.

Step 1. For $\omega = 0$, if $\arg[G_0(0)] = -\pi$, plot the horizontal line,

$$k = \frac{1}{|G_0(0)|} \text{ on plane } (L, k).$$

Step 2. Calculate $n_{\max}$ from (3.9) and plot $L_n$, $n = n_{\min}, n_{\min} + 1, ..., n_{\max}$, on plane $(L, k)$.

Step 3. Start from the left-most region near to the origin and take the number of unstable poles of this region same as that of $G_0(s)$, and then know its stability; count the number of unstable poles of the region, one by one, from left to right, with help of Corollary 3.1, and then know its stability.

Step 4. If $G_0(0) < 0$, there is the horizontal line $k = \frac{1}{|G_0(0)|}$ dividing

the plane $(L,k)$ into the lower and upper portions. Apply the same procedure as for the lower one in Step 3.

**Example 3.2.** Consider a process with time delay,

$$G(s) = \frac{s+1}{s^5 + s^4 + 30s^3 + 10s^2 + 100s + 1} e^{-Ls}$$

This process is stable. The gain plot in Figure 3.9 shows that the gain does not monotonically reduce with frequency and requires us to apply Algorithm 3.2. For Step 1, $G_0(0) = 1$ does not meet (3.3), and produces no line. For Step 2, we have $\omega_1 = 0.89$ with $[\underline{\omega}_1, \overline{\omega}_1] = [0.89, 2.57]$, $\omega_2 = 1.95$ with $[\underline{\omega}_2, \overline{\omega}_2] = [0.10, 1.95]$, $\omega_3 = 3.94$ with $[\underline{\omega}_3, \overline{\omega}_3] = [3.94, 5.39]$ and $\omega_4 = 5$ with $[\underline{\omega}_4, \overline{\omega}_4] = [2.9, 5]$. Let $L_{max} = 25$, we have, $n_1 = 10.26$, $n_2 = 7.6$, $n_3 = 21.8$ and $n_4 = 20.1$. By (3.9), we get $n_{max} = 22$. The maximum phase of $G_0(j\omega)$ is $\Phi = 0$, and (5) gives $n > -0.5$, so $n_{min} = 0$. The 23 boundary functions $L_i$, $i = 0, 1, ..., 22$, are drawn on plane $(L,k)$ in Figure 3.10. These boundary functions divide the plane $(L,k)$ into regions. Step 3 tells that the left-most region near to the origin has the same number of unstable poles with $G_0(s)$, which has no unstable poles. Thus this region is stable and shaded in green. It is found that all the other regions are unstable.
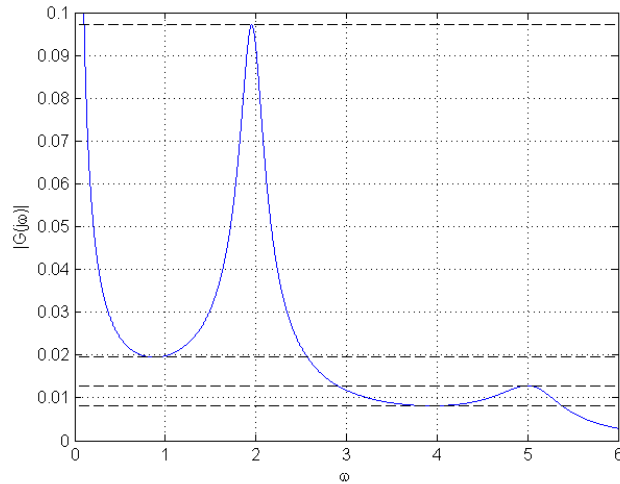
Figure 3.9: Gain plot of $G_0(s)$ of Example 3.2
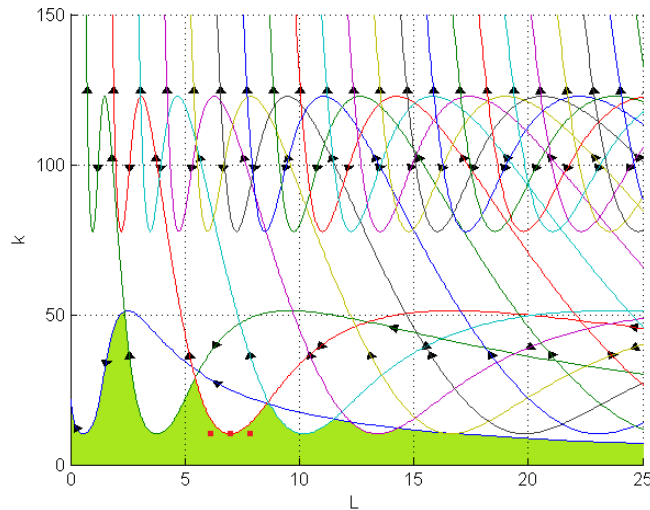


Figure 3.10: Stabilizing region of Example 3.2

To verify our Lemma 3.4, we take $\omega = 1.95$, at which the gain rate of $kG_0(s)e^{-Ls}$, with $(L,k) = (6.99, 10.3)$ marked with a square, is zero. Its Nyquist plot has unique intersection with the critical point. Let look at the two points $(L,k) = (6.29, 10.3)$ and $(L,k) = (7.69, 10.3)$, also marked in a square, which are respectively on the left hand side and the right hand side of $(L,k) = (6.99, 10.3)$. Observe that both points stay in the same region, and thus they give the closed-loop system with $kG_0(s)e^{-Ls}$ the same number of

unstable poles, indeed, as predicted by our Lemma 3.4.

**Example 3.3.** Consider an unstable delay process,

$$G(s) = \frac{-80(s+1)}{(s+10)(s^2 - 2s + 30)} e^{-Ls}.$$

This process has two unstable poles at $s = 1 \pm j5.3852$. Its gain does not monotonically reduce, and Algorithm 3.2 should be used. $G(0) = -0.267$ meets (3.3) and produces the horizontal line $k = 3.75$ as in Figure 3.17. We have $\omega_1 = 0$ with $[\underline{\omega_1}, \overline{\omega_1}] = [0, 16.93]$. With $L_{max} = 5$, $n_{max}$ is found to be 14. The maximum phase of $G_0(j\omega)$ is $\Phi = 0.41$, and (5) gives $n > -0.5653$, so $n_{min} = 0$. We plot $L_i$, $i = 0,1,...,14$, in the plane $(L,k)$ as in Figure 3.11. These boundary functions divide the plane $(L,k)$ into regions. The left-most region near the origin in the lower portion has the same number of unstable poles as $G_0(s)$, which has two unstable poles. With help of Corollary 3.1, the number of unstable poles of the region, one by one, from left to right is obtained. The stable region is the shaded one in Figure 3.11. In the upper portion of the plane $(L,k)$, we take $(L,k) = (0.1, 4)$ in the left-most region to find the number of unstable poles of closed-loop system with $kG(s)$. Its Nyquist plot in Figure 3.12 shows that this closed-loop system has one unstable pole. All the other regions in the upper portions are unstable
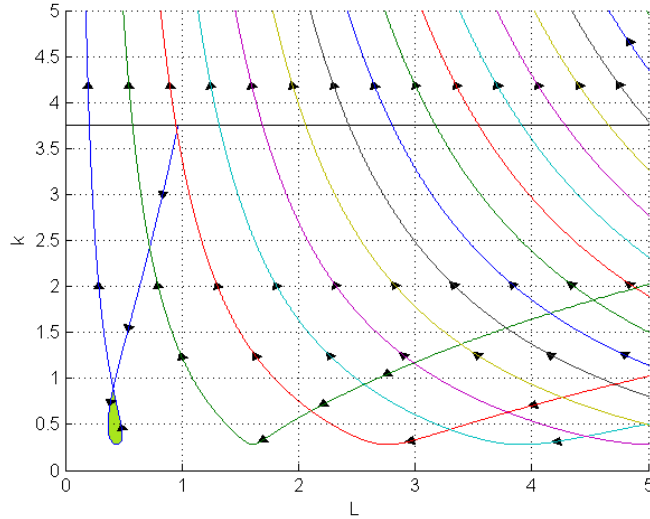
Figure 3.11: Stabilizing region of Example 3.3
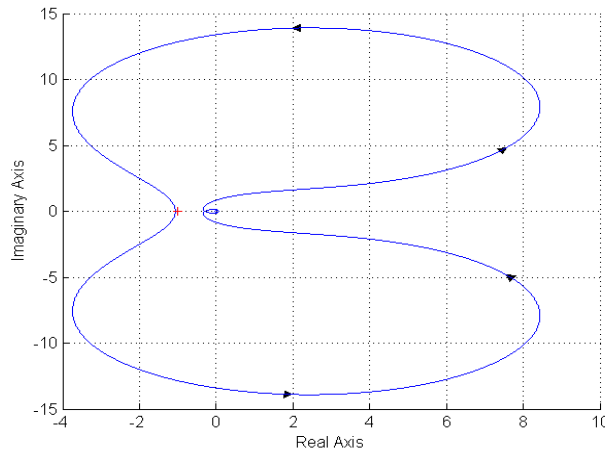


Figure 3.12: Nyquist plot of Example 3.3 with $(L, k) = (4, 0.1)$

In all three examples considered so far, we have $n_{\min} = 0$. This may not always be the case. For instance, consider the process in Example 3.3 but change its sign to

$$G_1(s) = -G(s) = \frac{80(s+1)}{(s+10)(s^2 - 2s + 30)} e^{-Ls}.$$

For this process, the maximum phase of $G_0(j\omega)$ is $\Phi = 3.552$, and (3.5) gives $n > -1.065$, so $n_{\min} = -1$. The stability result is exhibited in Figure 3.13, where the stable region is on the left hand side of $L_{-1}$.
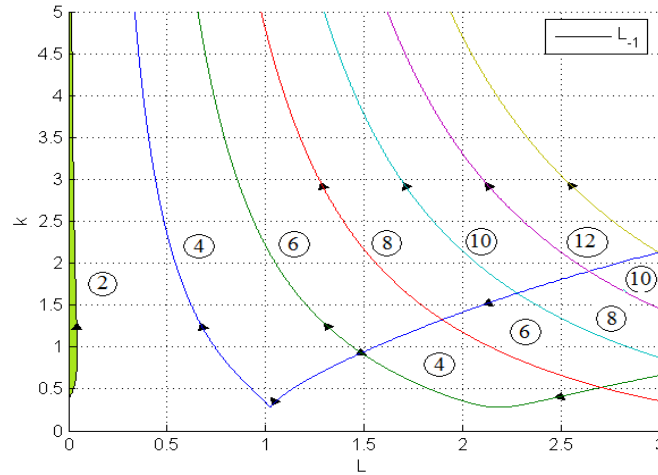
Figure 3.13: Stabilizing region of $G_1(s)$ of Example 3.3

## 3.6. Conclusion

In this chapter, a graphical method for exactly computing the stabilizing gain and delay ranges is presented. This is achieved by determining the boundary functions which may change system's stability. The proposed method is very general and applicable to any strictly proper process, and thus significantly relaxes the restrictions with the existing works. It is also powerful and can produce the exact and complete set of controller gain and delay for a stable closed-loop, which is hard to find with analytical methods. A variety of examples are given and some of them show very complex stabilizing ranges which are out of imagination.

Note that the time delay case has not been addressed in D-decomposition literature. In D-decomposition literature, coefficients of the characteristic equation must appear as a linear combination or as a polynomial of the two parameters of interest. In such a case, the number of solutions of the real part and imaginary part equations is finite since the equations are polynomial. However, when the time delay is considered as a parameter of interest, it

introduces the transcendental element in characteristic equation and coefficients no longer occur in polynomial form. The real and imaginary equations become trigonometric equations which are difficult to solve and have infinite number of solutions.

The present work solely focuses on time delay processes because time delay is important in process control. It may cause instability, oscillation and poor performance to the control loop. This chapter provides new development with advantages that fill the gap in D-decomposition method for time delay processes. Due to the nature of exponential function introduced by time delay in open loop transfer function, we change D-decomposition technical approach with our approach as described in the Introduction paragraph to find the direct solution without the need of solving complex equations. It should be emphasized that such a change and new development in this chapter are necessary for delay processes, since the time delay case gives infinite number of solution curves. The existing D-decomposition method fails because it is impossible to find and plot all these solutions.

Our work also provides essential techniques to reduce the number of solution curves needed to be plotted as much as possible by careful studies of the solution curves properties. This technical development is documented in the paper as six Lemmas which are all new and novel. In the end, for the monotonic gain case, we need to draw only one solution curve, while for the non-monotonic case, we need to draw several solution curves only. This produces great simple, efficient and elegant solution.

Note also that after plotting solution curves in (k, L) plane, one still needs to determine the stability of each region. This is not simple task if there are

many regions and the number of poles of the system is large or infinite. The D-decomposition method shades all solution curves to find the regions with maximum number of stable poles; and subsequently, verifies if those regions are indeed stable regions. The shading rule uses the sign of the Jacobian to decide which sides of the curves are corresponding to the left half plane. This means the Jacobian equation needs to be solved to determine its sign in different ranges of frequency. This additional equation solving could be troublesome, especially for the nonlinear case, and adds computational load and complexity to the method. Further, even after all curves are shaded, the procedure of finding the regions with most stable poles is not systematic. The stability test for those favorable regions is not straightforward, either. They need to calculate all roots of the characteristic equation corresponding with an arbitrary point in a region and to compare the number of stable roots with the total number of roots of that equation. This method works for simple processes but it may not work for other complex processes.

On the other hand, our method is able to significantly simplify the stability check and even identify stable regions by inspection without any numerical computational check. The proposed six Lemmas show how a delay perturbation changes the number of the Nyquist curve's encirclements with respect to the critical point as well as the change to the number of unstable/stable poles. This turns out to depend on the rate of gain change, which is novel and has never been discovered before. This is obviously different from Jacobian based D-decomposition method.

More specifically, with helps of newly developed Lemmas, we establish 2 Algorithms corresponding with processes with monotonic gain reduction and

processes with non-monotonic gain. In many cases, stability test is not necessary for any region. It is because, we already know the number of unstable poles in one region connected to open loop, which is the number of unstable poles of the process. We can then infer the number of unstable poles in other regions with help of our proposed corollaries to the lemmas. Thus, the stable regions are found trivially in most of cases. This is an obvious advantage of our method over D-decomposition method and is possible since we adopt control view with open and closed loops in mind. Moreover, Nyquist chart can determine stability while D-decomposition method can never get them because it starts from characteristic equation in mind and focuses on solving it for the roots.

# Chapter 4

# Stabilizing Loop Gain and Delay for Bi-proper Processes

## 4.1. Introduction

No manufacturing process can be put into operation until it has been proven to be stable, and stability of a system is thus an important and basic problem in process control. Even though this problem has been studied for decades, it is still an active field of investigation in control society. Moreover, obtaining a complete set of stabilizing parameters set can be extremely beneficial for other problems in controller design, such as optimization of some performance criteria. Therefore, significant effort has been spent to find the complete stabilizing ranges of system or controller parameters. Delay free processes are relatively simple as its spectrum is finite. However, this is not the case for processes with time delay under feedback control. Time delay, which is usually encountered in industrial processes, can make process stabilization more difficult because it introduces infinite number of poles into the system characteristic equation. The problem has been studied extensively in control community [10]–[14], [16], [31], [33], [34], and most of the solutions focus on finding analytical solutions for limited classes of delay processes. Thus, a graphical method should be a good alternative to solve the stabilizing problem for general delay processes.

One of the popular approaches in graphical methods is D-decomposition technique, which maps the stability boundary from the root

plane into the parameter space. The D-decomposition method solves the characteristic equation of a system with a set of parameters for all of its imaginary roots. Then, the resulting solutions are drawn on parameter space. They divide the parameter space into regions, in which the number of positive real part roots is invariant. The stable regions are those regions for which this number is zero. A great number of works have applied this method for processes with fixed time delay [4], [6], [26], [51]–[55]. In these works, the characteristic equation appears as a polynomial of parameters while the time delay is fixed and not a parameter. Because of such restriction, the number of solution in the parameter space is finite and the stable regions can be found by checking stability of all regions.

But there are inevitable uncertainties in the process and its models. Delay cannot be known precisely in practice. It is uncertain and usually is known to be in a range. Delay should be treated as a parameter in stability analysis. When time delay is one of the parameters, the number of boundary solutions in the D-decomposition framework is no longer finite but infinite. Thus, it is impossible to draw all solutions and look for the stable regions. The delay case is simply mentioned in [3], which is in Russia, and in its English translation [2], provided no technical details on how to handle the infinite number of solutions. Therefore, it is impractical to use the method there. In face of such a great difficulty, our graphical method in previous chapter can be used to compute the exact stabilizing gain and delay ranges for a strictly proper process. To effectively reduce the infinite number of boundary curves due to the delay, properties of these curves were investigated thoroughly. This greatly helped to simplify the stability determination of the resulting regions.

As a result, all stable regions could be identified and the stabilizing gain ranges were obtained in term of delay. It however assumed strict properness of the process.

This chapter continues our previous work focusing on the case of processes with bi-proper transfer functions. Although they are less popular in industry, such processes may be found in practices such missiles [35] and robotic processes [36]. Thus, they should be addressed for general applicability and completion of the method. Extension the method to accommodate the bi-proper processes also occurred to complementary root locus method [37]. Note that the generalization from a strict proper case to a bi-proper case is not trivial for our previous method. If $G_0(s)$ is a strict proper transfer function, its gain eventually reduces to zero, i.e. $\lim_{\omega \to \infty} |G_0(j\omega)| = 0$, and its Nyquist plot ends at the origin. $kG_0(s)e^{-Ls}$ will always go to the origin at $\omega = \infty$ for any finite value of $k$, regardless of $L$. Therefore, at $\omega = \infty$, does not affect closed-loop stability, and can be excluded from stability analysis. As a result, this will significantly simplify technical development in previous chapter. On the other hand, a bi-proper process has a non-zero finite gain at infinity frequency. As a result, this creates additional scenarios to consider, such as monotonic gain increase, and infinite encirclements of the critical point by Nyquist curve of a delay process. The most challenging issue is that there are infinite boundary functions within a limited delay range, which is impossible to draw and thus infer stability regions. Whereas it is shown that finite boundary functions are sufficient to determine stability region for a strictly proper case.

For example, consider the following strict process:

$$G(s) = \frac{(s^2+1.63s+20.69)(s^2+1.51+1.79)(s^2+0.46s+1.44)}{(s^2+2s+65)(s^2+s+0.5)(s^2+1.4s+4.49)(s^2+s+3)}e^{-Ls}.$$

It follows from Chapter 3 that 20 is the maximum number of boundary functions that can intersect with each other within the rectangular bounded by $0 \le L \le 10$ and $0 \le k \le 200$ of the plane $(L,k)$. Indeed, as can be seen in Figure 4.1, there are 26 boundary curves inside the rectangular area but only $L_n$, $n = 0,1,...,19$, intersect with each other. Thus, for this process, we only need to draw 20 boundary functions in order to find the stable regions.
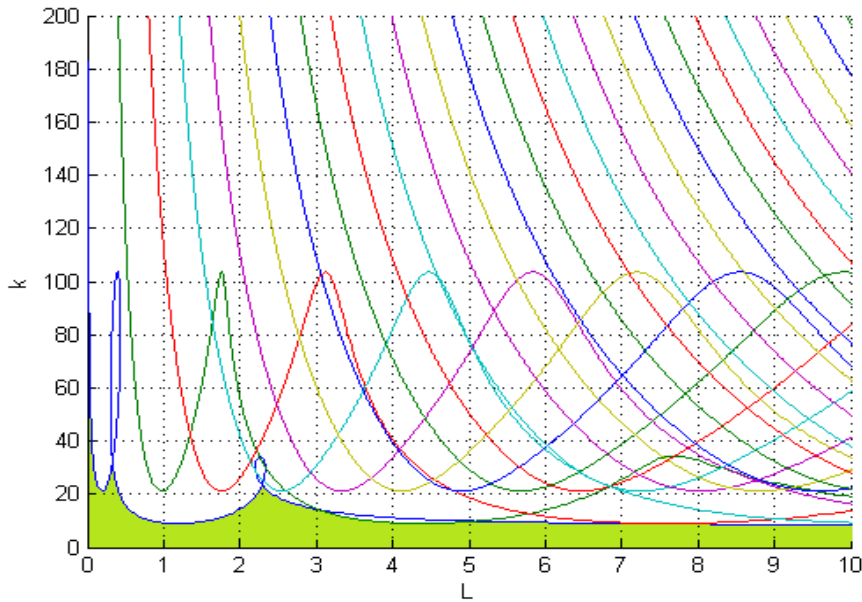


Figure 4.1: Stabilizing graph of $G(s)$

When two zeros are added, the above process becomes bi-proper:

$$G_1(s) = \frac{(5.1-s)(s+6.9)(s^2+1.63s+20.69)(s^2+1.51+1.79)(s^2+0.46s+1.44)}{(s^2+2s+65)(s^2+s+0.5)(s^2+1.4s+4.49)(s^2+s+3)}e^{-Ls}$$

,

For which, an infinite number of boundary functions intersect with each other within the rectangular, as can be inferred from Figure 4.2. However, it is impossible to plot infinite boundary functions and check the stability of all

resulting regions. This exhibits a significant challenge for the bi-proper processes. This paper will show that not all of the intersections between boundary functions are needed, and only a finite number of boundary functions are required to find stabilizing ranges. For $G_1(s)$ above, this number is 14, so we can plot all these boundary functions on the plane $(L, k)$ and find the stable region as in Figure 4.3, where the stable region is shaded.
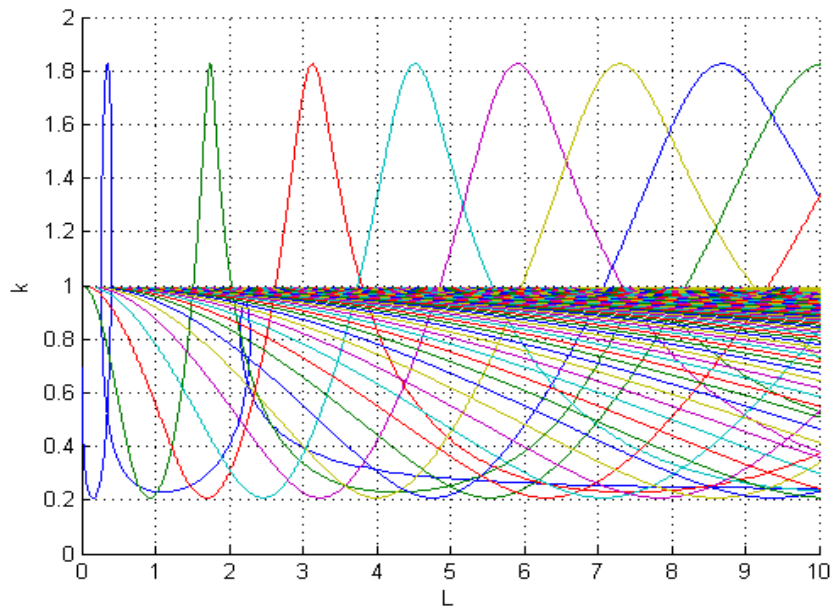


Figure 4.2: Boundary curves graph of $G_1(s)$
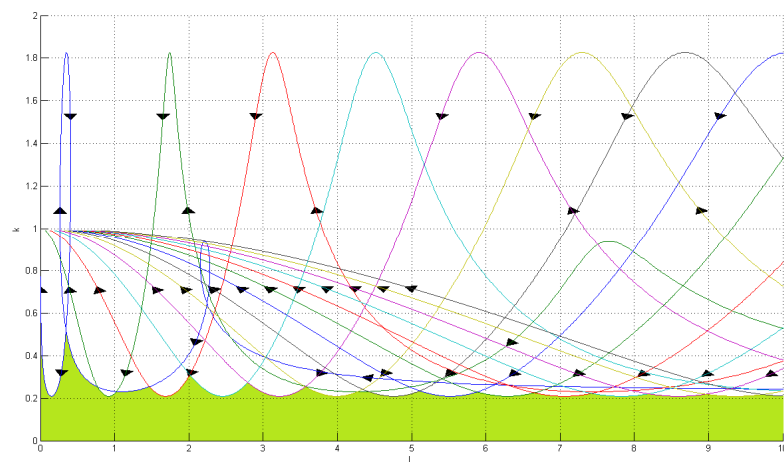


Figure 4.3: Stabilizing Graph of $G_1(s)$

This chapter will address all technical issues pertaining to a bi-proper case. In particular, we provide some theoretical results which enable us to determine stability regions with finite number of boundary functions. In the end, our method becomes complete in the sense that it covers all possible processes and thus generally applicable. The remainder of the chapter is organized as follows. Section 4.2 presents the problem of computing the stabilizing parameter ranges for a bi-proper process and preliminaries for solving such problem. The simplified solution for processes with monotonic gain is given in Section 4.3. In Section 4.4, the solution for processes with non-monotonic gain is developed. Finally, Section 4.5 draws the conclusions.

## 4.2. The Problem Formulation and Preliminaries

A bi-proper process is a process that has finite non-zero gain at infinity frequency. In this paper, we consider the control configuration under the conventional unity output feedback in Figure 1.1, where $G(s) = G_0(s)e^{-Ls}$ is a process with $G_0(s)$ being a *fixed* bi-proper transfer function with no delay, and $K(s) = k$ is a proportional controller. The stabilizing gain problem is formulated as follows.

**Problem 4.1.** For a process, $G(s) = G_0(s)e^{-Ls}$, under the proportional controller, $K = k$, with the gain $k > 0$, find the regions in the 2D space, $(L, k)$, such that their interior points give stable closed-loop while their boundary points produce unstable closed-loop (with poles in the closed right half plane).

Let the open-loop transfer function be $Q(s) = ke^{-sL}G_0(s)$. Like what was seen in previous chapter that the closed-loop system may change its stability

only when $L$ and $k$ satisfy, for $\omega > 0$,

$$k = \frac{1}{|G_0(j\omega)|}, \; G_0(j\omega) \neq 0, \qquad\qquad \text{(4.1)}$$

$$L_n = \frac{\arg[G_0(j\omega)] + (2n+1)\pi}{\omega}, n = 0, 1, 2, \ldots; \qquad \text{(4.2)}$$

while for $\omega = 0$ and with $k > 0$ the condition becomes

$$\arg[G_0(0)] = -(2n+1)\pi, \qquad\qquad \text{(4.3)}$$

under which,

$$k = \frac{1}{|G_0(0)|}, \quad L \geq 0. \qquad\qquad \text{(4.4)}$$

For each $n$, equations (4.1) and (4.2) define a boundary function, which relates all $L$ and $k$ that makes the Nyquist plot of the $Q(s) = ke^{-sL}G_0(s)$ intersect with the critical point. Equation (4.4) defines another boundary function which is actually a horizontal line in the plane of $(L, k)$. The plot of all the boundary functions defined by (4.1), (4.2) and (4.4) divide the plane $(L, k)$ into regions. Each interior point in a so-formed region gives the corresponding closed-loop system with the same number of unstable poles.

By convention, let

$$\arg[G_0(0)] = \begin{cases} 0, \text{ if } G_0(0) > 0; \\ -\pi, \text{ if } G_0(0) < 0. \end{cases}$$

Note that only non-negative delay is realistic, which requires (2) to meet

$$L_n = \frac{\arg[G_0(j\omega)] + (2n+1)\pi}{\omega} \geq 0.$$

This yields

$$n \geq \frac{-\Phi - \pi}{2\pi}, \qquad\qquad \text{(4.5)}$$

where $\Phi$ is the maximum phase of $G_0(j\omega)$. Denote $n_{\min}$ as the smallest integer number that satisfies (4.5). Thus, (4.2) is valid only for $n = n_{\min}, n_{\min} + 1, ...$, which is used in the rest of this chapter.

In general, all the boundary functions $L_n$ need to be plotted on the plane of $(L, k)$ in order to determine the stability of regions. However, there are an infinite number of boundary functions $L_n$, and, an infinite number of the resulting regions. It is impossible to plot and check the stability of all these regions. To overcome this problem, we develop new Lemmas beside those that are proved in Chapter 3. For convenient reference purpose, we include Lemmas from Chapter 3 as well as new Lemmas in the new order as following:

**Lemma 4.1.** *For* $m \neq n$ *, a boundary function* $L_m$ *intersects with another* $L_n$ *only if there are* $\omega_m$ *and* $\omega_n$ *with* $\omega_m \neq \omega_n$ *such that* $|G_0(j\omega_m)| = |G_0(j\omega_n)|$.

**Lemma 4.2.** *Let the Nyquist plot of the open-loop* $kG_0(s)e^{-sL}$ *for* $\omega > 0$ *has the unique intersection with the critical point of* $(-1 + j0)$ *at a frequency* $\omega = \omega^* \in (0, \infty)$. *If the gain of its frequency response decreases at this frequency, that is,* $d\left|kG_0(j\omega)e^{-j\omega L}\right|/d\omega\Big|_{\omega=\omega^*} < 0$, *then the closed-loop system with* $kG_0(s)e^{-s(L+\varepsilon)}$ *has two more unstable poles than the closed-loop system with* $kG_0(s)e^{-s(L-\varepsilon)}$ *for some* $\varepsilon > 0$.

**Lemma 4.3.** *Let the Nyquist plot of the open-loop* $kG_0(s)e^{-sL}$ *for* $\omega > 0$ *has the unique intersection with the critical point of* $(-1 + j0)$ *at a frequency* $\omega = \omega^* \in (0, \infty)$ *. If the gain of its frequency response increases at this*

*frequency, that is,* $d\left|kG_0(j\omega)e^{-j\omega L}\right|/d\omega\Big|_{\omega=\omega^*}>0$, *then the closed-loop system with* $kG_0(s)e^{-s(L+\varepsilon)}$ *has two fewer unstable poles than the closed-loop system with* $kG_0(s)e^{-s(L-\varepsilon)}$ *for some* $\varepsilon>0$.

**Remark 4.1.** Let $\bar{\omega}$ be the largest frequency which meets $d\left|kG_0(j\omega)e^{-j\omega L}\right|/d\omega=0$. Then, the sign of $d\left|kG_0(j\omega)e^{-j\omega L}\right|/d\omega$ does not change for $\omega\in(\bar{\omega},\infty)$. Since the gain rate of a rational transfer function is continuous, there are three possible cases for the gain rate in $\omega\in(\bar{\omega},\infty)$:

1) $d\left|kG_0(j\omega)e^{-j\omega L}\right|/d\omega<0$ : the gain monotonically decreases for $\omega\in(\bar{\omega},\infty)$. In the case of intersection, **Lemma 4.2** is applicable for this case.

2) $d\left|kG_0(j\omega)e^{-j\omega L}\right|/d\omega>0$ : the gain monotonically increases for $\omega\in(\bar{\omega},\infty)$. In the case of intersection, **Lemma 4.3** is applicable for this case.

3) $d\left|kG_0(j\omega)e^{-j\omega L}\right|/d\omega=0$: the gain rate is zero for $\omega\in(\bar{\omega},\infty)$. Since the transfer function is a rational function, this implies the gain rate is always zero, i.e. the gain is constant for every frequency. In this case, variation of $L$ does not affect the stability of the closed loop system. Only the change in controller gain $k$ may affect the stability. For $L>0$, if the loop gain $\left|kG_0(j\omega)\right|>1$, the Nyquist plot has infinite number of clockwise encirclement of the critical point; if $\left|kG_0(j\omega)\right|<1$, the Nyquist plot has no clockwise encirclement of the critical point. Thus, for a process with constant gain $\left|G_0(j\omega)\right|=C$, the stabilizing gain range is $k<\dfrac{1}{C}$ if $G_0$ is stable and null if $G_0$ is unstable. The stabilization of a bi-proper process with constant gain is, therefore, fully determined.

A bi-proper $G_0(s)$ has its gain at infinity frequency which is bounded but non-zero, and the Nyquist curve may intersect with the critical point at this frequency. Let

$$k_\infty = \lim_{\omega \to \infty} \frac{1}{|G_0(j\omega)|}. \qquad (4.6)$$

For $k > k_\infty$, the final gain of $kG_0(j\omega)e^{-Ls}$ is greater than 1. Moreover, with nonzero delay $L$, the phase of $kG_0(s)e^{-sL}$ decreases with frequency, implying the infinite number of clockwise encirclements of the Nyquist plot with regard to the critical point.

**Lemma 4.4.** *Let $G_0(s)$ be a bi-proper process. Then, for $L > 0$ and $k > k_\infty$, the Nyquist plot of $kG_0(s)e^{-sL}$ has infinite number of clockwise encirclement.*

**Remark 4.2.** It can be deduced from Lemma 4.4 that for $L > 0$ and $k > k_\infty$, the closed-loop system with $kG_0(s)e^{-sL}$ is unstable. Thus, the gain range to consider for stabilizing problem is limited to $0 \le k \le k_\infty$. As a result, all frequencies that give the process gain smaller than process gain at infinity, i.e. $\omega$ such that $|G_0(j\omega)| < \lim_{\omega \to \infty}|G_0(j\omega)|$, are excluded from calculations. This reflexes the special feature of a bi-proper process and greatly simplifies the computation of boundary functions. However, Lemma 4.4 holds only for $L > 0$. On the other hand, for $L = 0$, the process has no delay and the stabilizing gain ranges can be determined for delay-free $G_0$, which is available and thus excluded. Thus, we suppose $L > 0$ for the rest of this paper.

It should be pointed out that in a real practice; physical systems restrict

delay and gain. Thus, we suppose that $0 \le L \le L_{max}$ and $0 \le k \le \overline{k}$ are the physical constraints of delays and gain for our process. Furthermore, it is deduced from Remark 4.2 that, for stabilizing a bi-proper process, the controller gain is also limited to $0 \le k \le k_{\infty}$. Hence, we define $k_{max} = \min\{\overline{k}, k_{\infty}\}$ and the stabilizing graph is confined to the rectangular area bounded by $0 \le L \le L_{max}$ and $0 \le k \le k_{max}$ of the plane $(L, k)$.

**Lemma 4.5.** *Let $\phi_{min}$ be the minimum phase of $G_0(j\omega)$ in $[\omega_1, \omega_2]$. Then, there holds*

$$L_n(\omega)\big|_{\omega \in [\omega_1, \omega_2]} > L_{max} \quad for \quad n > n_{max},$$

*where $n_{max}$ is the smallest integer such that*

$$n_{max} \ge \frac{\omega_2 L_{max} - \phi_{min} - \pi}{2\pi}. \tag{4.7}$$

**Lemma 4.6.** *Let $L_n$ be the boundary function defined as in (3.2), then* $\lim_{\omega \to \infty} L_n(\omega) = 0$.

**Proof.** It follows that

$$L_n\big|_{\omega = \infty} = \frac{\arg[G_0(j\omega)] + (2n+1)\pi}{\omega}\bigg|_{\omega = \infty} = 0,$$

for any finite *n,* since $G_0(s)$ does not contain time delay and its phase is finite, too.

## 4.3. Processes with Monotonic Gain

For processes with strictly proper transfer function, the gain eventually reduces to zero, and the class of monotonic gain (either always increasing or decreasing) is only applicable for the processes with monotonic gain reduction.

However, for bi-proper processes, since the gain is non-zero at infinity frequency, the class of monotonic gain includes both increasing and decreasing cases.

A transfer function $G_0(s)$ is said to have monotonic gain increase if there holds $|G_0(j\omega_1)| < |G_0(j\omega_2)|$ for $0 \le \omega_1 < \omega_2$. For such a case, the maximum process gain is the gain at infinity frequency. It follows from Remark 4.2 that the whole range of frequency should be excluded from calculation of boundary functions. Thus, there is no $L_n$ in the rectangular area given by $0 \le k \le k_{max}$ and $L > 0$. Observe that, because the loop gain is less than one, the Nyquist plot of $kG_0(s)e^{-sL}$ corresponding to any point $(L, k)$ in this rectangular area will not have any encirclement of the critical point. Hence, this area is stable if $G_0$ is stable and vice versa. We then have the following proposition.

**Proposition 4.1.** Let $G_0$ be a process with monotonic gain increase, then the region bounded by $L > 0$ and $k_{max} > k > 0$ of the plane $(L, k)$ is stable (or unstable) if $G_0$ is stable (or unstable).

**Example 4.1.** Consider the following process,

$$G(s) = \frac{(s+1)(s+2)}{(s+3)(s+4)} e^{-Ls},$$

This process is stable. One sees from gain plot of $G_0(s) = \frac{(s+1)(s+2)}{(s+3)(s+4)}$ in Figure 4.4 that the process has monotonic gain increase, so Preposition 4.1 is applicable. Since $\lim_{\omega \to \infty} |G_0(j\omega)| = 1$, $k_{max} = k_\infty = 1$. $G_0(s)$ is stable, and the region below $k = 1$ is the stable region, that is, the process with any delay is

stabilizable providing that $k < 1$.
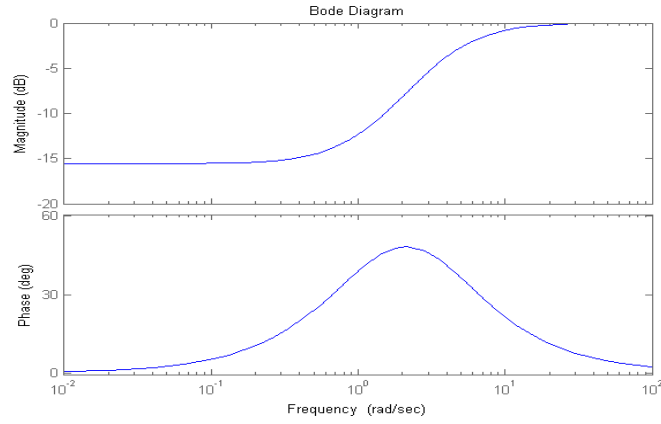


Figure 4.4: Bode plot of $G_0(s)$ of Example 4.1

**Example 4.2.** Consider the following process,

$$G(s) = \frac{s+0.5}{s-1}e^{-Ls},$$

The process has one unstable pole at $s=1$. The gain of $G_0(j\omega)$ increases monotonically with frequency and $k_{max} = k_\infty = 1$. Since this process is unstable, the region below $k=1$ is unstable.
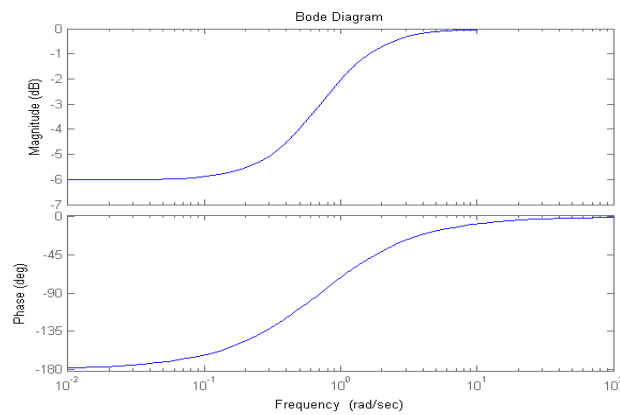


Figure 4.5: Bode plot of $G_0(s)$ of Example 4.2

It follows from Remark 4.2 that, before calculating boundary functions, we discard all frequencies with $|G_0(j\omega)| < \lim_{\omega \to \infty} |G_0(j\omega)|$. Note that after such

procedure, the process may have monotonic gain decrease for the remaining frequencies. For such a process as well as process with monotonic gain decrease for the whole range of frequencies, we can apply the counterpart for a strictly proper process to determine stable regions.

**Algorithm 4.1**. Consider a process with monotonic gain reduction.

Step 1. For $\omega = 0$, if $\arg[G_0(0)] = -\pi$, plot the horizontal line, $k = \dfrac{1}{|G_0(0)|}$, on the plane $(L, k)$. The region below this line is stable (or unstable) if $G_0$ is stable (or unstable).

Step 2. For $\omega \neq 0$, plot $L_{n_{min}}$ with (3.1) and (3.2) on the plane $(L, k)$. If $G_0(0) > 0$, the region on the left hand side of $L_{n_{min}}$ is stable (or unstable) if $G_0(s)$ is stable (or unstable). If $G_0(0) < 0$, check stability of the region on the left hand side of $L_{n_{min}}$.

**Example 4.3.** Consider a process,

$$G(s) = \frac{s^2 + s + 1}{(s-1)(s+0.1)} e^{-Ls}.$$

This process has one unstable pole at $s = 1$. Its gain does not monotonically change with frequency. However, note that $k_\infty = 1$ and $k$ for the boundary function $L_n$ is greater than $k_\infty$ for $\omega \in [0.7016, \infty]$. Thus $\omega \in [0.7016, \infty]$ is not of interests for our calculations. For $\omega \in [0, 0.7016]$, the gain decreases monotonically so that we can apply Algorithm 4.1. For Step 1, $G_0(0) = -10$ meets (3.3), and produces the horizontal line $k = 0.1$ in Figure 4.7. For Step 2, we have maximum phase of $G_0(j\omega)$ is $\Phi = 0$, and (3.5) gives $n > -0.5$ so $n_{min} = 0$ and $L_0$ is plotted on the plane $(L, k)$. Since $G_0(0) < 0$, we take

$(L, k) = (0.1, 0.7)$ in the region on the left hand side of $L_{n_{\min}}$ to check whether or not it is stable. Its Nyquist plot in Figure 4.8 shows that the closed-loop system has no unstable pole. This is the only stable region and shaded in green as in Figure 4.7.
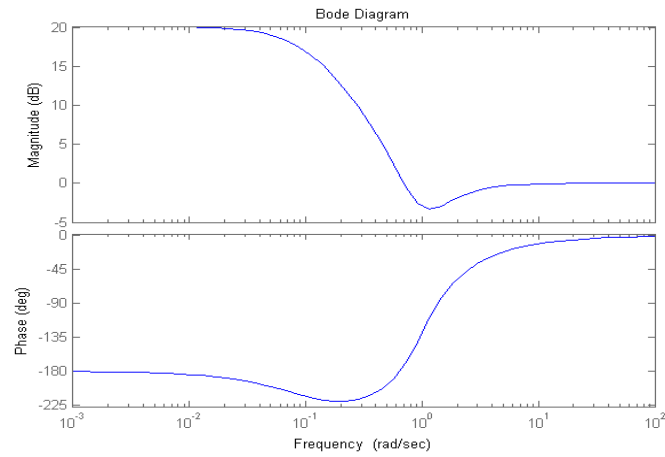

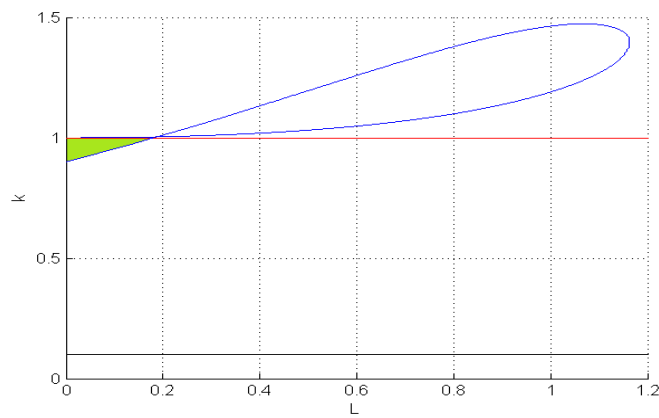
Figure 4.6: Bode plot of $G_0(s)$ of Example 4.3



Figure 4.7: Stabilizing graph of Example 4.3
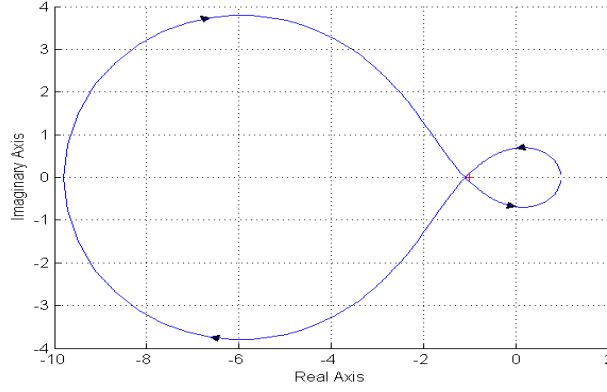
Figure 4.8: Nyquist plot of Example 4.3 with $(L, k) = (0.97, 0.001)$

## 4.4. Processes with Non-monotonic Gain

In this section, we consider a process that does not have monotonic gain change. For such a process, its gain may increase first and then decrease. As a result, there exist two or more frequencies with the same gain. It follows from Lemma 4.1 that the corresponding boundary functions may intersect with each other at these frequencies. In such a case, the stabilizing regions cannot be simply obtained by plotting only one boundary function as for processes with monotonic gain but call for plotting all boundary curves that may intersect with each other. In order to obtain the stabilizing ranges, we need to determine how many boundary functions are necessary to draw in the rectangular area bounded by $0 \leq L \leq L_{\max}$ and $0 \leq k \leq k_{\max}$ of the plane $(L, k)$.

It is worthy of remark that, for a strictly proper process, the number of boundary functions in any rectangular area of the plane $(L, k)$ is finite for a limited controller gain $k_{\max}$. This is because there holds $|kG_0(j\omega)| = 1$ on any boundary function, which then excludes from consideration those frequencies at which $|G_0(j\omega)|k_{\max} < 1$, which is true for a frequency large enough but finite as the gain of a strictly proper process eventually goes to zero as the

88

frequency goes to infinity. This implies that the range of frequency that defines the boundary functions is finite and so is $n_{max}$ from (4.7). However, it is not the case for a bi-proper process, since its gain is nonzero at infinity frequency, and $|G_0(j\omega)|k_{max} < 1$ may never hold for any large frequency. In addition, it follows from Lemma 4.6 that $\lim_{\omega \to \infty} L_n(\omega) = 0$. Thus, both coordinates of $(L, k)$ might stay within the rectangular area bounded by $0 \leq L \leq L_{max}$ and $0 \leq k \leq k_{max}$, and it could be infinite number of boundary functions there. This poses a great challenge. Our main task at hands is to determine all the stable regions inside it without need to draw infinite number of boundary functions which is impossible to do.

In the plane of $(L, k)$, we indicate direction of frequency increase with an arrow on a boundary function. The upward arrow indicates increase of controller gain $k$, which corresponds to decrease of the process gain $|G_0(j\omega)|$, whereas the downward arrow indicates decrease of controller gain $k$, which corresponds to increase of the process gain $|G_0(j\omega)|$. It follows from Lemma 4.2 that if the arrow of $L_n$ is upward, the closed-loop system with $(L, k)$ in the region on the left of $L_n$ has two fewer unstable poles than the closed-loop system with $(L, k)$ in the region on the right of $L_n$. On the other hand, it follows from Lemma 4.3 that if the arrow of $L_n$ is downward, the closed-loop system with $(L, k)$ in the region on the left of $L_n$ has two more unstable poles than the closed-loop system with $(L, k)$ in the region on the right of $L_n$. Thus, if we follow the direction of the arrow, the region on the left hand side of any boundary curve has fewer numbers of unstable poles than

89

the region on the right hand side. For each boundary curve, we shade this region of the left hand side.

**Lemma 4.7.** The regions with the minimum number of unstable poles are the intersection of all the shaded regions. And the stable regions are necessarily in the intersection of all the shaded regions.

**Proof.**   Let $L_n$ and $L_m$ be two arbitrary boundary functions.

- $L_n$ and $L_m$ do not intersect with each other. Without loss of generality, we suppose that $n < m$, and $L_n$ is on the left hand side of $L_m$. These two boundary functions divide a rectangular area of plane $(L, k)$ into three regions. Let the region on the left hand side of $L_n$ be $S_1$, the region in between $L_n$ and $L_m$ be $S_2$ and the region on the right hand side of $L_m$ be $S_3$. At the same frequency, the arrows along both boundary functions have the same direction, thus the shaded regions of $L_n$ and $L_m$ are on the same side. If the arrow is upward in general (Figure 4.9.a), the shaded region of $L_n$ is $S_1$, and the shaded region of $L_m$ is $S_1 \cup S_2$. The intersection of these two shaded regions is $S_1$. It follows from Lemma 4.2 that $S_1$ is the region with the minimum number of unstable poles. Similarly, if the arrow is downward in general, the shaded region of $L_n$ is $S_2 \cup S_3$, and the shaded region of $L_m$ is $S_3$. The intersection of these two shaded regions is $S_3$ (Figure 4.9.b). It follows from Lemma 4.3 that $S_3$ is the region with the minimum number of unstable poles. Thus, in both cases, the region with the minimum number of unstable poles is the intersection of the two shaded regions.

90
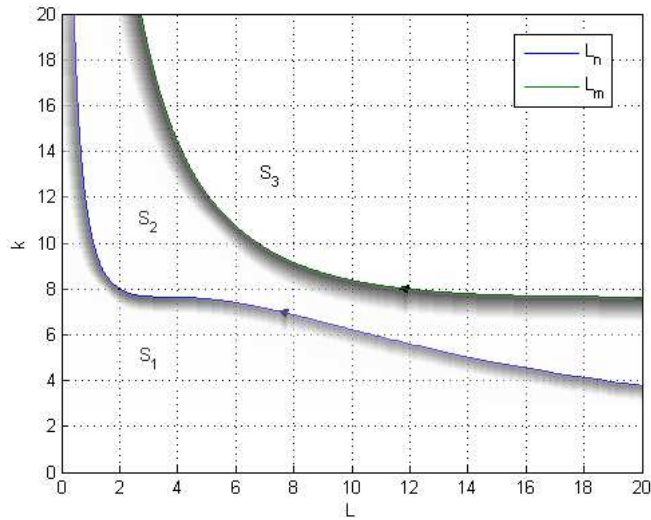
a)
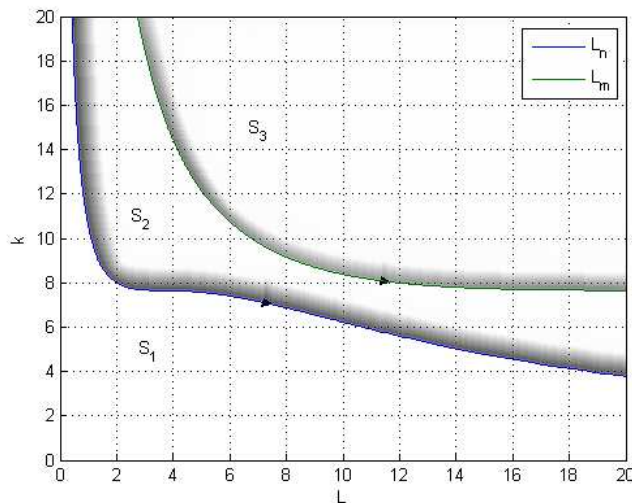


b)

Figure 4.9: $L_n$ and $L_m$ have no intersection.

- $L_n$ and $L_m$ intersect with each other. Consider one intersection point of two boundary functions. The rectangular area is then divided into 4 regions: $S_1$, $S_2$, $S_3$ and $S_4$; where $S_1$ is on the right hand side of $L_n$ and $L_m$; $S_2$ is on the right hand side of $L_n$ and on the left hand side of $L_m$; $S_3$ is on the left hand side of $L_n$ and $L_m$; $S_4$ is on the left hand

side of $L_n$ and on the right hand side of $L_m$. Let $N^+(S_i)$, $i = 1, 2, 3, 4$, be number of unstable poles for $S_i$. There are 4 combinations of arrows along $L_n$ and $L_m$:

- Arrows along $L_n$ and $L_m$ are both upward. It follows from Lemma 4.2 that $N^+(S_2) = N^+(S_1) + 2$, $N^+(S_3) = N^+(S_1) + 4$, $N^+(S_4) = N^+(S_1) + 2$. Thus, $S_1$ has the minimum number of unstable poles and it is also the intersection of the shaded regions of $L_n$ and $L_m$ (see Figure 4.10a).

- Arrows along $L_n$ and $L_m$ are both downward. . It follows from Lemma 4.3 that $N^+(S_2) = N^+(S_1) - 2$, $N^+(S_3) = N^+(S_1) - 4$, $N^+(S_4) = N^+(S_1) - 2$. Thus, $S_3$ has the minimum number of unstable poles and it is also the intersection of the shaded regions of $L_n$ and $L_m$ (see Figure 4.10b).

- Arrows along $L_n$ is upward and arrows along $L_m$ is downward. It follows from Lemma 4.2 for $L_n$ and Lemma 4.3 for $L_m$ that $N^+(S_2) = N^+(S_1) + 2$, $N^+(S_3) = N^+(S_1)$, $N^+(S_4) = N^+(S_1) - 2$. Thus, $S_4$ has the minimum number of unstable poles and it is also the intersection of the shaded regions of $L_n$ and $L_m$ (see Figure 4.10c).

- Arrows along $L_n$ is downward and arrows along $L_m$ is upward. Applying Lemma 4.3 for $L_n$ and Lemma 4.2 for $L_m$ yield $N^+(S_2) = N^+(S_1) - 2$, $N^+(S_3) = N^+(S_1)$, $N^+(S_4) = N^+(S_1) + 2$. Thus,

$S_2$ has the minimum number of unstable poles and it is also the intersection of the shaded regions of $L_n$ and $L_m$ (see Figure 4.10d).
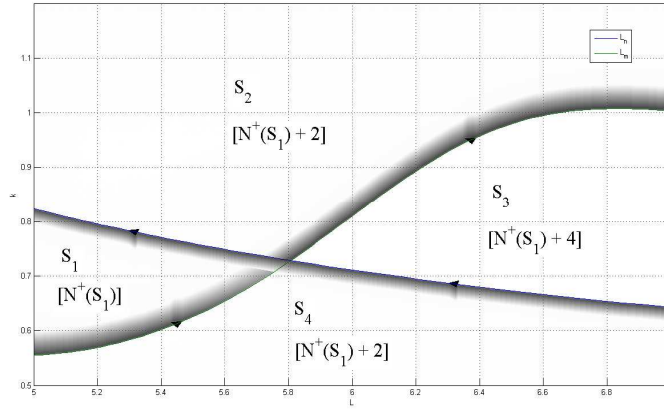


a)
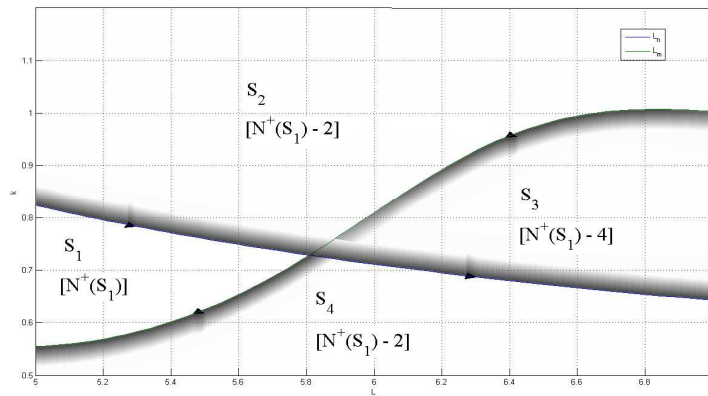


b)
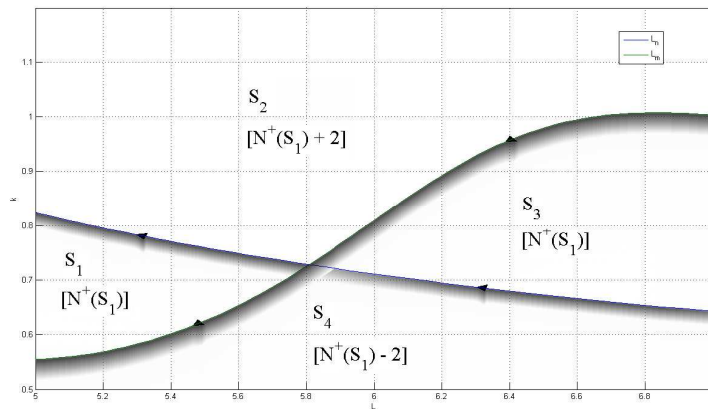


c)
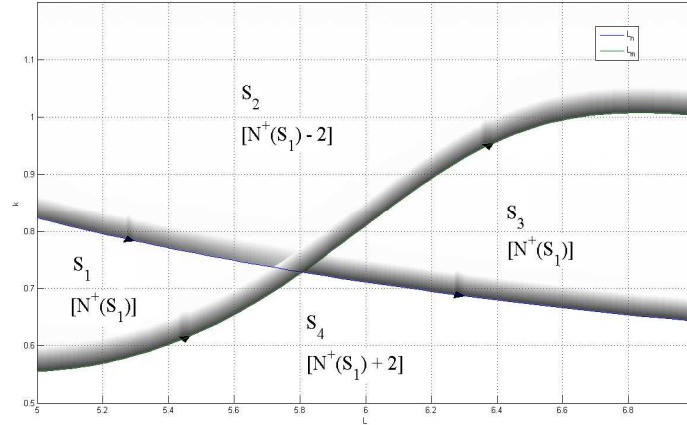
d)

Figure 4.10: $L_n$ and $L_m$ have intersection

In summary, for any two boundary curves, the region with the minimum number of unstable poles is the intersection of their two shaded regions.

If there are three boundary functions, $L_1$, $L_2$ and $L_3$. We take any two of them for consideration first, say $L_1$ and $L_2$. Apply the above analysis on two functions and conclude that the region with the minimum number of unstable poles is the intersection of their two shaded regions. Keep this intersection region with its boundary, arrow and shade, and remove the other portions of these two boundary functions. View the so-kept boundary as a boundary function and call it $L_4$. Apply the above analysis on two functions to $L_3$ and $L_4$, and conclude that the region with the minimum number of unstable poles is the intersection of their two shaded regions, which is the intersection of three original shaded regions. This induction is valid for any countable number of functions.

If there are three boundary functions, $L_1$, $L_2$ and $L_3$. We take any two of them for consideration first, say $L_1$ and $L_2$. Apply the above analysis on

94

two functions and conclude that the region with the minimum number of unstable poles is the intersection of their two shaded regions. Keep this intersection region with its boundary, arrow and shade, and remove the other portions of these two boundary functions. View the so-kept boundary as a boundary function and call it $L_4$. Apply the above analysis on two functions to $L_3$ and $L_4$, and conclude that the region with the minimum number of unstable poles is the intersection of their two shaded regions, which is the intersection of three original shaded regions. This induction is valid for any countable number of functions.

Note that the number of unstable poles in any region of the stabilizing graph is non-negative and a stable region has no unstable poles, or this number is zero, which reaches the minimum of this number. Thus, the stable regions, if any, must be the regions with the minimum number of unstable poles, or the intersection of all the shaded regions.

The proof is complete. □

With helps of the above lemma, we are able to state Proposition 4.2 as follows, which makes use of finite boundary functions only to determine stable regions. Recall that $\bar{\omega}$ defined before is the largest frequency which meets $d\left|kG_0(j\omega)e^{-j\omega L}\right|/d\omega=0$.

**Proposition 4.2.** Let $n_{\max}$ be the number obtained from (4.7) for $[0,\bar{\omega}]$. Then, $n_{\max}$ is the maximum number of boundary functions for determining the stable regions in the rectangular area bounded by $0 \leq L \leq L_{\max}$ and $0 \leq k \leq k_{\max}$ of the plane $(L,k)$.

**Proof.** Let $L_n\left(\omega \in [0,\infty)\right) = L_n\left(\omega \in [0,\bar{\omega}]\right) \cup L_n\left(\omega \in (\bar{\omega},\infty)\right)$ and

$L_n^A \triangleq L_n \left( \omega \in [0, \bar{\omega}] \right)$   and   $L_n^B \triangleq L_n \left( \omega \in (\bar{\omega}, \infty) \right)$ .   Consider each portion separately as follows.

A: $\omega \in [0, \bar{\omega}]$. It follows from Lemma 4.5 that $L_n^A > L_{max}$ for $n > n_{max}$, that is, all these $L_n^A$ stay outside of the rectangular area bounded by $0 \le L \le L_{max}$ and $0 \le k \le k_{max}$.

B: $\omega \in (\bar{\omega}, \infty)$. There are two possible cases: the gain of $G_0$ in this range monotonically increases or decreases. If $\left| G_0(j\omega) \right|$ increases monotonically, then $k(\omega)\big|_{\omega > \omega_m} > k_\infty$, and $L_n^B$ are outside of the rectangular area. If $\left| G_0(j\omega) \right|$ decreases monotonically, then $L_n^B$ for $n > n_{max}$ may be in the rectangular area but do not intersect with each other. $L_{n_{max}}^B$ divides the rectangular area into two separate regions: all $L_n^B$ with $n > n_{max}$ stay totally in the region on the right hand side of $L_{n_{max}}^B$, while all $L_n^B$ with $n < n_{max}$ stay totally in the region on the left hand side of $L_{n_{max}}^B$, which is the shaded region of $L_{n_{max}}^B$, due to the nature of gain decrease.

With the above analysis, the intersection of all the shaded regions of $L_n$ for $n \ge n_{max}$ in the rectangular area bounded by $0 \le L \le L_{max}$ and $0 \le k \le k_\infty$ is the same as the shaded region of $L_{n_{max}}$ alone as far as the rectangular area is concerned. Drawing the additional shaded regions of $L_n$ for $n > n_{max}$ does not refine the aforementioned intersection and is thus redundant to determine this intersection. It follows from Lemma 4.7 that the stable regions must be intersection of all the shaded regions, which is equivalent to the intersection of (i) intersection of the shaded regions of $L_n$ for $n < n_{max}$ and (ii) intersection

of the shaded regions of $L_n$ for $n \geq n_{\max}$, where the latter has been shown to be the same as the shaded region of $L_{n_{\max}}$ alone when restricted to the rectangular area. Therefore, $L_n$ with $n > n_{\max}$ are not needed to find stable regions in the rectangular area. The proof is complete. □

In the view of the above development, to find the stable regions, we draw $L_n$, $n = n_{\min}, n_{\min} + 1, ..., n_{\max}$, on the plane $(L, k)$. These boundary functions divide the rectangular area bounded by $0 \leq L \leq L_{\max}$ and $0 \leq k \leq k_{\max}$ into finite regions. Stability of each resulting region is determined with the help of the following Corollary 4.1.

**Corollary 4.1.** *On the plane of* $(L, k)$,

- *if the arrow of* $L_n$ *is upward, the region on the left hand side of* $L_n$ *has two fewer unstable pole the region on the right hand side of* $L_n$.

- *if the arrow of* $L_n$ *is down ward, the region on the left hand side of* $L_n$ *has two more unstable pole the region on the right hand side of* $L_n$.

If $G_0(0) < 0$, there is the horizontal line $k = \dfrac{1}{|G_0(0)|}$ in the plane $(L, k)$. This line divides the plane $(L, k)$ into two portions. Firstly, consider the lower portion. Start with the left-most region, that is, the one nearest to the origin. We can determine the number of unstable poles for the system corresponding to each point of this region by looking at one point inside it only. Then, we can infer from Corollary 4.1, the number of unstable poles of each region on its right, one region after another, from left to right. A region is stable if this number is zero. Note that the region near the origin has the same

number of unstable poles as that of $G_0(s)$, because, for $(L, k)$ near the origin, the closed-loop system with $kG_0(s)e^{-Ls}$ is close to the open loop $G_0(s)$. Finally, one can repeat the above procedure for the upper portion.

Now, we present a complete procedure as follows to obtain stabilizing gain ranges with respect to delay of a bi-proper process with non-monotonic gain.

**Algorithm 4.2.** Consider a bi-proper process with non-monotonic gain.

Step 1. For $\omega = 0$, if $\arg[G_0(0)] = -\pi$, plot the horizontal line,

$$k = \frac{1}{|G_0(0)|} \text{ on plane } (L, k).$$

Step 2. Calculate $n_{max}$ from (4.7) for $[0, \bar{\omega}]$. Plot $L_n$, $n = n_{min}, n_{min} + 1, ..., n_{max}$, on plane $(L, k)$.

Step 3. If $G_0(0) > 0$, start from the left-most region nearest the origin, take the number of unstable poles of this region same as that of $G_0(s)$, and then know its stability; Then, count the number of unstable poles of the next region, one by one, from left to right, with help of Corollary 4.1, and then know its stability.

Step 4. If $G_0(0) < 0$, there is the horizontal line $k = \frac{1}{|G_0(0)|}$ dividing the plane $(L, k)$ into the lower and upper portions. The lower portion is done as in Step 3. For the upper portion, start from the left-most region which is against k-axis, and check its stability; then, count the number of unstable poles of the next region, one by one, from left to right, with help of Corollary 4.1, and then know its stability.

**Example 4.4.** Consider a process with time delay,

$$G(s) = \frac{(5.1-s)(s+6.9)(s^2+1.63s+20.69)(s^2+1.51+1.79)(s^2+0.46s+1.44)}{(s^2+2s+65)(s^2+s+0.5)(s^2+1.4s+4.49)(s^2+s+3)}e^{-Ls}$$

This process is stable and of non-minimum phase. The gain plot in Figure 4.11 shows that the gain does not monotonically change with frequency and requires us to apply Algorithm 4.2. We have that $\lim_{\omega\to\infty}|G_0(j\omega)|=1$, so $k_\infty=1$. For $\omega\in[3.56, 5.64]$, $|G_0(j\omega)|<1$, thus, this range is not of interests for our calculations. For $\omega=8.18$, $d\left|kG_0(j\omega)e^{-j\omega L}\right|/d\omega=0$ and the gain is monotonic decrease for $\omega>8.18$. Thus, $\bar{\omega}=8.18$ and the minimum phase of $G_0(j\omega)$ in $[0, 8.18]$ is $\phi_{min}=-2.219$. The maximum phase of $G_0(j\omega)$ is $\Phi=0.93$, which gives $n>-0.65$ from (3.5), so $n_{min}=0$. In this example, we let $k_{max}=k_\infty=1$ and $L_{max}=10$. Proceeding with Algorithm 4.2, for Step 1, $G_0(0)=4.28$ does not meet (3.3), and produces no line. For Step 2, we have $n_{max}=13$ from (4.7) so we plot the boundary functions, $L_i$, $i=0,1,...,13$, on plane $(L,k)$ as in Figure 4.3. They divide plane $(L,k)$ into regions. For Step 3, the left-most region near the origin has the same number of unstable poles as that of $G_0(s)$, which is zero, so this region is stable. With help of Corollary 4.1, the number of unstable poles for each next region is counted and its stability decided accordingly. In the end, all the stable regions are found as the given area and marked in green in Figure 4.3.

Figure 4.11: Bode plot of $G_0(s)$ of Example 4.4

**Example 4.5.** Consider a process with time delay,

$$G(s) = \frac{(7-s)(s+0.2)(s+3)(s+25)}{(s-0.1)(s+5)(s+20)(s+6)} e^{-Ls}$$

This process is unstable and of non-minimum phase. The Bode plot in Figure 4.12 shows that the gain does not monotonically change with frequency and requires us to apply Algorithm 4.2. We have that $\lim_{\omega \to \infty} |G_0(j\omega)| = 1$, so $k_\infty = 1$.

For $\omega \in [0.3, 2.53]$, $|G_0(j\omega)| < 1$, thus, this range is not of interests for our calculations. For $\omega = 9.57$, $d|kG_0(j\omega)e^{-j\omega L})|/d\omega = 0$ and the gain is monotonic decrease for $\omega > 9.57$. Thus, $\bar{\omega} = 9.57$ and the minimum phase of $G_0(j\omega)$ in $[0, 9.57]$ is $\phi_{\min} = -\pi$. The maximum phase of $G_0(j\omega)$ is $\Phi = -0.48$, which gives $n > -0.42$ from (3.5), so $n_{\min} = 0$. In this example, we let $k_{\max} = k_\infty = 1$ and $L_{\max} = 15$. Proceeding with Algorithm 4.2, for Step 1, $G_0(0) = -1.75$ meets (3.3), and produces the horizontal line $k = 0.5714$ in Figure 4.13. For Step 2, we have $n_{\max} = 23$ from (4.7) so we plot the boundary functions, $L_i$, $i = 0, 1, ..., 23$, on plane $(L, k)$ as in Figure 4.13.

They divide plane $(L,k)$ into regions. Since $G_0(0) < 0$, we skip Step 3 and proceed to Step 4. The lower region is unstable it has the same number of unstable poles as that of $G_0(s)$, which is one. For the upper region, we pick a point in the left-most region which is against k-axis which is $(L,k) = (1,0.8)$ to check its stability. The Nyquist plot of $kG_0(s)e^{-Ls}$ with $(L,k) = (1,0.8)$ in Figure 4.14 shows that the close-loop system is stable, so this region is stable. With help of Corollary 4.1, the number of unstable poles for each next region is counted and its stability decided accordingly. In the end, all the stable regions are found as the given area and marked in green in Figure 4.13.
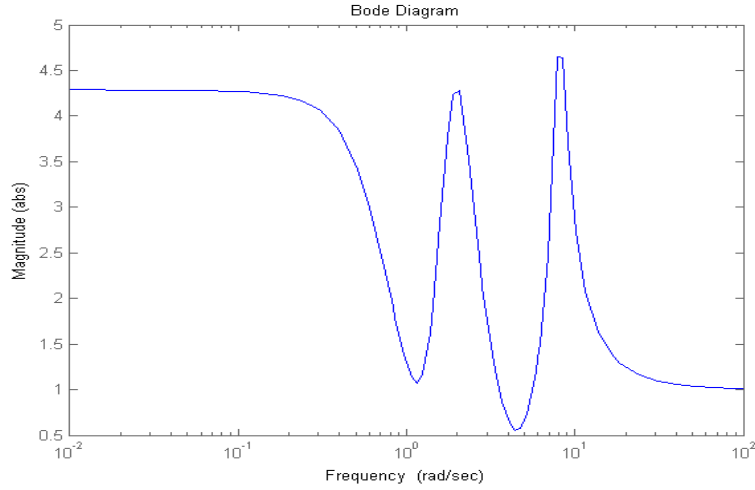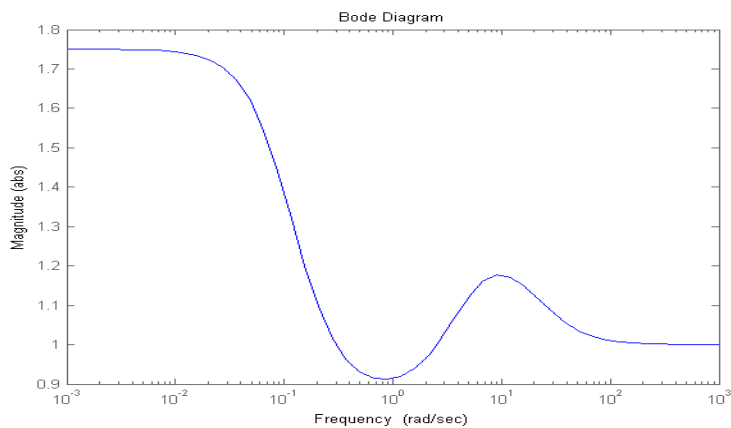


Figure 4.12: Bode plot of $G_0(s)$ of Example 4.5
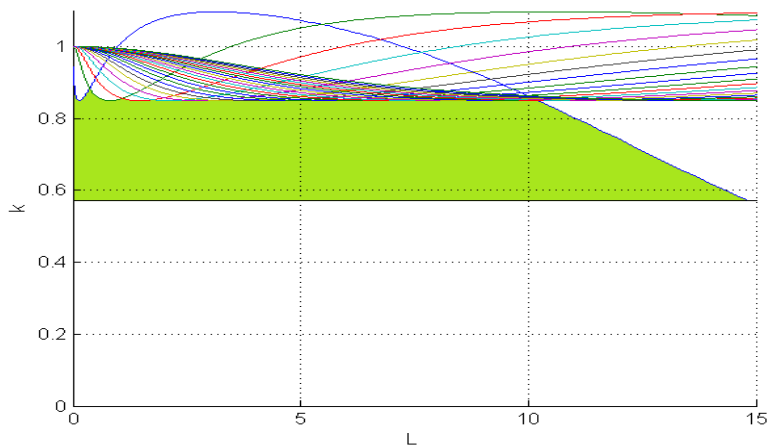


Figure 4.13: Stabilizing graph of Example 4.5
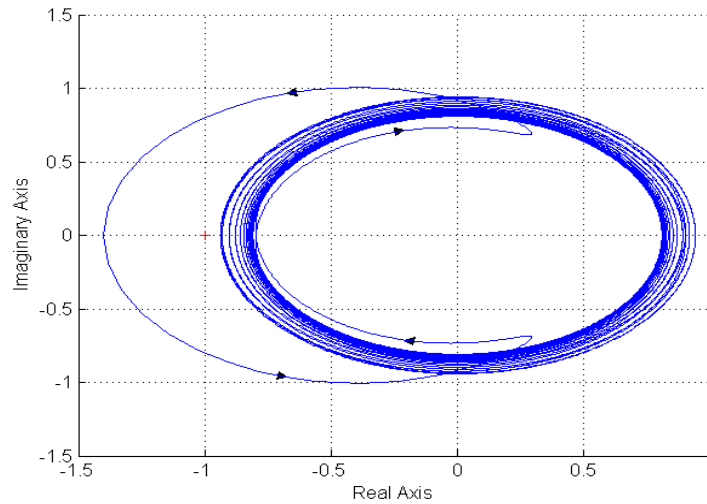
Figure 4.14: Nyquist plot of Example 4.5 with $(L, k) = (1, 0.8)$

## 4.5. Conclusion

The D-decomposition method for computing stabilizing loop gain and delay ranges has been extended to the case of bi-proper processes. The properties of boundary functions from such processes are investigated in great details. It is shown that finite boundary functions are sufficient to determine all stable regions for finite parameter intervals. The formula is given for calculating this number. Moreover, the algorithms are established to find exact stabilizing gain and delay ranges, and they are illustrated by many kinds of processes including stable/unstable poles and minimum/non-minimum zeros. These new results, together with those in our previous chapter, provide a complete solution for numerical parameterization of stabilizing loop gain and delay for a general delay SISO process.

# Chapter 5

# Stabilizing loop gains and delay for MIMO processes

## 5.1. Introduction

In this chapter, we first present a graphical method to compute the stabilizing gain ranges of a decentralized proportional controller for a linear time invariant (LTI) two-input and two-output (TITO) system. This method determines all possible stability boundaries. These boundaries divide the gain plane into regions and the stability of each region is checked to identify the stable ones. Subsequently, the loop gain margins are obtained from these stable regions. The proposed method is simple and easy to apply, especially, no iteration is required for computing stability boundaries.

Next, stabilizing parameterization is addressed for the common gain and delay case for TITO processes. The characteristic locus method is exploited to develop the solution with helps of the SISO results developed in the preceding chapters.

The chapter is organized as follows. Section 5.2 presents the procedure to compute exact stabilizing gains for a fixed- coefficient TITO process. An extension of D-decomposition approach to find stabilizing P controller for MIMO process with varying time delay is discussed in Section 5.3. Section 5.4 will conclude this chapter.

## 5.2. Stabilizing Gain Ranges for TITO Processes

Consider a unity output feedback system depicted in Figure 5.1, where the process and diagonal controller are described via their transfer function matrices $G(s)$ and $K$, respectively,

$$G(s) = \begin{bmatrix} g_{11} & g_{12} \\ g_{21} & g_{22} \end{bmatrix}, \ K = \begin{bmatrix} k_1 & 0 \\ 0 & k_2 \end{bmatrix}.$$

The loop gain margins are defined in [43], [44] and are adapted to the two-input two-output (TITO) case as follows.

**Problem 5.1.** For a $2 \times 2$ process, $G(s)$, under the decentralized gain controller, $K = diag\{k_1, k_2\}$, find the regions in 2D space, $(k_1, k_2)$, such that their interior points give stable closed-loop while their boundary points produce unstable closed-loop.
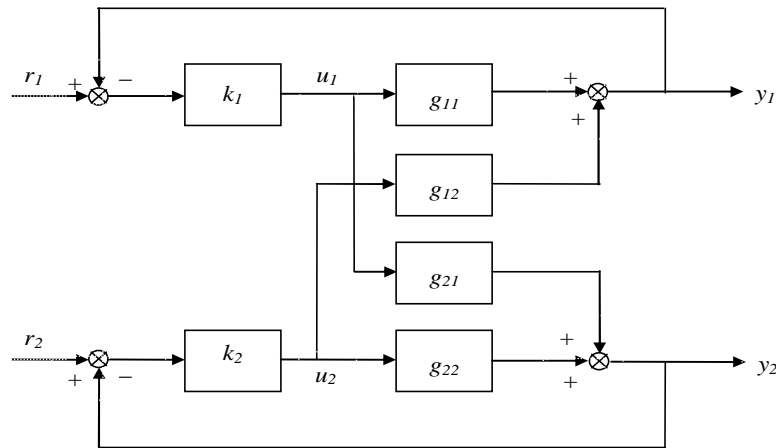


Figure 5.1: Diagram of a TITO control system

It follows [56] that the characteristic equation of the closed-loop system is

$$P_c(s) = P_G(s) P_K(s) \det[I + G(s)K(s)] = 0,$$

where $P_G(s)$ and $P_K(s)$ are the pole polynomials of $G(s)$ and $K(s)$,

respectively. In our case, $P_K(s) = 1$ and the characteristic equation becomes

$$P_G(s)\{1 + k_1 g_{11}(s) + k_2 g_{22}(s) + k_1 k_2 [g_{11}(s) g_{22}(s) - g_{12}(s) g_{21}(s)]\} = 0 \quad (5.1)$$

The roots of the above equation, or the poles of the closed-loop, are functions of gains, $k_1$ and $k_2$. The stability may change only when at least one pole moves across the imaginary axis [2], [3]. That means $s = j\omega$ satisfies (5.1), and by taking real and imaginary parts, it leads to

$$\alpha_1(\omega)k_1 + \alpha_2(\omega)k_2 + \alpha_{12}(\omega)k_1 k_2 + \alpha_0(\omega) = 0, \quad (5.2)$$

$$\beta_1(\omega)k_1 + \beta_2(\omega)k_2 + \beta_{12}(\omega)k_1 k_2 + \beta_0(\omega) = 0, \quad (5.3)$$

where

$$\alpha_1(\omega) = \Re e[P_G(j\omega)g_{11}(j\omega)],$$

$$\alpha_2(\omega) = \Re e[P_G(j\omega)g_{22}(j\omega)],$$

$$\alpha_{12}(\omega) = \Re e\{P_G(j\omega)[g_{11}(j\omega)g_{22}(j\omega) - g_{12}(j\omega)g_{21}(j\omega)]\},$$

$$\alpha_0(\omega) = \Re e[P_G(j\omega)],$$

$$\beta_1(\omega) = \Im m[P_G(j\omega)g_{11}(j\omega)],$$

$$\beta_2(\omega) = \Im m[P_G(j\omega)g_{22}(j\omega)],$$

$$\beta_{12}(\omega) = \Im m\{P_G(j\omega)[g_{11}(j\omega)g_{22}(j\omega) - g_{12}(j\omega)g_{21}(j\omega)]\},$$

$$\beta_0(\omega) = \Im m P_G[(j\omega)].$$

The solutions for $k_1$ and $k_2$ to (5.2) and (5.3) when $\omega$ varies from zero to infinity define the boundary curves in the plane of $(k_1, k_2)$. To solve (5.2) and (5.3) for $k_1$ and $k_2$ given a $\omega$, we get a quadratic equation in $k_1$

$$[\beta_1(\omega)\alpha_{12}(\omega) - \alpha_1(\omega)\beta_{12}(\omega)]k_1^2 + [\beta_1(\omega)\alpha_2(\omega) - \alpha_1(\omega)\beta_2(\omega) +$$
$$+\alpha_{12}(\omega)\beta_0(\omega) - \beta_{12}(\omega)\alpha_0(\omega)]k_1 + [\alpha_2(\omega)\beta_0(\omega) - \beta_2(\omega)\alpha_0(\omega)] = 0 \quad (5.4)$$

and a function of $k_2$ in term of $k_1$

$$k_2 = -\frac{\alpha_1(\omega)k_1 + \alpha_0(\omega)}{\alpha_{12}(\omega)k_1 + \alpha_2(\omega)}. \quad (5.5)$$

In fact, (5.4) and (5.5) define a parametric map in $\omega$ from $k_1$ to $k_2$ as following: For $\omega \neq 0$, the solutions for $k_1$ are obtained from (5.4), and the solutions for $k_2$ from (5.5). In case of $\omega = 0$, the characteristic equation is real, where (5.3) disappears, and (5.2) becomes

$$k_2 = -\frac{\alpha_1(0)k_1 + \alpha_0(0)}{\alpha_{12}(0)k_1 + \alpha_2(0)}, \quad (5.6)$$

which defines explicit function from $k_1$ to $k_2$.

The boundary curves divide the plane $(k_1, k_2)$ into several regions. All the interior points in one particular region will share the same number of unstable poles if any, thus, preserve the stability property, i.e. either stable or unstable. To determine whether a region is stable or not, one only needs to check one point of any choice. One may use the generalized Nyquist criterion (GNC) to test for this, especially when the process has delay, for which there is infinite number of poles and pole-based stability test is not applicable.

We summarize our development so far as follows.

**Algorithm 5.1**. Compute the exact stabilizing loop gain ranges.

Step 1. For $\omega = 0$, plot the function $k_2 = -\dfrac{\alpha_1(0)k_1 + \alpha_0(0)}{\alpha_{12}(0)k_1 + \alpha_2(0)}$ on the plane

$(k_1, k_2)$.

Step 2. Calculate $k_1$ and $k_2$ from (5.4) and (5.5) for $\omega \neq 0$ and plot

all of them on the plane $(k_1, k_2)$.

Step 3. Use the GNC to check the stability of each resulting region.

Note that Step 3 above can be significantly simplified if one finds the gain ranges of the common gain controller $K(s) = kI_2$ for stability with the GNC. The controller represents a straight line in the plane and may intersect with the above regions. The segment of the common gain controller dictates stability property of its intersected region.

Suppose we take a subset from the solution to Problem 5.1 as

$$k_i \in \left[ \underline{k}_i, \overline{k}_i \right], \qquad i = 1, 2.$$

Then, the closed-loop remains stable even when the gain for the $i$th loop, $k_i$, varies between $\underline{k}_i$ and $\overline{k}_i$, provided that other loop gains, $k_j$, $j = 1, 2$, $j \neq i$, are arbitrary but also within their respective ranges. $\left[ \underline{k}_i, \overline{k}_i \right]$ is called by [43] the gain margin for the $i$th loop. It is also subjected to other loops' gain margins within $\left[ \underline{k}_j, \overline{k}_j \right]$, $j = 1, 2$, $j \neq i$. The loop gain margins defined as above can be easily found using Algorithm 5.1, by taking a rectangle in any stable region.

Controller for system integrity is designed to ensure that the closed-loop stability is maintained when any combination of the individual controller or actuator fails [57]. One sees that failure of controller or actuator in loop 1 (or loop 2) is equivalent to setting $k_1 = 0$ (or $k_2 = 0$) for a TITO system. Thus, a controller with gains of $(k_1, k_2)$ has integrity if its closed-loop system is always stable for each of four sets of gains: $(k_1, k_2)$, $(k_1, 0)$, $(0, k_2)$ and $(0, 0)$. A sufficient condition for this integrity is that the loop gain margins are

$[0, k_1]$ and $[0, k_2]$, or the rectangular with vertices of $(k_1, k_2)$ and the origin is a stable region. The above exact and sufficient conditions for system integrity can be easily checked using Algorithm 5.1.

**Example 5.1.** Consider the Wood-Berry binary distillation column process [58],

$$G(s) = \begin{bmatrix} \dfrac{12.8}{16.7s+1} e^{-s} & \dfrac{-18.9}{21s+1} e^{-3s} \\ \dfrac{6.6}{10.9s+1} e^{-7s} & \dfrac{-19.4}{14.4s+1} e^{-3s} \end{bmatrix}.$$

This process is a well-studied process in process control. The process does not have unstable poles but its unity feedback is unstable. Algorithm 5.1 is employed to find the stabilizing ranges of $k_1$ and $k_2$. Step 1 gives the red curves while Step 2 yields the blue one as in Figure 5.2. These curves divide the gain-plane into regions. In Step 3, it follows from the GNC that the stabilizing common gain range for this process is $-0.12 < k < 0.0671$. The dashed line in Figure 5.2 is the common gain line, and it intersects with several regions. The stable region (shaded) is the one that intersects with the dashed line at the segment $[-0.12, 0.0671]$. In this stable region, we can determine the loop gain margins. For example, let the range of $k_1$ to be $[0,1]$, a maximum rectangle with a side of $[0,1]$ is determined inside the stable region with the maximum range of $k_2$ being $[-0.255, 0.0515]$. It results in the following gain margins

$$k_1 \in [0,1] \text{ and } k_2 \in [-0.255, 0.0515].$$

It means that the system remains stable when $k_1$ varies in $[0,1]$ given that $k_2$ varies in $[-0.255, 0.0515]$ and vice versa.

For the system integrity problem, the controller with $(k_1, k_2) = (1, 0.05)$ has integrity because four points, $(1, 0)$, $(1, 0.05)$, $(0, 0.05)$ and $(0, 0)$, are all in stable regions. Whereas the controller with $(k_1, k_2) = (1, 0.08)$ has no integrity because only three points $(1, 0)$, $(1, 0.08)$ and $(0, 0)$ are in stable regions, while the point $(0, 0.08)$ is not in stable regions.

In this example, the method in [45] cannot be applied because of instability of the unity feedback system, that is, the region that contains $(k_1, k_2) = (1, 1)$ is unstable.



Figure 5.2:　Stabilizing region of $(k_1, k_2)$ for Example 5.1

**Example 5.2.** Consider a stable TITO process,

$$G(s) = \begin{bmatrix} \dfrac{s-1}{(s+1)(s+3)} & \dfrac{-0.5s+1}{0.5s^3 + 2.5s^2 + s + 3} \\ \dfrac{0.3}{s+2} e^{-0.3s} & \dfrac{0.5s+1}{s^2 + 2s + 5} e^{-0.7s} \end{bmatrix}.$$

The process is unity feedback stable. To find the stabilizing region we only need to obtain the region that contains $(k_1, k_2) = (1, 1)$. Algorithm 5.1 produces Figure 5.3. The stabilizing region is marked as the shaded one. It is exactly the same region as shown in [44]. However, this new method is much simpler
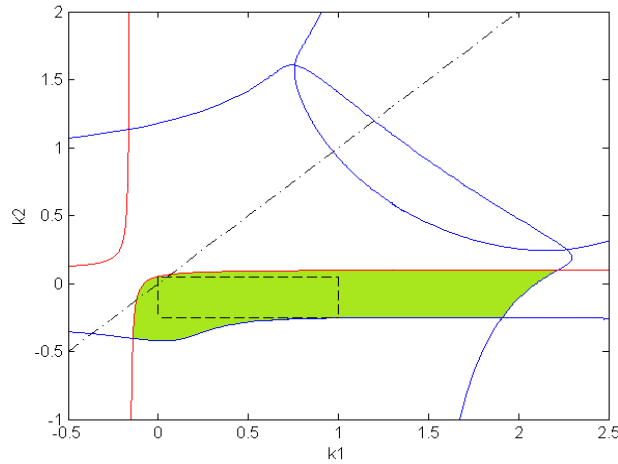
technically and effective computationally.
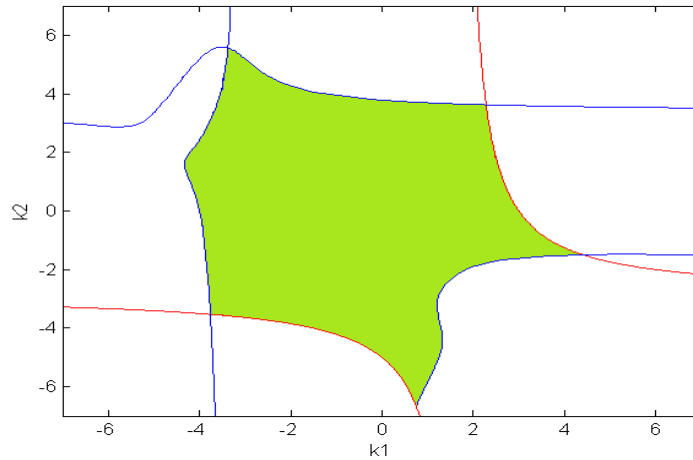


Figure 5.3:    Stabilizing region of $(k_1, k_2)$    for Example 5.2

**Example 5.3**. Consider an unstable process,

$$G(s) = \begin{bmatrix} \dfrac{1}{s-1}e^{-0.5s} & \dfrac{2}{s+1}e^{-0.25s} \\ \dfrac{3}{s+2}e^{-0.5s} & \dfrac{4}{s+3}e^{-0.25s} \end{bmatrix}.$$

The process has one unstable pole at $s = 1$. It is not stable in the unity feedback structure and cannot be stabilized by a common gain controller, either. Thus, the method in [45] cannot be applied. The stabilizing region is found by checking the stability of each region. For $(k_1, k_2) = (1.8, 0.05)$, the Nyquist plot of $KG$ has one counter-clockwise encirclement of the critical point, thus the corresponding closed loop is stable (Figure 5.4). The stable region (shaded) is the region that includes $(k_1, k_2) = (1.8, 0.05)$ (Figure 5.5).
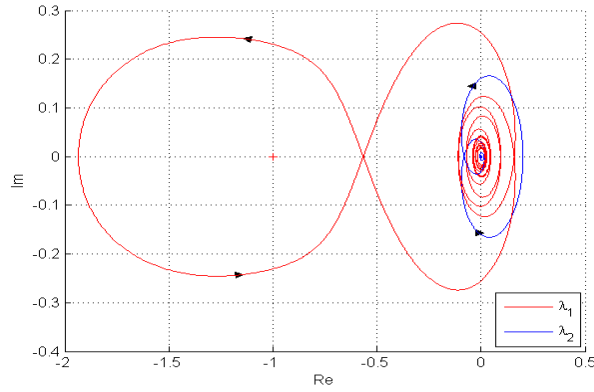
Figure 5.4:　Characteristic loci of　$KG(s)$　with　$(k_1, k_2) = (1.8, 0.05)$　of

Example 5.3
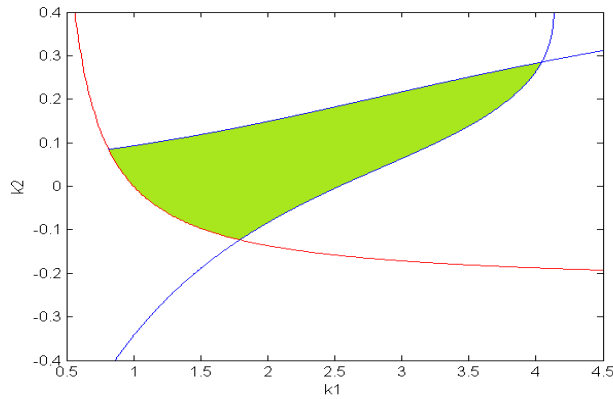


Figure 5.5:　Stabilizing region of　$(k_1, k_2)$　of Example 5.3

## 5.3. Stabilizing Gain and Delay for TITO Processes

Consider the following process,

$$G(s) = G_0(s)e^{-Ls} = \begin{bmatrix} g_{11}(s) & g_{12}(s) \\ g_{21}(s) & g_{22}(s) \end{bmatrix} e^{-Ls},$$

where　$G_0$　is non-singular and　$g_{ij}$,　$i, j = 1, 2$, may have fixed time delay. It

is to be stabilized by the controller

$$K(s) = kI_2 = \begin{bmatrix} k & 0 \\ 0 & k \end{bmatrix}.$$

We define the stabilizing problem as following:

**Problem 5.2.** For a TITO process, $G(s) = G_0(s)e^{-Ls}$, under the centralized gain controller, $K = kI_2$, find the regions in 2D space, $(L, k)$, such that their interior points give stable closed-loop while their boundary points produce marginally stable or unstable closed-loop.

**Theorem 5.1** [56]**.** Suppose that G(s) has $P_o$ unstable poles. Then the feedback system with the proportional controller $K(s) = kI$ is stable if and only if the characteristic loci of $kG(s)$, taken together, encircles the critical point, $(-1 + j0)$, $P_o$ times anti-clockwise.

Let $\lambda(G_0)$ and $\lambda(KG)$ be characteristic loci of $G_0$ and $KG$, respectively. We have

$$\det\left[\lambda(G_0)I - G_0\right] = 0$$
$$\Leftrightarrow \det\left[k\lambda(G_0)e^{-Ls} - kG_0e^{-Ls}\right] = 0 \tag{5.7}$$

so $\lambda(KG) = ke^{-Ls}\lambda(G_0)$. Since $G_0$ is a $2\times2$ matrix, it has two characteristic loci. Thus, we denote $\lambda_i(j\omega) = \lambda[G_0(j\omega)], i = 1, 2$. By Theorem 5.1, the closed-loop system may change its stability with regard to $L$ and/or $k$ only when the number of encirclements of the characteristic loci of $kG(s)$ with respect to the critical point changes. To find a stabilizing region for $(L, k)$, we locate its boundary where $k\lambda_i(j\omega)e^{-j\omega L}$, $i = 1, 2$, passes through the critical point at some frequency $\omega$. That case satisfies $k\lambda_i(j\omega)e^{-j\omega L} = (-1 + j0)$, which implies, for $\omega > 0$, that

$$\left|\lambda_i(j\omega)\right| = 1 \tag{5.8}$$

$$\arg\left[\lambda_i(j\omega)\right] = -(2n+1)\pi \tag{5.9}$$

Thus, one has

$$k = \frac{1}{\left| \lambda_i \left( j\omega \right) \right|} \tag{5.10}$$

$$L_n = \frac{\arg\left[ \lambda_i \left( j\omega \right) \right] + (2n+1)\pi}{\omega}, n \in \{...,-1,0,1,...\} \tag{5.11}$$

while for $\omega = 0$, $k\lambda_i(0) = -1$ with $k > 0$ requires

$$\arg\left[ \lambda_i(0) \right] = -\pi, \tag{5.12}$$

under which,

$$k = \frac{1}{\left| \lambda_i(0) \right|}, \quad L \geq 0. \tag{5.13}$$

Note that only positive delay is realistic, which requires (5.11) to meet

$$L_n = \frac{\arg\left[ \lambda_i \left( j\omega \right) \right] + (2n+1)\pi}{\omega} > 0.$$

This yields

$$n > \frac{-\Phi_i - \pi}{2\pi}, \tag{5.14}$$

where $\Phi_i$ is the maximum phase of $\lambda_i(j\omega)$. Denote $n_{\min}$ as the smallest integer number that satisfies (5.14). Thus, (5.11) is valid only for $n = n_{\min}, n_{\min} + 1,...$, which is used in the rest of this chapter.

Notice that the system has a 2x2 transfer matrix, and it has two characteristic loci. Thus, for each valid *n,* equations (5.10) and (5.11) define *two* boundary functions, each from one characteristic locus. This is an implicit mapping from the delay, $L$, to the gain, $k$, which is parameterized in terms of the frequency, $\omega$. Equation (5.13) defines another boundary function, which is an explicit mapping from $L$ to $k$ and is actually a horizontal line in the $(L,k)$ plane. The boundary functions defined by (5.10), (5.11) and

(5.13) based on the frequency response of the fixed part of the process, $G_0$, can be drawn in the 2D plane, $(L, k)$. They divide the plane into regions. Each interior point in a so-formed region will have the same number of encirclements of the critical point by the characteristic loci of the corresponding open-loop as that of any other points in the region. Thus, all the points in the same region produce either closed-loop stability or instability. There will be no stability difference among the points in one region. Therefore, one only needs to check stability of one region by looking at any single point inside that region. Single point stability test is simple and can be done in many ways. For instance, one may use Theorem 5.1 to test for stability.

In general, all the boundary functions $L_n$ are needed to be plotted on the plane of $(L, k)$ in order to determine the stability of regions. However, there are an infinite number of boundary functions $L_n$, and, an infinite number of the resulting regions. It is impossible to plot and check the stability of all these regions. To overcome this problem, we need to study prosperities of such boundary functions carefully. Observe that, in previous chapters, for SISO case, we examine the intersection of the Nyquist curve of the open loop system with the critical point. In particular, we investigate how a delay perturbation changes the number of the curve's encirclements with respect to the critical point. In the current TITO case, the local behavior analysis is still true for intersection of the Nyquist plot of a characteristic locus with the critical point. Thus, we adapt those Lemmas from the early chapters to our TITO case as follows.

**Lemma 5.1.** *For $m \neq n$, a boundary function $L_m$ intersects with*

another $L_n$ only if there are $\omega_m$ and $\omega_n$ with $\omega_m \neq \omega_n$ such that $\left| \lambda_i \left( j\omega_m \right) \right| = \left| \lambda_i \left( j\omega_n \right) \right|$.

**Lemma 5.2.** *Let a characteristic locus of $kG_0(s)e^{-sL}$ for $\omega > 0$ has the unique intersection with the critical point of $(-1 + j0)$ at a frequency $\omega = \omega^* \in (0, \infty)$. If the gain of its frequency response decreases at this frequency, that is, $\left. d \left| k\lambda_i \left( j\omega \right) e^{-j\omega L} \right| / d\omega \right|_{\omega = \omega^*} < 0$, then the closed-loop system with $kG_0(s)e^{-s(L+\varepsilon)}$ has two more unstable poles than the closed-loop system with $kG_0(s)e^{-s(L-\varepsilon)}$ for some $\varepsilon > 0$.*

**Lemma 5.3.** *Let a characteristic locus of $kG_0(s)e^{-sL}$ for $\omega > 0$ has the unique intersection with the critical point of $(-1 + j0)$ at a frequency $\omega = \omega^* \in (0, \infty)$. If the gain of its frequency response increases at this frequency, that is, $\left. d \left| k\lambda_i \left( j\omega \right) e^{-j\omega L} \right| / d\omega \right|_{\omega = \omega^*} > 0$, then the closed-loop system with $kG_0(s)e^{-s(L+\varepsilon)}$ has two fewer unstable poles than the closed-loop system with $kG_0(s)e^{-s(L-\varepsilon)}$ for some $\varepsilon > 0$.*

**Lemma 5.4.** *Let $\phi_{\min}$ be the minimum phase of $\lambda_i(j\omega)$ in $[\omega_1, \omega_2]$. Then, there holds*

$$\left. L_n(\omega) \right|_{\omega \in [\omega_1, \omega_2]} > L_{\max} \ \ for \ \ n > n_{\max},$$

*where $n_{\max}$ is the smallest integer such that*

$$n_{\max} \geq \frac{\omega_2 L_{\max} - \phi_{\min} - \pi}{2\pi}. \tag{5.15}$$

In the plane of $(L, k)$, we indicate direction of frequency increase with an arrow on a boundary function. The upward arrow indicates increase of

controller gain $k$, which corresponds to decrease of the characteristic locus gain $|\lambda_i(j\omega)|$. Whereas, the downward arrow indicates decrease of controller gain $k$, which corresponds to increase of the characteristic locus gain $|\lambda_i(j\omega)|$. It follows from Lemma 5.2 that if the arrow of $L_n$ is upward, the closed-loop system with $(L,k)$ in the region on the left of $L_n$ has two fewer unstable poles than the closed-loop system with $(L,k)$ in the region on the right of $L_n$. On the other hand, it follows from Lemma 5.3 that if the arrow of $L_n$ is downward, the closed-loop system with $(L,k)$ in the region on the left of $L_n$ has two more unstable poles than the closed-loop system with $(L,k)$ in the region on the right of $L_n$. Thus, if we follow the direction of the arrow, the region on the left hand side of any boundary curve has fewer numbers of unstable poles than the region on the right hand side. For each boundary curve, we shade this region of the left hand side.

**Lemma 5.5.** *The regions with a minimum number of unstable poles are the intersection of all the shaded regions. And the stable regions are necessarily in the intersection of all the shaded regions.*

Let $\bar{\omega}$ be the largest frequency which meets $d|k\lambda_i(j\omega)|/d\omega = 0$. Since the characteristic loci converge to zero at infinity, there holds $d|k\lambda_i(j\omega)|/d\omega < 0$ for $\omega \in (\bar{\omega}, \infty)$.

**Lemma 5.6**. *Let $n_{\max}$ be the number obtained from (5.15) for $[0,\bar{\omega}]$. Then, $n_{\max}$ is the maximum number of boundary functions for determining stable regions in the rectangular area bounded by $0 \le L \le L_{\max}$ and $0 \le k \le k_{\max}$ of the plane $(L,k)$.*

**Corollary 5.1.** *On the plane of* $(L, k)$,

- *if the arrow of* $L_n$ *is upward, the region on the left hand side of* $L_n$ *has two fewer unstable pole than the region on the right hand side of* $L_n$.

- *if the arrow of* $L_n$ *is down ward, the region on the left hand side of* $L_n$ *has two more unstable pole than the region on the right hand side of* $L_n$.

It follows from Lemma 5.5 that the stable regions (if any) are in the intersection of all shaded regions which is the left hand side of the boundary functions corresponding to both characteristic loci. Moreover, it can be deduced from Lemma 5.1 and Lemma 5.2 that if a characteristic locus has monotonic gain decrease, the intersection of all its boundary functions is on the left hand side of its $L_{n_{\min}}$. Thus, if the gain of a characteristic loci is monotonic, we only need to plot the corresponding $L_{n_{\min}}$ and consider the stability of only the region on the left hand side of $L_{n_{\min}}$. On the other hand, if a characteristic locus has non-monotonic gain, it follows from Lemma 5.6 that we need to plot $L_n$ with $n = n_{\min}, n_{\min} + 1, ..., n_{\max}$ on $(L, k)$ plane to find the stable regions. Therefore, the algorithm to find the stabilizing gain ranges is summarized as following:

**Procedure 5.2**. Consider a TITO process, $G_0(s)e^{-Ls}$,

Step 1. Compute and plot gains of two characteristic loci of $G_0(s)$, $\lambda_i(j\omega), i = 1, 2.$

Step 2. For $\omega=0$ , plot the horizontal line(s), $k=\dfrac{1}{\left|\lambda_i(0)\right|}$ if

$\arg\left[\lambda_i(0)\right]=-\pi, i=1,2,$ on $(L,k)$ plane.

Step 3. If $\lambda_i$ is monotonic for $\omega>0$, plot the $L_{n_{\min}}$ with (5.10) and

(5.11) on $(L,k)$ plane; Otherwise, if $\lambda_i$ is not monotonic for

$\omega>0$ , calculate $n_{\max}$ from (5.15) for $[0,\bar{\omega}]$ . Plot the

corresponding $L_n$, $n=n_{\min}, n_{\min}+1,...,n_{\max}$, on $(L,k)$ plane.

Step 4a. If there is no horizontal line drawn in Step 1, start from the

left-most region nearest the origin, take the number of unstable

poles of this region same as that of $G_0(s)$, and obtain its

stability; Then, count the number of unstable poles of the next

region, one by one, from left to right, with help of Corollary 5.1,

and then obtain its stability.

Step 4b. Otherwise, the horizontal lines drawn in Step 1 divide $(L,k)$

plane into a maximum of 3 portions. For each portion, start

from the left-most region which is against the k-axis, and check

its stability; then, count the number of unstable poles of the

next region, one by one, from left to right, with help of

Corollary 5.1, and then obtain its stability.

**Example 5.4** Consider a process,

$$G(s)=\begin{bmatrix} \dfrac{2.5}{s-1} & \dfrac{1}{s+1} \\ \dfrac{3}{s+1} & \dfrac{1}{s+1} \end{bmatrix}e^{-Ls}$$

which has an unstable pole at $s=1$. Follow Procedure 5.2 step by step. For

118

Step 1, the gain plots of two characteristic loci are shown in Figure 5.6. Both loci of this process have monotonic gain reduction. In Step 2, $\lambda_1(0) = -3.2122$ meets the condition (5.12), giving the line $k = 0.3113$ on $(L, k)$ plane as in Figure 5.7, while $\lambda_2(0) = 1.7122$ fails it. For Step 3, both characteristic loci are monotonic, with $n_{\min} = 0$, we plot $L_0$ from both characteristic loci on $(L, k)$ plane; the red curve is the boundary curve from one characteristic locus, while the blue curve is of the other one. Since there is a horizontal line in Step 2, this line divides the plane into two portions. Following Step 4b, the most left region in the upper portion is checked for stability at one selected point $(L, k) = (0.1, 1)$. The Nyquist plot shows that this region is stable (Figure 5.8). Using a similar check, the left most region in the lower portion is unstable. In the end, the stable region is marked in green in the stabilizing graph (Figure 5.7).
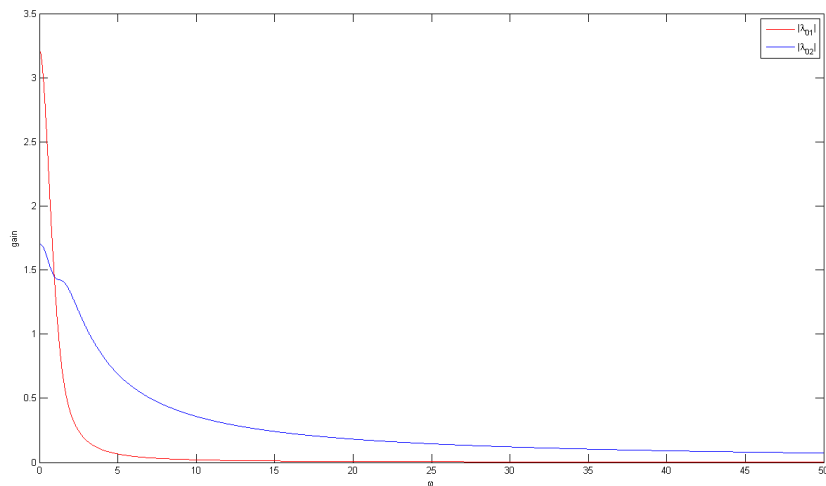


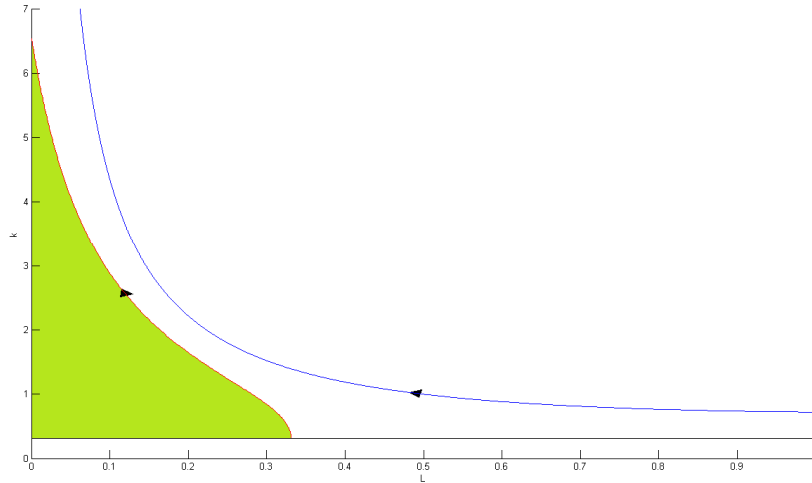Figure 5.6: Gain plot of $\lambda_i(s)$ of Example 5.4

Figure 5.7: Stabilizing graph of Example 5.4
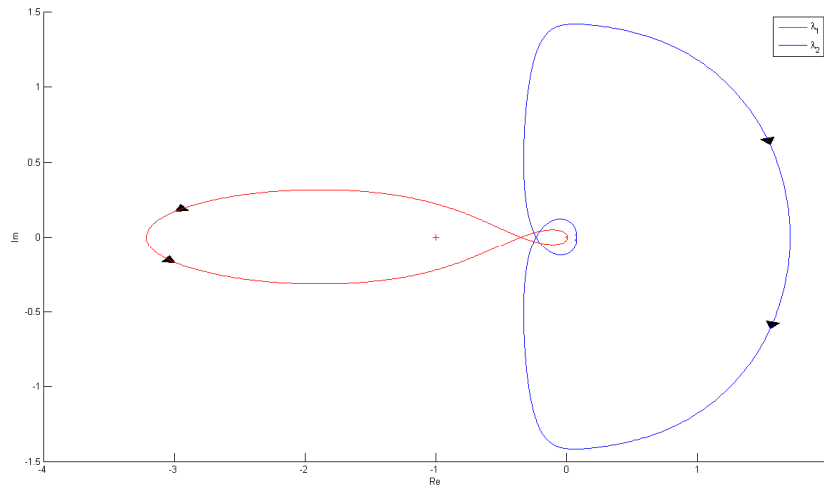


Figure 5.8: Nyquist plot of Example 5.4 with $(L, k) = (0.1, 1)$

**Example 5.5.** Consider

$$G(s) = \frac{1}{s^4 + 1.75s^3 + 7.5s^2 + 4s + 8} \begin{bmatrix} 0.0625s + 0.25 & s^2 + s + 4 \\ 0.25s^2 + 0.1875s + 0.75 & s + 4 \end{bmatrix} e^{-Ls}$$

This process is stable. For Step 1, the gain plot in Figure 5.9 shows that both characteristic loci are non-monotonic, $\bar{\omega}_1 = 1.19$ and $\bar{\omega}_2 = 2.38$. In Step 2, since only $\lambda_1(0) = -0.0534$ meets the condition (5.12), there is one horizontal

line $k = 18.7103$ on the plane $(L, k)$. In Step 3, since both characteristic loci are non-monotonic, we calculate $n_{\max}$. The phase plot in Figure 5.10 shows that $\phi_{\min 1} = -1.586$ and $\phi_{\min 2} = -3.597$. Let $L_{\max} = 10$, we have $n_{\min} = 0$, $n_{\max 1} = 2$ and $n_{\max 2} = 4$. We then plot all boundary curves $L_0$, $L_1$, $L_2$ of $\lambda_1$ and $L_0$, $L_1$, $L_2, L_3$, $L_4$ of $\lambda_2$ on $(L, k)$ plane (Figure 5.11). Since one horizontal line results from Step 2, this line divides the plane into two portions. Following Step 4b, the left most region in the lower portion is checked for stability at one selected point $(L, k) = (0.1, 1)$. The Nyquist plot shows that this region is stable (Figure 5.12). With a similar check, the left most region in the upper portion is unstable. In the end, the stable region is marked in green in the stabilizing graph (Figure 5.11).



Figure 5.9: Gain plot of $\lambda_0(s)$ of Example 5.5

Figure 5.10: Phase plot of $\lambda_0(s)$ of Example 5.5
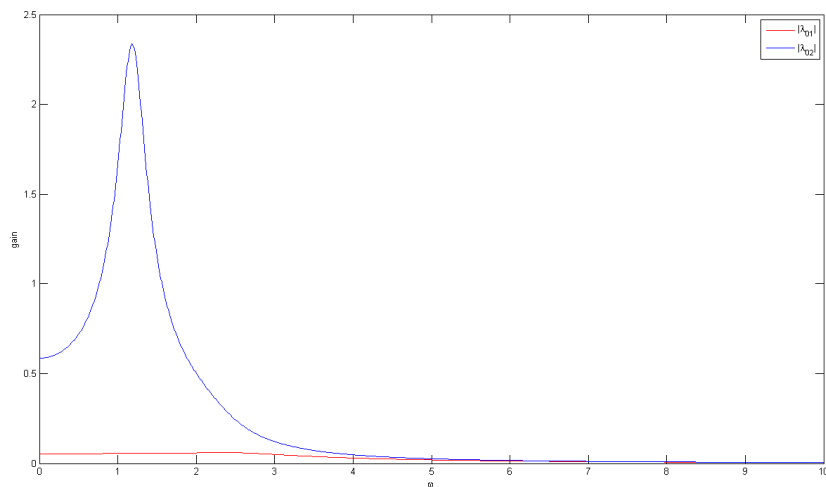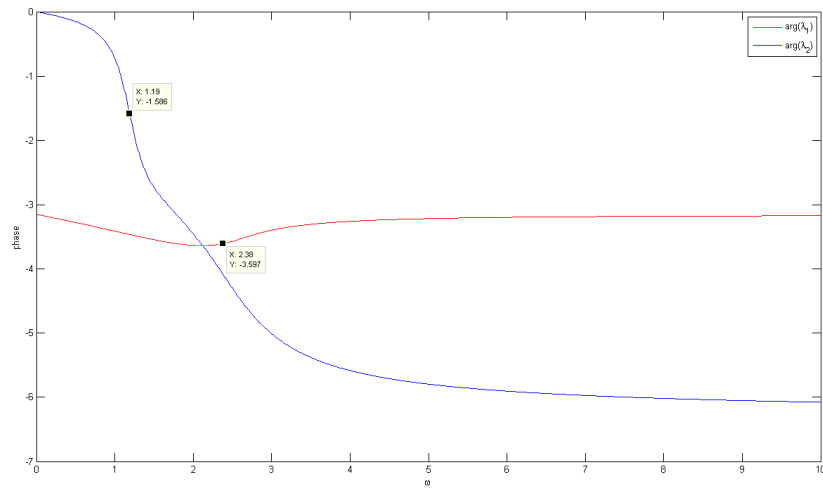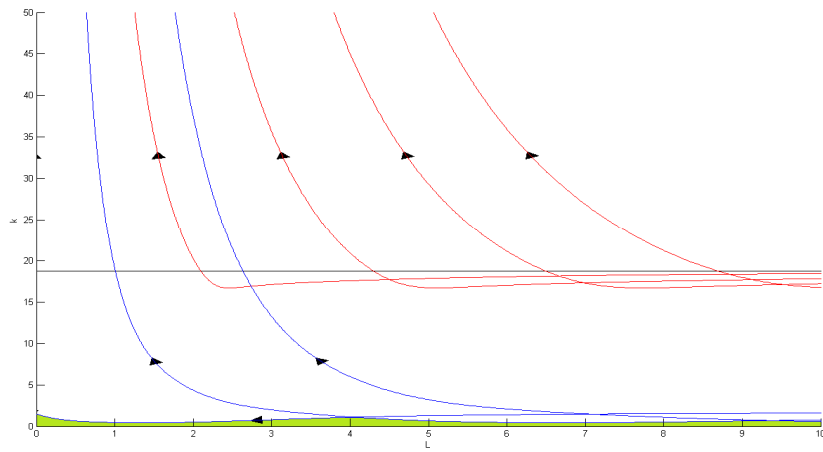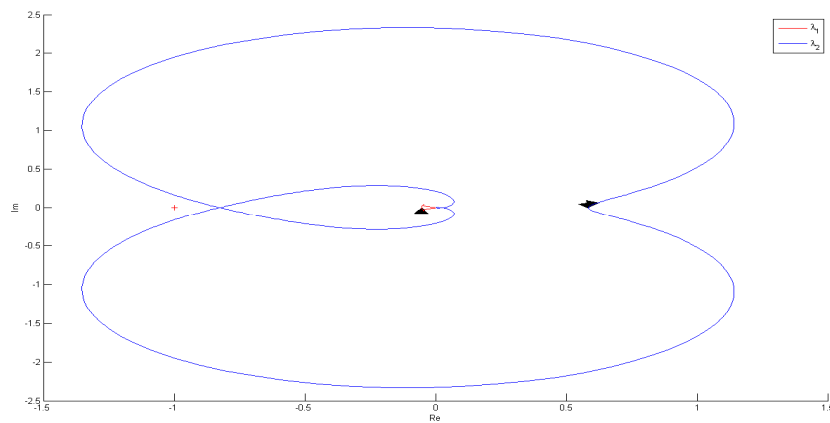


Figure 5.11: Stabilizing graph of Example 5.5



Figure 5.12: Nyquist plot of Example 5.5 with $(L, k) = (0.1, 1)$

**Example 5.6.** Our method can be applied to any square system, say,

$$G(s) = \begin{bmatrix} \dfrac{-1}{s+1} & \dfrac{2}{s+1} & \dfrac{3}{s+1} \\[2mm] \dfrac{4}{s+2} & \dfrac{-5}{s+2} & \dfrac{6}{s+2} \\[2mm] \dfrac{1}{s+3} & \dfrac{3}{s+3} & \dfrac{-2}{s+3} \end{bmatrix} e^{-Ls}$$

This process has no unstable pole. Adapting Algorithm 5.2 for three characteristic loci produces the stabilizing graph in Figure 5.13.
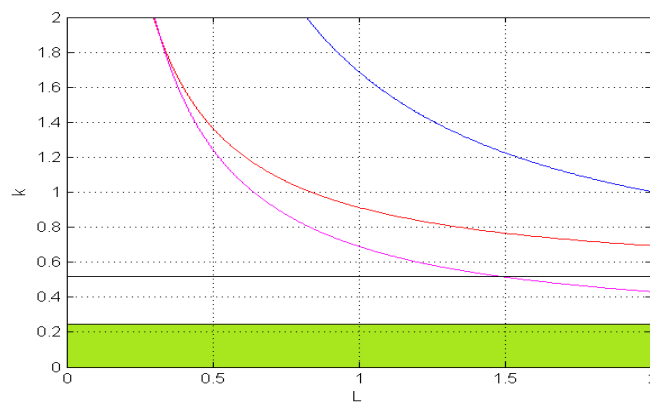


Figure 5.13: Stabilizing graph for Example 5.6

Though the stabilizability delay is unbounded for this stable process, the stabilizing gain range is quite small. For instance, when the delay is in the range $L \in [0,1.5]$ the stabilizing gain range is $k \in [0, 0.2458]$.

## 5.4. Conclusions

In this chapter, a simpler yet effective method is presented for accurately computing stabilizing gain ranges for TITO processes with fixed delay. It determines stability boundaries which separate the stable and unstable regions. The method can be applied for general TITO processes with delays. The method is simple technically and effective computationally. It can be employed to determine, as by-products, controller integrity as well as the loop gain margins. Since any control system must maintain its stability for loop

gain changes, loop gain margin are important specifications for TITO system analysis and design. The extension to general MIMO processes is possible but visualization will be lost. For TITO processes with uncertain/varying time delay, the characteristic loci approach is proposed to obtain the common gain stabilizer in term of time delay.

# Chapter 6

# Conclusion

## 6.1. Main Findings

### A. Parametric Approach to Computing Stabilizing PID Regions

A graphical method is presented to design stabilizing PID controller for a general process with/without time delay. By introducing the parameterized stability boundary band concept, the stabilizing region in $(K_p, K_i)$ plane with $K_d$ varies in a range is established. For a process with monotonic $\lambda(\omega)$, the entire stabilizing ranges of three parameters of PID controller are given. For a process with non-monotonic $\lambda(\omega)$, the method produces stable regions while suggesting some techniques to find conditionally stable regions.

### B. Stabilizing Loop Gain and Delay for Strictly Proper Processes

The exact and complete stabilizing gain and delay ranges are computed by determining the boundary functions which may change system's stability on the parameters plane. The proposed method is very general and applicable to any strictly proper process, and thus significantly relaxes the restrictions with the existing works. It is also powerful and can produce the exact and complete set of controller gain and delay which results in a stable closed-loop, which is difficult to find with analytical methods. A variety of examples are given and some of them show very complex stabilizing ranges which are beyond of imagination.

### C. Stabilizing Loop Gain and Delay for Bi-proper Processes

The D-decomposition method for computing stabilizing loop gain and delay ranges is extended to the case of bi-proper processes. The properties of boundary functions from such processes are investigated in great details. It has been shown that finite boundary functions are sufficient to determine all stable regions for finite parameter intervals. The formula is given for calculating this number. Moreover, the algorithms are established to find exact stabilizing gain and delay ranges, and they are illustrated by many kinds of processes including stable/unstable poles and minimum/non-minimum zeros. These new results, together with those for strictly proper processes, provide a complete solution for numerical parameterization of stabilizing loop gain and delay for a general delay SISO process.

**D. Stabilizing Loop Gain and Delay for MIMO Processes**

For a TITO process with fixed time delay, a method to find the stable regions in controller gains plane is proposed. It first determines all possible stability boundaries. These boundaries divide the gain plane to regions and the stability of each region is checked to identify the stable ones. Subsequently, the loop gain margins as well as controller integrity are obtained from these stable regions. The proposed method is simple and easy to apply with no iteration is required for computing stability boundaries.

For a TITO process with common varying delay, characteristic loci approach is employed to find the stable regions in the delay-gain plane. The common stabilizing gain ranges in term of the delay are obtained from such stable regions. This method is also applicable for any square MIMO process with a common delay as uncertainty parameter.

## 6.2. Suggestions for Future Work

The limitation of the D-decomposition method is the number of parameters due to the difficulty of graphical presentation and visualization. It is interesting to extend the afore-mentioned method to more than two parameters. In [4]–[6], this technique was applied to determine the stability boundary in the 3D space and find the stable regions of such space. However, the stabilizing graph produced by this approach is difficult to visualize. Thus, the key issue in the extended problem is on how to handle more parameters while keeping the feasible visualization. Chapter 2 on PID handles 3D case with a different approach which enables visualization.

On the other hand, if we go with numerical method without graphical representation, there are several difficulties as follows. Firstly, as we only have two real equations from the complex characteristic equation, the solutions of the equations at a given frequency are unique and determined for the case of two parameters. Therefore, the parameter space is divided into clearly separate regions with defined boundary. In case of more than 3 parameters, solutions of the equation are not unique and they will be given in term of other parameters. As a result, the region division is no longer clear, as we can observe in section 2.3 that the boundary bands intersects with each other, which causes much more complications than the boundary curves intersection in the 2-parameters problem. Secondly, if the characteristic equation is nonlinear in term of parameters, there may be infinite number of boundary bands and possible infinite number of their overlapping, which would cause great difficulty in stability analysis of resulting regions. Based on the framework of this thesis, further research may be conducted in the following directions.

## A. Parametric Approach to Computing Stabilizing PID Regions

In chapter 2, we presented the parametric approach to designing stabilizing PID controller for a general process with/without time delay. For a process with monotonic $\lambda(\omega)$, the complete set of all stable regions and conditional stable regions can be obtained. For a process with non-monotonic $\lambda(\omega)$, the method produces stable regions while suggesting some techniques to find conditionally stable region. Thus, more research works can be done on how to simplify solution for the case of non-monotonic $\lambda(\omega)$.

## B. Stabilizing Parameterization in Face of General Uncertain Processes

It is well known that the mathematical representation of a process is susceptible to uncertainties arising from modeling error, nonlinearities or operating condition [59]. The extension of D-decomposition method to design robust PI/PD controllers for such processes can be explored. Because of the uncertainty in process, at a frequency, the frequency response's magnitude and phase are no longer a single point but lies in a region in the Nyquist plane. As a result, the stability boundary curve of such a process in controller parameter plane is no longer a curve but a boundary band. The shape of the boundary band is an interesting aspect to investigate. The stable regions will give a complete set of robust controllers.

## C. Decentralized Controller for TITO Processes with Varying Common Time Delay

Consider a decentralized controller for a TITO process with varying common time delay. For such a problem, the transfer functions of the process and the diagonal controller, $G(s)$ and $K$, are described as follows.

$$G(s) = \begin{bmatrix} g_{11} & g_{12} \\ g_{21} & g_{22} \end{bmatrix} e^{-Ls}, \quad K = \begin{bmatrix} k_1 & 0 \\ 0 & k_2 \end{bmatrix}.$$

Like the PID case studied in Chapter 2, and using either $k_1$, or $k_2$ or $L$ as a parameter, the stability boundary in the other two parameters plane will become a boundary band. Finding the stable regions in the parameters plane gives solution to the stabilizing problem.

**D. Decentralized Controller for Three-input Three-output Processes**

A three-inputs three-outputs process can be found in industry such as a simplified hybrid solid oxide fuel cell gas turbine process [60]. Designing a decentralized controller for such a process can be another focus. The process and the controller can be described via transfer function matrices as follows.

$$G(s) = \begin{bmatrix} g_{11} & g_{12} & g_{13} \\ g_{21} & g_{22} & g_{23} \\ g_{31} & g_{23} & g_{33} \end{bmatrix}, \quad K = \begin{bmatrix} k_1 & 0 & 0 \\ 0 & k_2 & 0 \\ 0 & 0 & k_3 \end{bmatrix}.$$

Then, the parametric boundary band is obtained by viewing either $k_1$, or $k_2$ or $k_3$ as the parameter. The stabilizing problem is solved by finding all stable and conditionally stable regions in the parameters plane.

## Bibliography

[1]     T. H. K.J. Åström, *PID Controllers: Theory, Design, and Tuning*, 2nd ed. Instrument Society of America, Research Triangle Park, NC, 1995.

[2]     Y. I. Neimark, "D-decomposition of quasipolynomial space (to stability of linear distributed system)," *Am. Math. Soc. Transl.*, pp. 95–131.

[3]     Y. I. Neimark, "D-decomposition of quasipolynomial space (to stability of linear distributed system," *Appl. Math. and Mech.*, vol. 13, pp. 349–380, 1949.

[4]     N. Hohenbichler, "All stabilizing PID controllers for time delay systems," *Automatica*, vol. 45, no. 11, pp. 2678–2684, Nov. 2009.

[5]     M. T. Soylemez, N. Munro, and H. Baki, "Fast calculation of stabilizing PID controllers," vol. 39, pp. 121–126, 2003.

[6]     S. E. Hamamci, "An Algorithm for Stabilization of Fractional-Order Time," vol. 52, no. 10, pp. 1964–1969, 2007.

[7]     J. Fang, D. Zheng, and Z. Ren, "Computation of stabilizing PI and PID controllers by using Kronecker summation method," *Energy Convers. Manag.*, vol. 50, no. 7, pp. 1821–1827, Jul. 2009.

[8]     L. Jinggong, X. Yali, and L. Donghai, "Calculation of PI Controller Stable Region Based on D-Partition Method," no. 2, pp. 2185–2189, 2010.

[9]     N. H. El-Farra  Mhaskar, P., and Christofides, P. D., N. H. El-Farra, P. Mhaskar, and P. D. Christofides, "Hybrid predictive control of nonlinear systems: Method and applications to chemical processes," *Int. J. Robust Nonlinear Control*, vol. 14, pp. 199–225, 2004.

[10]    G. C. Goodwin, S. F. Graebe, M. E. Salgado, and G. C. Goodwin  Graebe, S.F., and Salgado, M.E., *Control System Design*. Prentice Hall, 2001.

[11]    J. E. Normey-Rico  Camacho, E.F., J. E. Normey-Rico, and E. . Camacho, *Control of Dead-Time Processes*. Springer London, 2007.

[12]    Y. He, Q.-G. Wang, C. Lin, and M. Wu, "Delay-range-dependent stability for systems with time-varying delay," *Automatica*, vol. 43, no. 2, pp. 371–376, 2007.

[13]    M. Wu, Y. He, J.-H. She, and G.-P. Liu, "Delay-dependent criteria for robust stability of time-varying delay systems," *Automatica*, vol. 40, no. 8, pp. 1435–1439, 2004.

[14] X.-M. Zhang, M. Wu, J.-H. She, and Y. He, "Delay-dependent stabilization of linear systems with time-varying state and input delays," *Automatica*, vol. 41, no. 8, pp. 1405–1412, 2005.

[15] G. Huijun and C. Tongwen, "New Results on Stability of Discrete-Time Systems With Time-Varying State Delay," *Autom. Control. IEEE Trans.*, vol. 52, no. 2, pp. 328–334, 2007.

[16] W. Min, L. Fang, S. Peng, H. Yong, and R. Yokoyama, "Improved Free-Weighting Matrix Approach for Stability Analysis of Discrete-Time Recurrent Neural Networks With Time-Varying Delay," *Circuits Syst. II Express Briefs, IEEE Trans.*, vol. 55, no. 7, pp. 690–694, 2008.

[17] O. J. Smith, "A controller to overcome dead time," *ISA J.*, vol. 6, no. 2, pp. 28–33, 1959.

[18] Z. J. Palmor, "Time delay compensation – smith predictor and its modifications," in in *The Control Handbook*, W. S. Levine, Ed. CRC Press, 1996, pp. 224–237.

[19] A. S. Rao and M. Chidambaram, "Analytical design of modified Smith predictor in a two-degrees-of-freedom control scheme for second order unstable processes with time delay," *ISA Trans.*, vol. 47, no. 4, pp. 407–419, 2008.

[20] J. E. Normey-Rico and E. F. Camacho, "Unified approach for robust dead-time compensator design," *J. Process Control*, vol. 19, no. 1, pp. 38–47, 2009.

[21] S. Uma, M. Chidambaram, A. Seshagiri Rao, and C. K. Yoo, "Enhanced control of integrating cascade processes with time delays using modified Smith predictor," *Chem. Eng. Sci.*, vol. 65, no. 3, pp. 1065–1075, 2010.

[22] P. García and P. Albertos, "Dead-time-compensator for unstable MIMO systems with multiple time delays," *J. Process Control*, vol. 20, no. 7, pp. 877–884, 2010.

[23] P. Albertos and P. García, "Robust control design for long time-delay systems," *J. Process Control*, vol. 19, no. 10, pp. 1640–1648, 2009.

[24] S. Mondié and W. Michiels, "Finite Spectrum Assignment of Unstable Time-Delay Systems with a Safe Implementation," *IEEE Trans. Automat. Contr.*, vol. 48, pp. 2207–2212, 2003.

[25] A. Manitius and A. Olbrot, "Finite spectrum assignment problem for systems with delays," *Autom. Control. IEEE Trans.*, vol. 24, no. 4, pp. 541–552, 1979.

[26] Z. Shafiei, A. T. Shenton, and Z. Shafiei Shenton, A.T., "Tuning of PID-type controllers for stable and unstable systems with time delay," *Automatica*, vol. 30, no. 10, pp. 1609–1615, 1994.

[27] R. Lanzkron and T. Higgins, "D-decomposition analysis of automatic control systems," *Autom. Control. IRE Trans.*, vol. 4, no. 3, pp. 150–171, 1959.

[28] G. J. Silva Datta, A., and Bhattacharyya, S.P., *PID controller for time-delay systems*. Boston: Birkhauser, 2004.

[29] A. Roy and K. Iqbal, "PID controller tuning for the first-order-plus-dead-time process model via Hermite-Biehler theorem," *ISA Trans.*, vol. 44, no. 3, pp. 363–378, 2005.

[30] G. J. Silva, A. Datta, and S. P. Bhattacharyya, "PI stabilization of first-order systems with time delay," *Automatica*, vol. 37, no. 12, pp. 2025–2031, 2001.

[31] C. Xiang, Q. G. Wang, X. Lu, L. A. Nguyen, and T. H. Lee, "Stabilization of second-order unstable delay processes by simple controllers," *J. Process Control*, vol. 17, no. 8, pp. 675–682, 2007.

[32] S. C. Lee, Q.-G. Wang, and C. Xiang, "Stabilization of all-pole unstable delay processes by simple controllers," *J. Process Control*, vol. 20, no. 2, pp. 235–239, 2010.

[33] S. C. Lee, Q.-G. Wang, and L. B. Nguyen, "Stabilizing control for a class of delay unstable processes.," *ISA Trans.*, vol. 49, no. 3, pp. 318–325, 2010.

[34] S. C. Lee and Q.-G. Wang, "Stabilization conditions for a class of unstable delay processes of higher order," *J. Taiwan Inst. Chem. Eng.*, vol. 41, no. 4, pp. 440–445, 2010.

[35] T. Shima and O. M. Golan, "Bounded differential games guidance law for dual-controlled missiles," *Control Syst. Technol. IEEE Trans.*, vol. 14, no. 4, pp. 719–724, 2006.

[36] L. Zhiwei, S. Fujii, Y. Saitoh, E. Muramatsu, and K. Watanabe, "Feedback-error Learning for Explicit Force Control of a Robot Manipulator Interacting with Unknown Dynamic Environment," in *Robotics and Biomimetics, 2004. ROBIO 2004. IEEE International Conference on*, 2004, pp. 262–267.

[37] M. C. M. Teixeira, Assun, #231, #227, E. o, R. Cardim, N. A. P. Silva, and E. R. M. D. Machado, "On Complementary Root Locus of Biproper Transfer Functions," *Math. Probl. Eng.*, vol. 2009, 2009.

[38] V. Blondel and D. Bertilsson, "An upper bound for the gain of stabilizing proportional controllers," *Syst. Control Lett.*, vol. 24, no. 2, pp. 83–86, 1995.

[39] L. Naimark and E. Zeheb, "All constant gain stabilizing controllers for an interval delay system with uncertain parameters," *Automatica*, vol. 33, no. 9, pp. 1669–1675, 1997.

[40] A. Tannenbaum, "On the multivariable gain margin problem," *Automatica*, vol. 22, no. 3, pp. 381–383, 1986.

[41] R. R. E. de Gaston and M. G. Safonov, "Exact calculation of the multiloop stability margin," *IEEE Trans. Automat. Contr.*, vol. 33, no. Compendex, pp. 156–171, 1988.

[42] M. G. Safonov, "Stability margins of diagonally perturbed multivariable feedback systems," in *Proceedings of the 20th IEEE Conference on Decision and Control including the Symposium on Adaptive Processes, 16-18 Dec. 1981*, 1981, pp. 1472–1478.

[43] Q.-G. Wang, C. Lin, Z. Ye, G. Wen, Y. He, and C. C. Hang, "A quasi-LMI approach to computing stabilizing parameter ranges of multi-loop PID controllers," *J. Process Control*, vol. 17, no. 1, pp. 59–72, 2007.

[44] Z.-Y. Nie, Q.-G. Wang, M. Wu, and Y. He, "Exact computation of loop gain margins of multivariable feedback systems," *J. Process Control*, vol. 20, no. 6, pp. 762–768, 2010.

[45] Z.-Y. Nie, M. Wu, Q.-G. Wang, and Y. He, "A novel computational method for loop gain and phase margins of TITO systems," *J. Franklin Inst.*, vol. 350, no. 3, pp. 503–520, 2013.

[46] E. N. Gryazina and B. T. Polyak, "Stability regions in the parameter space: D-decomposition revisited," *Automatica*, vol. 42, no. 1, pp. 13–26, Jan. 2006.

[47] D. D. Šiljak, *Nonlinear systems: the parameter analysis and design*. Wiley, 1968, p. 34.

[48] B. John and J. B. Moore, "CONTROL SYSTEM DESIGN USING EXTENSIONS. OF THE PARAMETER PIANE CONCEPT," 1967.

[49] A. Visioli, *Practical PID Control*. Springer London, 2006.

[50] G. F. Franklin, J. D. Powell, and A. Emami-Naeini, *Feedback control of dynamic systems*, 3rd ed. Reading, Mass.: Pearson Prentice Hall, 1994, p. xvii, 910 p.

[51] Z. Shafiei and A. T. Shenton, "Frequency-domain design of pid controllers for stable and unstable systems with time delay," *Automatica*, vol. 33, no. 12, pp. 2223–2232, 1997.

[52] Y. Song, M. O. Tadé, and T. Zhang, "Stabilization and algorithm of integrator plus dead-time process using PID controller," *J. Process Control*, vol. 19, no. 9, pp. 1529–1537, Oct. 2009.

[53] K. Saadaoui, S. Testouri, and M. Benrejeb, "Robust stabilizing first-order controllers for a class of time delay systems," *ISA Trans.*, vol. 49, no. 3, pp. 277–282, 2010.

[54] Y.-Y. Li, G.-Q. Qi, and A.-D. Sheng, "Frequency parameterization of H∞ PID controllers via relay feedback: A graphical approach," *J. Process Control*, vol. 21, no. 4, pp. 448–461, Apr. 2011.

[55] D.-J. Wang, "A PID controller set of guaranteeing stability and gain and phase margins for time-delay systems," *J. Process Control*, vol. 22, no. 7, pp. 1298–1306, 2012.

[56] Q.-G. Wang, *Decoupling Control 2003*. Springer, 2003.

[57] P. J. Campo and M. Morari, "Achievable closed-loop properties of systems under decentralized control: conditions involving the steady-state gain," *Autom. Control. IEEE Trans.*, vol. 39, no. 5, pp. 932–943, 1994.

[58] R. K. Wood and M. W. Berry, "Terminal composition control of a binary distillation column," *Chem. Eng. Sci.*, vol. 28, no. 9, pp. 1707–1717, 1973.

[59] M. Morari and E. Zafiriou, *Robust process control*. Prentice Hall, 1989.

[60] A. Tsai, "Multivariable Robust Control of a Simulated Hybrid Solid Oxide Fuel Cell Gas Turbine Plant Multivariable Robust Control of a Simulated Hybrid," 2007.

**Author's publications**

Journal Papers:

1. See Chek Lee, Qing-Guo Wang, Binh Nguyen Le, "Stabilizing control for a class of delay unstable processes", ISA Transaction, Vol. 49 no.3 (7/2010), pp. 318-325 (2010).

2. Chao Yu, Binh-Nguyen Le, Xian Li, Qing-Guo Wang, "Randomized Algorithm for Determining Stabilizing Parameter Regions for General Delay Control Systems", Journal of Intelligent Learning Systems and Applications, Vol 5 no 2 (5/2013), pp. 99-107 (2013).

3. Binh Nguyen Le, Qing-Guo Wang, Tong Heng Lee, "A Graphical Approach to Computing Loop Gain Margins for TITO systems", accepted to Transactions of the Institute of Measurement and Control.

4. Binh Nguyen Le, Qing-Guo Wang, Tong Heng Lee, "Development of D-decomposition method for Computing Stabilizing Gain Ranges for General Delay Systems", accepted to Journal of Process control.

5. Binh Nguyen Le, Qing-Guo Wang, Tong Heng Lee, "On Computation of Stabilizing Gain Ranges for Bi-Proper Delay Systems", submitted to ISA Transactions.

Conference Papers:

1. Qing-Guo Wang, Binh Nguyen Le, Tong Heng, Lee, "Graphical Methods for Computation of Stabilizing Gain Ranges for TITO systems", 9th IEEE International Conference on Control and Automation. Santiago, Chile, December 19-21, 2011.

2. Qing-Guo Wang, Binh Nguyen Le, Tong Heng, Lee, "Parametric Approach to Computing Stabilizing PID Regions", submitted to 11th

IEEE International Conference on Control and Automation. Taichung,

Taiwan, June 18-20, 2014.